



**NTNU – Trondheim**  
Norwegian University of  
Science and Technology

# LDV Measurements in Centrifugal Pump Diffuser

**Karl Oskar Pires Bjørgen**

Master of Science in Mechanical Engineering

Submission date: June 2015

Supervisor: Torbjørn Kristian Nielsen, EPT

Co-supervisor: Alessandro Nocente, EPT

Norwegian University of Science and Technology  
Department of Energy and Process Engineering



EPT-M-2015-9

**MASTER THESIS**

for

Stud.techn Karl Oskar Pires Bjørgen

Spring 2015

LDV Measurements in Centrifugal Pump Diffuser  
*LDV malinger i sentrifugalpumpe***Background**

The use of centrifugal pumps in the petroleum industry is growing in the last years due to many advantages this kind of machines can give. These pumps often operate with multiphase flows or with special fluids. The present work focuses on a multistage centrifugal pump used for produced water from an offshore oil platform. Produced water is a multiphase fluid and the dispersed oil is removed downstream. In order to achieve a high separation efficiency, the dispersed phase needs to have certain characteristics which are strongly influenced by the motion it experiences inside the pump. Hence is fundamental to determine the exact flow conditions in the channels of the machine.

**Objective**

Perform a series of CFD calculations with open source software using different meshes, pointing out the influence that mesh has on the accuracy of the simulations.  
Improve the LDV measurements on the diffuser and the return channel of the centrifugal pump rig in the Waterpower laboratory, and validate the simulations.

**The following tasks are to be considered:**

- 1 Literature survey
  - a. CFD mesh characteristics and influence on the simulation results.
  - b. LDV, Imaging investigation technique with high frequency cameras
  - c. Measurement and acquisition systems (software and hardware)
- 2 Software knowledge
  - a. CFD codes (OpenFOAM, ANSYS Fluent)
  - b. Meshing softwares
  - c. Post processing softwares (LabVIEW, Matlab)
- 3 The student shall obtain an esteem of the mesh sensitivity of the multistage centrifugal pump Model, perform a series of LDV measurements and evaluate the possibility and the utility of optical measurements on the centrifugal pump rig in Waterpower laboratory. In case of positive response the student shall perform optical measurements and use all the previously obtained experimental data to validate the CFD model as reference for the mesh sensitivity test.

Within 14 days of receiving the written text on the master thesis, the candidate shall submit a research plan for his project to the department.

When the thesis is evaluated, emphasis is put on processing of the results, and that they are presented in tabular and/or graphic form in a clear manner, and that they are analyzed carefully.

The thesis should be formulated as a research report with summary both in English and Norwegian, conclusion, literature references, table of contents etc. During the preparation of the text, the candidate should make an effort to produce a well-structured and easily readable report. In order to ease the evaluation of the thesis, it is important that the cross-references are correct. In the making of the report, strong emphasis should be placed on both a thorough discussion of the results and an orderly presentation.

The candidate is requested to initiate and keep close contact with his/her academic supervisor(s) throughout the working period. The candidate must follow the rules and regulations of NTNU as well as passive directions given by the Department of Energy and Process Engineering.

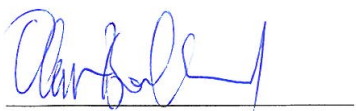
Risk assessment of the candidate's work shall be carried out according to the department's procedures. The risk assessment must be documented and included as part of the final report. Events related to the candidate's work adversely affecting the health, safety or security, must be documented and included as part of the final report. If the documentation on risk assessment represents a large number of pages, the full version is to be submitted electronically to the supervisor and an excerpt is included in the report.

Pursuant to “Regulations concerning the supplementary provisions to the technology study program/Master of Science” at NTNU §20, the Department reserves the permission to utilize all the results and data for teaching and research purposes as well as in future publications.

The final report is to be submitted digitally in DAIM. An executive summary of the thesis including title, student's name, supervisor's name, year, department name, and NTNU's logo and name, shall be submitted to the department as a separate pdf file. Based on an agreement with the supervisor, the final report and other material and documents may be given to the supervisor in digital format.

- Work to be done in lab (Water power lab, Fluids engineering lab, Thermal engineering lab)  
 Field work

Department of Energy and Process Engineering, 14. January 2015



Olav Bolland  
Department Head



Torbjørn Nielsen  
Academic Supervisor

Co-Supervisors : Trygve Husveg, PhD  
Alessandro Nocente, PhD candidate



## Abstract

This thesis describes experimental research on the flow inside a vaned diffuser of a centrifugal pump. The measurements were conducted inside one of the ten curved diffuser channels on the single-stage centrifugal pump test rig located at the Water Power Laboratory at the Norwegian University of Science and Technology (NTNU). The measuring technique used during the experiment was laser Doppler velocimetry (LDV), providing velocity data with a high spatial resolution and accuracy. Procedures for operating the test rig and the LDV system are included in the thesis. Detailed quantification of the two-dimensional steady flow is represented as the ensemble-averaged velocity and the root-mean-square (RMS) of the velocity fluctuations at design point and off-design point. Visualization of the flow properties are presented as velocity magnitude plots and velocity vector plots. The results show a well-behaved flow without flow separation at the diffuser walls when operating at design point and off-design point. However, the flow appears to be highly three-dimensional and fluctuating throughout the entire diffuser channel, which is expected in a curved diffuser. The main characteristic of the observed flow is a high velocity core near the concave wall, persisting until the outlet of the diffuser channel. Also a near-stagnation condition of the flow in a low velocity region near the convex wall is observed. The velocity fluctuation distribution has a characteristic S-shape in the upstream part of the diffuser with peak values located at high viscous shear stress zones, while in the downstream part it is uniformly distributed. The results show an overall good repeatability, especially for the downstream part of the diffuser channel, while the data acquired in the upstream part are more scattered. As the purpose of this thesis is to compare the measured velocity data with a Computational Fluid Dynamics (CFD) simulation, the reliability of the data is paramount. Based on the evaluation of the experimental setup and the uncertainty analysis presented in this thesis, the results are concluded to be suited for the intended purpose.



## Sammendrag

Denne oppgaven beskriver eksperimentell forskning på vannstrømningen inne i en diffusorkanal i en sentrifugalpumpe. Målingene ble gjennomført inne i en av de ti kurvede diffusorkanalene i ettrinnssentrifugalpumpen som befinner seg i Vannkraftlaboratoriet ved Norges Teknisk-Naturvitenskaplige Universitet (NTNU). Måleteknikken brukt under eksperimentet var laser Doppler velocimetry (LDV), som ga hastighetsmålinger med en høy romlig oppløsning og nøyaktighet. Prosedyrer for drift av testriggeren og LDV-systemet er inkludert i oppgaven. Det todimensjonale hastighetsfeltet er presentert som gjennomsnittshastigheten og kvadratisk middelvei av hastighetsfluktuasjonene, både for optimal drift og ikke-optimal drift av pumpen. Strømningskarakteristikkene er presentert gjennom hastighetsmagnitudediagram og vektordiagram. Resultatene viser at strømmingen følger diffusorgeometrien og at ingen strømningsavløsning ved diffusorveggene finner sted, både for optimal drift og ikke-optimal drift. Likevel kan strømmingen inne i diffusorkanalen karakteriseres som tredimensjonal og svært fluktuerende. Hovedkarakteristikken av strømmingen er en høyhastighetskjerne nær den konkave veggen som vedvarer gjennom hele kanalen. Ved den konvekse veggen oppnås det nesten stagnasjon av strømmingen. Hastighetsfluktasjonsprofilen er ved innløpet til diffusorkanalen formet som en S, hvor topppunktene tilsvarer områder i strømmingen med høy viskøs skjærspenning. Ved utløpet er hastighetsfluktasjonsprofilen jevnt fordelt over bredden av kanalen. Resultatene viser generelt god repeterbarhet, spesielt for nedstrømsdelen av kanalen, mens oppstrømsdelen viser større spredning av måleverdiene. Ettersom målet med denne oppgaven er å sammenligne målingene med en Computational Fluid Dynamics (CFD) simulering, er repeterbarheten av målingene svært viktig. Basert på evalueringen av det eksperimentelle oppsettet og usikkerhetsanalysen presentert i denne oppgaven, er resultatene gode nok for det tilsiktede formål.



## Acknowledgements

I would like to thank professor Torbjørn K. Nielsen for guiding me through the process of this thesis. His advises have been valuable for solving practical and theoretical issues. I would also like to thank PhD candidate Alessandro Nocente for his cooperation and guidance, for making the countless hours in the laboratory educational and enjoyable and for giving me advises about the writing process. In addition, I would like to thank Typhonix for giving me and NTNU the chance to contribute to research on this interesting topic, and Trygve Opland in the laboratory for making the pump run as optimal as possible. Furthermore, my fellow students at the Water Power Laboratory for making my time here enjoyable, for that I am very grateful. I would also like to show my gratitude to professor James Dawson for giving me advises on how to operate the LDV system. Finally, I would like to thank Ingrid Vik Bakken for reading my thesis and giving me advises on writing technique and language, and my parents, Rolf Bjørgen and Maria Pires Bjørgen, for their personal support throughout my studies.



# Contents

<b>List of Figures</b>	<b>xi</b>
<b>List of Tables</b>	<b>xv</b>
<b>Abbreviations</b>	<b>xvii</b>
<b>Nomenclature</b>	<b>xix</b>
<b>1 Introduction</b>	<b>1</b>
1.1 Background . . . . .	1
1.2 Objective . . . . .	2
1.3 Previous Work . . . . .	3
<b>2 Theory</b>	<b>5</b>
2.1 Multistage Centrifugal Pump . . . . .	5
2.2 The Flow in a Diffuser . . . . .	6
2.2.1 Straight diffuser . . . . .	6
2.2.2 Curved diffuser . . . . .	9
2.3 Laser Doppler Velocimetry . . . . .	12
2.3.1 Principles of LDV . . . . .	12
2.3.2 The fringe model . . . . .	15
2.3.3 Frequency shift . . . . .	15
2.3.4 Seeding particles . . . . .	16
2.3.5 Dimensions of the measurement volume . . . . .	17
<b>3 Experimental Work</b>	<b>19</b>
3.1 The Typhoon Pump . . . . .	19
3.2 The Single-stage Centrifugal Pump Test Rig . . . . .	20
3.2.1 Sensors . . . . .	21
3.2.2 Operating the test rig . . . . .	21
3.2.3 The characteristic curve . . . . .	21
3.2.4 Operating conditions . . . . .	22
3.2.5 Geometry of the diffuser . . . . .	24



3.3	Laser Doppler Velocimetry System . . . . .	24
3.3.1	The measurement volume . . . . .	25
3.3.2	Operating the LDV system . . . . .	26
3.3.3	Seeding particles . . . . .	28
3.4	Preparation . . . . .	28
3.4.1	Health, safety and environment . . . . .	28
3.4.2	Coordinate system . . . . .	28
3.4.3	Measurement points . . . . .	28
3.4.4	Alignment of the traverse table . . . . .	29
3.4.5	Number of samples . . . . .	29
3.5	Procedures . . . . .	30
3.5.1	Measurement campaigns . . . . .	31
<b>4</b>	<b>Data Analysis</b>	<b>33</b>
4.1	BSA Flow Software Raw Data . . . . .	33
4.2	Statistical Analysis . . . . .	34
4.3	Post-processing the Raw Data . . . . .	35
4.3.1	Steady velocity distribution . . . . .	35
4.3.2	Turbulence . . . . .	36
4.4	Evaluation of the Raw Data . . . . .	37
4.4.1	Skewness . . . . .	37
4.4.2	Filtering the data . . . . .	38
4.5	Plotting Routines . . . . .	40
4.5.1	Velocity vector plot . . . . .	40
4.5.2	Three-dimensional plot . . . . .	40
4.5.3	Widthwise cross-sectional plot . . . . .	41
<b>5</b>	<b>Results</b>	<b>43</b>
5.1	Steady Velocity Distribution . . . . .	45
5.2	RMS of the Total Velocity Fluctuation Distribution . . . . .	54
<b>6</b>	<b>Evaluation of the Experiment</b>	<b>57</b>
6.1	The Test Rig . . . . .	57
6.1.1	Water temperature change . . . . .	57
6.1.2	The geometry of the diffuser . . . . .	59
6.1.3	Other factors . . . . .	60
6.2	The LDV System . . . . .	60
6.3	Uncertainty Analysis . . . . .	63
6.3.1	Sources of error . . . . .	63
6.3.2	Repeatability . . . . .	67
<b>7</b>	<b>Discussion</b>	<b>71</b>

7.1	Flow Characteristics . . . . .	71
7.1.1	Flow direction . . . . .	71
7.1.2	Velocity magnitude . . . . .	73
7.1.3	Turbulence . . . . .	74
7.1.4	Off-design points . . . . .	76
7.2	Comparison Between Experimental and Numerical Results . . . . .	76
<b>8</b>	<b>Conclusions</b>	<b>81</b>
<b>9</b>	<b>Further Work</b>	<b>83</b>
	<b>References</b>	<b>85</b>
	<b>Appendices</b>	
<b>A</b>	<b>Calibration</b>	<b>87</b>
A.1	Calibration of the Pressure Transducer . . . . .	87
A.2	Calibration of the Flow Meter . . . . .	90
A.3	Calibration of the Torque Meter . . . . .	95
<b>B</b>	<b>Typhoon Performance Report</b>	<b>97</b>
<b>C</b>	<b>HSE Risk Assessments</b>	<b>101</b>



# List of Figures

2.1	Technical drawing of the three-stage Typhoon pump. (Typhonix) . . . .	5
2.2	The straight diffuser. . . . .	7
2.3	The dimensions of a curved diffuser. . . . .	10
2.4	The principle of LDV [1]. . . . .	12
2.5	A seeding particle in the flow, which scatters the light received from the two laser beams. . . . .	14
2.6	Intersection of the coherent laser beams forming fringes. [2] . . . . .	15
2.7	The graph to the left shows LDV with a frequency shift of $f_0$ , while the graph to the right shows equation 2.16, which represents an ambiguity of the received frequency $\Delta f_s$ . . . . .	16
3.1	The return vanes of Typhoon 1, 2 and 3, from left to right respectively. (Typhonix) . . . . .	19
3.2	The test rig. . . . .	20
3.3	Layout drawing of the single-stage centrifugal pump test rig. . . . .	21
3.4	Characteristic curve of the single-stage centrifugal pump test rig. . . . .	22
3.5	Temperature change of the water while running the pump. . . . .	23
3.6	The LDV probe pointing toward the measurement domain. . . . .	25
3.7	Schematic drawing of the LDV system. . . . .	26
3.8	The diffuser domain. The origin is inside the red circle. . . . .	29
3.9	Steadiness of $u$ and $v$ at $(x, y) = (140 \text{ mm}, 49.2 \text{ mm})$ . . . . .	30
4.1	Histogram of the velocities in the point $(x, y) = (122 \text{ mm}, 45.7 \text{ mm})$ , which is approximately skew normally distributed. The red line represents the velocity mean. . . . .	37
4.2	The neglected points. . . . .	39
4.3	The widthwise cross-sectional profiles. . . . .	41
5.1	Steady velocity vector plots in the diffuser. . . . .	45
(a)	M1 . . . . .	45
(b)	M2 . . . . .	45
5.2	Steady velocity vector plots in the diffuser. . . . .	46

(a)	M3 . . . . .	46
(b)	M3 - A . . . . .	46
5.3	Steady velocity vector plots in the diffuser. . . . .	47
(a)	M3 - B . . . . .	47
(b)	M4 . . . . .	47
5.4	Steady velocity vector plots in the diffuser. . . . .	48
(a)	M4 - A . . . . .	48
(b)	M4 - B . . . . .	48
5.5	Steady velocity vector plots in the diffuser for a) $1.5Q_{BEP}$ and b) $0.75Q_{BEP}$ . . . . .	49
(a)	M7 . . . . .	49
(b)	M8 . . . . .	49
5.6	3d plots of the steady velocity magnitude in the diffuser. . . . .	50
(a)	M1 . . . . .	50
(b)	M2 . . . . .	50
5.7	3d plots of the steady velocity magnitude in the diffuser. . . . .	51
(a)	M3 . . . . .	51
(b)	M4 . . . . .	51
5.8	3d plots of the steady velocity magnitude in the diffuser for a) $1.5Q_{BEP}$ and b) $0.75Q_{BEP}$ . . . . .	52
(a)	M7 . . . . .	52
(b)	M8 . . . . .	52
5.9	3d plots of the RMS of the total velocity fluctuation in the diffuser. . . . .	54
(a)	M1 . . . . .	54
(b)	M2 . . . . .	54
5.10	3d plots of the RMS of the total velocity fluctuation in the diffuser. . . . .	55
(a)	M3 . . . . .	55
(b)	M4 . . . . .	55
6.1	Investigation of the effect of temperature change on the velocity profile close to the diffuser inlet. . . . .	58
6.2	Operating conditions of the pump during M2. . . . .	59
6.3	Velocity magnitude profile along $z$ , at $(x, y) = (90 \text{ mm}, 26.5 \text{ mm})$ and $(x, y) = (130 \text{ mm}, 41.5 \text{ mm})$ . . . . .	60
6.4	Sample size and data rate plot of M3. . . . .	61
(a)	. . . . .	61
(b)	. . . . .	61
6.5	The scratches on the Plexiglas cover of the pump. . . . .	62
6.6	Data with noise from the LDV system. . . . .	66
(a)	Zero-noise . . . . .	66
(b)	Tail-noise . . . . .	66

6.7	The mean velocity magnitudes of the measurement campaigns at $Q_{BEP}$ (points), the average of the mean velocity magnitudes (red line) and the RMS of the deviation (green dotted line). . . . .	68
	(a) $x = 140 \text{ mm}$ . . . . .	68
	(b) $x = 120 \text{ mm}$ . . . . .	68
6.8	The mean velocity magnitudes of the measurement campaigns at $Q_{BEP}$ (points), the average of the mean velocity magnitudes (red line) and the RMS of the deviation (green dotted line). . . . .	69
	(a) $x = 100 \text{ mm}$ . . . . .	69
	(b) $x = 80 \text{ mm}$ . . . . .	69
6.9	The mean velocity magnitudes of the measurement campaigns at $Q_{BEP}$ (points), the average of the mean velocity magnitudes (red line) and the RMS of the deviation (green dotted line). . . . .	70
	(a) $x = 60 \text{ mm}$ . . . . .	70
	(b) $x = 40 \text{ mm}$ . . . . .	70
7.1	Flow angle contour plot for M3. . . . .	72
7.2	Widthwise cross-sectional plot of the velocity magnitude for M3. . . . .	73
7.3	Widthwise cross-sectional plot of the RMS of the total velocity fluctuations for M3. . . . .	75
7.4	Steady velocity magnitude plot of the CFD simulation from Ansys Fluent. . . . .	77
7.5	Velocity profiles for all measurement campaigns at $Q_{BEP}$ compared to the numerical model performed in Ansys Fluent. . . . .	78
	(a) $x = 140 \text{ mm}$ . . . . .	78
	(b) $x = 120 \text{ mm}$ . . . . .	78
7.6	Velocity profiles for all measurement campaigns at $Q_{BEP}$ compared to the numerical model performed in Ansys Fluent. . . . .	79
	(a) $x = 100 \text{ mm}$ . . . . .	79
	(b) $x = 80 \text{ mm}$ . . . . .	79
7.7	Velocity profiles for all measurement campaigns at $Q_{BEP}$ compared to the numerical model performed in Ansys Fluent. . . . .	80
	(a) $x = 60 \text{ mm}$ . . . . .	80
	(b) $x = 40 \text{ mm}$ . . . . .	80
A.1	Calibration curve for the Swirl flow meter. . . . .	91
A.2	Calibration curve for the torque meter. . . . .	95





# List of Tables

3.1	The dimensions of the diffuser channel. . . . .	24
3.2	Technical specifications for the LDV system. . . . .	25
3.3	Calculated dimensions of the measurement volume. . . . .	26
3.4	The measurement campaigns (* means that the measurement is omitted). . . . .	32
4.1	The columns in the BSA Flow Software raw file. . . . .	33
6.1	Flow rate deviation from $Q_{BEP} = 16.67 \text{ l/s}$ . . . . .	64
A.1	The flow meters that were involved in the calibration procedure. . . . .	90
A.2	Calibration data from step one. . . . .	92
A.3	Calibration data from step two. . . . .	93
A.4	Calibration data from step one, the temperature ( $T_{water}$ ), and the density of the water. . . . .	94
A.5	Calibration data for the torque meter. . . . .	96



# Abbreviations

BEP	Best Efficiency Point
BSA	Burst Spectrum Analyzer
CAD	Computer-Aided Design
CFD	Computational Fluid Dynamics
HSE	Health, Safety and Environment
NTNU	Norges Teknisk-Naturvitenskaplige Universitet
LDV	Laser Doppler Velocimetry
LPTV	Laser Particle Tracking Velocimetry
PhD	Philosophiae Doctor
PIV	Particle Image Velocimetry
PM	Photomultiplier
PSP	Polyamid Particles
RANS	Reynolds-Averaged Navier-Stokes
RMS	Root-Mean-Square
SNR	Signal-to-Noise Ratio



# Nomenclature

$a$	Acceleration	$[m/s^2]$
$A$	Cross-sectional area	$[m^2]$
$AR$	Diffuser area ratio	$[-]$
$AS$	Diffuser aspect ratio	$[-]$
$AT$	Arrival time	$[ms]$
$b$	Depth of diffuser channel	$[mm]$
$c$	Speed of light	$[m/s]$
$C_p$	Static pressure recovery coefficient	$[-]$
$d$	Distance	$[m]$
$d_I$	Laser beam diameter	$[mm]$
$D$	Diameter	$[m]$
$D_h$	Hydraulic diameter	$[m]$
$e$	Internal energy per unit mass	$[J/kg]$
$\vec{e}$	Unit vector	$[-]$
$E$	Expander ratio	$[-]$
$f$	Frequency	$[Hz]$
$\vec{f}$	Body forces per unit mass	$[N/kg]$
$\Delta f_s$	Frequency shift	$[Hz]$
$F$	Focal length of the front lens	$[mm]$
$H$	Total head	$[m]$
$I$	Turbulence intensity	$[-]$
$k$	Turbulent kinetic energy	$[m^2/s^2]$
$l$	Beam spacing	$[mm]$
$L_{in}$	Length of convex wall in a curved diffuser	$[mm]$
$L_{out}$	Length of concave wall in a curved diffuser	$[mm]$
$N$	Length of the center-line in a curved diffuser	$[mm]$
$N$	Number of samples in a measurement point	$[-]$

$N_f$	Number of fringes	$[-]$
$p$	Static pressure	$[N/m^2]$
$\dot{q}$	Rate of volumetric heat addition per unit mass	$[J/kg\,s]$
$Q$	Flow rate	$[m^3/s]$
$Re$	Reynolds number	$[-]$
$T$	Temperature	$[^\circ C]$
$TT$	Transit time	$[\mu s]$
$u$	$x$ -velocity	$[m/s]$
$u'$	Velocity fluctuation in $x$ -direction	$[m/s]$
$U$	Mean velocity in $x$ -direction	$[m/s]$
$U'$	Total velocity fluctuation	$[m/s]$
$\vec{U}$	Velocity vector	$[m/s]$
$v$	$y$ -velocity	$[m/s]$
$v'$	Velocity fluctuation in $y$ -direction	$[m/s]$
$V$	Mean velocity in $y$ -direction	$[m/s]$
$w$	$z$ -velocity	$[m/s]$
$w'$	Velocity fluctuation in $z$ -direction	$[m/s]$
$W$	Mean velocity in $z$ -direction	$[m/s]$
$W$	Width of diffuser channel	$[mm]$
$\alpha$	Kinetic energy flux profile factor	$[-]$
$\Delta\beta$	Turning angle of center-line in a curved diffuser	$[^\circ]$
$\delta_f$	Spacing between fringes	$[mm]$
$\theta$	Angle between the two laser beams in crossed beam configuration	$[^\circ]$
$\theta_{eff}$	The effective diverging angle in a curved diffuser	$[^\circ]$
$\lambda$	Wavelength	$[nm]$
$\mu$	Dynamic viscosity	$[kg/m\,s]$
$\rho$	Density	$[kg/m^3]$
$\sigma$	Velocity standard deviation	$[m/s]$
$\phi$	Angle between $x$ -axis and the velocity in LDV	$[^\circ]$
$\psi$	Flow angle with respect to the $x$ -axis	$[^\circ]$

## Common subscripts

1	inlet of diffuser
2	outlet of diffuser
i	incoming beam
s	beam received by the photodetector
I	incoming beam from a crossed beam configuration
x	in $x$ -direction
y	in $y$ -direction
z	in $z$ -direction
BEP	Best efficiency point
n	sample number
RMS	root-mean-square





# Chapter 1

## Introduction

### 1.1 Background

Oil and gas retrieved from reservoirs underneath the seabed usually contain water as well as hydrocarbons. As the oil, gas and water mixture is extracted from the well, they are separated from each other. In the oil and gas industry the separated water is called produced water and is an oil-in-water emulsion, where the water is the continuous phase while the oil is the dispersed phase. Due to environmental regulations the produced water is required to be rinsed before released into the ocean. In the rinsing process a device called hydrocyclone is utilized in order to separate the oil droplets from the water. The hydrocyclone is also known as an "enhanced gravity separator". The reason for this is that it uses centrifugal forces for the separation process. The working principle of the hydrocyclone is simple and involves no moving parts. The produced water is tangentially injected into the cylindrical casing of the hydrocyclone. The fluid is forced into a spiral motion by the curved walls and forms a vortex. Centrifugal forces create an outward radial pressure gradient in the cylindrical casing with a low pressure core in the center. Since the oil has a lower density than water, a buoyancy force pointing toward the center is exerted on the oil droplets. The buoyancy force consequently accelerates the oil droplets to the center of the hydrocyclone where the oil is extracted. The separation efficiency of the hydrocyclone is closely connected to the hydrocyclone's ability to move the oil droplets [3]. This is related to the terminal velocity  $V_s$ , which for a spherical oil droplet with a diameter of  $D$  and the density  $\rho_s$ , submerged in a viscous fluid with the density  $\rho_f$  and the dynamic viscosity  $\mu_f$ , and having the acceleration  $a$ , is described by Stokes law:

$$V_s = \frac{aD^2 (\rho_s - \rho_f)}{18\mu_f} \quad (1.1)$$

Since the acceleration and fluid properties are hard to change, a change in droplet

size is most convenient. An increase of the oil droplet size will increase the terminal velocity of the oil droplet and consequently improve the separation efficiency of the hydrocyclone, without the use of additional mechanical or chemical treatment processes.

This thesis is a part of a research and development program on a separation-friendly multistage centrifugal pump called Typhoon, designed to pump produced water. The aim of the program is to optimize the design of the Typhoon pump so that it reduces problems connected to droplet break-up and emulsification of fluid phases compared to conventional pumps. The project is a collaboration between the pump design company Typhonix from Bryne in Norway and the Norwegian University of Science and Technology (NTNU) in Trondheim. PhD candidate Alessandro Nocente has numerically modeled a single-stage version of the pump using the commercial Computational Fluid Dynamics (CFD) software Ansys Fluent in order to obtain more knowledge on the flow characteristics inside the pump, and possibly further optimize the design.

## 1.2 Objective

The main purpose of this thesis is to obtain experimental data from the pump while operating under the same conditions as the CFD simulation, and to compare the results. If the numerical model is validated by the experimental data, modifications can be made and simulated in order to further optimize the design of the Typhoon pump.

The centrifugal pump diffuser consists of ten curved diffuser channels. In order to measure the velocity inside the pump, a single-stage version of the Typhoon pump was mounted in the Water Power Laboratory of NTNU during the autumn of 2014. The velocity and turbulence characteristics were investigated inside one of the diffuser channels of the pump with use of laser Doppler velocimetry (LDV). LDV is a complex technique which measures the velocity in a point with a high temporal and spatial resolution. All results presented here were acquired during the spring semester of 2015.

The second part of the thesis description, which involves a mesh sensitivity analysis for the numerical model, was not completed, and therefore not included in the thesis. Thus the focus for this thesis is on obtaining satisfying experimental results. This was in agreement with my supervisor professor Torbjørn Nielsen and PhD candidate Alessandro Nocente.

### 1.3 Previous Work

Typhonix started this project in 2010 on their own initiative. In the first phase of the development project the optimal geometry and configuration of Typhoon was established and an increase in oil droplet size was observed at an early stage. Tests with various combinations of operation and process conditions were performed in order to establish the cause of droplet growth. One of the main findings of the work was that increased fluid residence time had a large impact on droplet growth. Additionally, a hydrocyclone test rig was built in Typhonix's laboratory in order to verify the increase in separation efficiency when having larger oil droplets [3].

The internal flow of the Typhoon pump was also studied experimentally and theoretically in Foslie's master thesis [4] from 2013. The experimental part consisted of measuring the velocity profile at the outlet of the impeller, i.e. the inlet of the diffuser, by using pitot-static probes. The results were considered to be unreliable and a non-intrusive velocity measuring technique like LDV was recommended for further work.

Furthermore, various types of centrifugal pumps have been subject to previous experimental work. The unsteady flow field inside a diffuser of a centrifugal pump for various operating points were investigated by Eisele et al. [5] in 1997 by using LDV and laser particle tracking velocimetry (LPTV). Their main conclusions were that the flow in a vaned diffuser is strongly three-dimensional and unsteady; that the magnitude of the periodic unsteadiness is strongest at the impeller outlet and diminishes rapidly downstream of the diffuser inlet; and that the magnitude of the non-periodic unsteadiness, i.e. the turbulence, increases throughout the diffuser passage. Pedersen et al. [6] studied in 2003 the unsteady flow field inside an impeller of a centrifugal pump operating at design and off-design point by using LDV and particle image velocimetry (PIV). Pedersen provided detailed measurements of the unsteady flow inside the impeller and concluded that both LDV and PIV are highly suited for measurements in turbo machinery and that PIV is less time-consuming than LDV.

Experimental studies on curved diffusers were performed in 1962 by Fox and Kline [7]. The flow regime inside a curved diffuser with various geometry parameter combinations was qualitatively investigated through injecting dye to the flow. The dye follows the streamlines in the flow, enabling possible flow separation to be observed visually. Their conclusion was that the flow inside a curved diffuser is highly unsteady and three-dimensional. Additionally, the geometrical parameter combinations causing flow separation were presented.



## 2.1 Multistage Centrifugal Pump

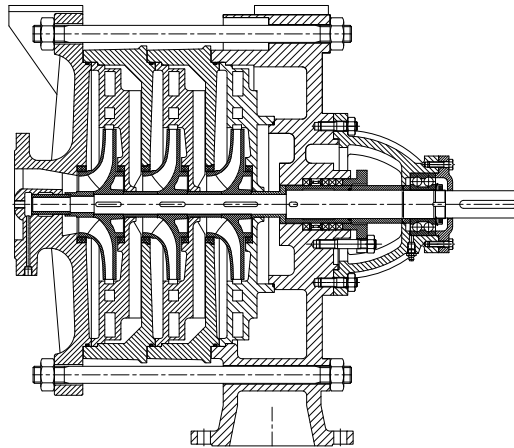


*Figure 2.1: Technical drawing of the three-stage Typhoon pump. (Typhonix)*

A centrifugal pump consists of an impeller attached to a shaft, which is driven by a motor. The impeller is surrounded by a casing with an inlet and an outlet. The inlet leads the liquid axially to the impeller inlet. Between the outlet of the impeller and the outlet of the casing, there is a diverging passage called the diffuser, which is normally a volute or several channels formed by vanes. As the impeller rotates, the liquid inside of it is forced to flow along the impeller blades, because of centrifugal forces exerted on the liquid from the rotating blades. The impeller blades are usually curved in the opposite direction of the rotation. The added momentum to the liquid then forces it to exit the impeller, enter the diffuser and eventually exit through the

outlet of the casing. The impeller increases the kinetic energy of the liquid, while the diffuser converts the kinetic energy into increased static pressure. The result is an increase of static pressure on the liquid from the inlet to the outlet of the pump, the static pressure increase divided by the specific weight of the fluid is also known as the total head. The total head produced by a centrifugal pump is a function of the flow rate through the pump, this relation is called the characteristic curve.

In a multistage centrifugal pump this process is repeated through two or more pump stages. The liquid exits from the first diffuser and is guided to the next stage, i.e. the next impeller inlet, before it continues to the next stage. The total head is the sum of each stage's head build-up. Figure 2.1 shows a multistage centrifugal pump with three stages, i.e. three impellers and diffusers. The inlet of the pump is located on the left-hand side, while the outlet is located in the lower part. The shaft is vertically centered and connected to three impellers, each coupled with a surrounding diffuser.

## 2.2 The Flow in a Diffuser

A diffuser is a component used in many fluid applications, such as the draft tube located at the exit of a Francis turbine, wind tunnels or centrifugal pumps. The main function of a diffuser is to convert kinetic energy into static pressure, i.e. the cross-sectional area increases in the streamwise direction in a diffuser, consequently the static pressure will rise due to the reduction of kinetic energy. This is only valid for subsonic flows. While the geometry of a diffuser is quite simple, the flow characteristics inside are particularly complex.

### 2.2.1 Straight diffuser

The performance of the diffuser is often measured by the increase in static pressure through the diffuser. This can be further investigated by looking at the combination of the equations for conservation of mass, and conservation of energy for a control volume around the fluid inside the diffuser [8]. For an incompressible steady flow the density is assumed to be constant, i.e.  $\rho_1 = \rho_2 = \rho = \text{constant}$ , hence the conservation of mass reduces to:

$$U_1 A_1 = U_2 A_2 \tag{2.1}$$

Where  $U_1$  and  $U_2$  are the inlet and outlet axial velocities in the  $x$ -direction, respectively.  $A_1$  and  $A_2$  are the cross-sectional areas at the inlet and outlet, respectively.



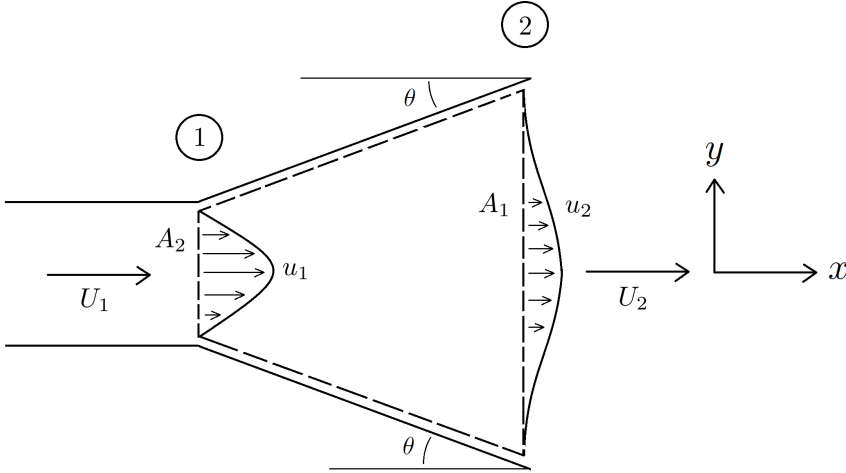


Figure 2.2: The straight diffuser.

The average axial velocity is defined as:

$$U = \frac{1}{A} \int_A u \, dA \quad (2.2)$$

$u$  is the axial velocity over the area  $A$ . The conservative form of the energy equation for the fluid is shown below [9]:

$$\frac{\partial}{\partial t} \left[ \rho \left( e + \frac{|\vec{U}|^2}{2} \right) \right] + \vec{\nabla} \cdot \left[ \rho \left( e + \frac{|\vec{U}|^2}{2} \right) \vec{U} \right] = \rho \dot{q} - \vec{\nabla} \cdot \vec{U} p + \rho \vec{f} \cdot \vec{U} \quad (2.3)$$

The viscous and thermal conductivity terms are neglected.  $\vec{U}$  is the velocity vector of the fluid at the position and time  $(x, y, z, t)$  and  $|\vec{U}|$  is the velocity magnitude.  $u$ ,  $v$  and  $w$  are the velocity magnitudes in the directions  $x$ ,  $y$  and  $z$  respectively.  $p$  is the pressure,  $e$  is the internal energy per unit mass,  $\dot{q}$  is the rate of volumetric heat addition per unit mass and  $\vec{f}$  is the sum of body forces per unit mass working on the fluid. The simplified diffuser case is considered to have steady incompressible subsonic flow, no heat transfer nor body forces acting on the control volume.

Rewriting equation 2.3 yields:

$$\vec{\nabla} \cdot \left[ \left( e + \frac{|\vec{U}|^2}{2} + \frac{p}{\rho} \right) \vec{U} \right] = 0 \quad (2.4)$$

The following expression is obtained by integrating equation 2.4 over the control volume and applying the Divergence Theorem<sup>1</sup>:

$$\iiint_V \vec{\nabla} \cdot \left[ \left( e + \frac{|\vec{U}|^2}{2} + \frac{p}{\rho} \right) \vec{U} \right] dV = \iint_A \left[ \left( e + \frac{|\vec{U}|^2}{2} + \frac{p}{\rho} \right) \vec{U} \right] \cdot \vec{n} dA = 0 \quad (2.5)$$

Further simplifications are necessary. Only the axial velocity component along the center-line of the diffuser is used, changes in internal energy from  $A_1$  to  $A_2$  are neglected<sup>2</sup>. The static pressure is uniformly distributed over the surfaces. When evaluating the integral at all surfaces, the scalar product  $\vec{U} \cdot \vec{n}$  is equal to zero at all surfaces, except at the inlet and outlet. Equation 2.5 can then be simplified to:

$$p_1 \iint_{A_1} u dA + \frac{\rho}{2} \iint_{A_1} u^3 dA = p_2 \iint_{A_2} u dA + \frac{\rho}{2} \iint_{A_2} u^3 dA \quad (2.6)$$

Equation 2.6 is heavily simplified, but still gives an indication of how the static pressure and the kinetic energy flux are balanced at inlet and the outlet. Defining the kinetic energy flux profile factor  $\alpha$  as:

$$\alpha = \frac{1}{A} \iint_A \left( \frac{u}{U} \right)^3 dA \quad (2.7)$$

$\alpha$  is the ratio between the kinetic energy flux based on the actual velocity profile  $u$ , and the kinetic energy flux based on a uniform velocity profile  $U$ . For a real diffuser the velocity profile is usually zero at the walls and peaked at the center-line, i.e.  $\alpha \geq 1$ . However, if the real velocity profile is uniform,  $\alpha$  becomes equal to 1.

---

<sup>1</sup>Divergence theorem:  $\iiint_V \vec{\nabla} \cdot \vec{F} dV = \iint_A \vec{F} \cdot \vec{n} dA$ ,  $\vec{n}$  is defined as the normal vector pointing outwards from the volume  $V$ .

<sup>2</sup>Viscous dissipation is neglected.

Applying equation 2.7, 2.1 and 2.2 to equation 2.6, yields:

$$\frac{p_2 - p_1}{\frac{1}{2}\rho U_1^2} = \alpha_1 - \alpha_2 \left( \frac{A_1}{A_2} \right)^2 \quad (2.8)$$

Equation 2.8 shows how the kinetic energy flux at the inlet and outlet affects the static pressure recovery, here represented as the change in static pressure normalized with the inlet dynamic pressure. For optimal performance of the diffuser, the static pressure recovery should be maximized. The cross-sectional area of the diffuser is always expanding, i.e.  $\frac{A_1}{A_2} < 1$ . To achieve the ideal situation for the diffuser, the inlet velocity profile should be as peaked as possible, i.e. maximizing  $\alpha_1$ , and the outlet velocity profile should be as uniform as possible, i.e.  $\alpha_2 = 1$ .

On the contrary, if the velocity profile at the inlet is uniform and the flow at the diffuser walls separates and produces a non-uniform velocity profile at the outlet, e.g. the extreme case of a jet flow where  $\alpha_1 = 1$  and  $\alpha_2 = (A_2/A_1)^2$ , the static pressure recovery is equal to zero. A jet flow in a diffuser is defined as a flow which is completely separated at the walls, meaning that the diverging cross-sectional area has no effect. This concludes that flow separation at the walls reduces the performance of a diffuser. Viscous dissipation, which is not included in this analysis, also diminishes the static pressure recovery.

### 2.2.2 Curved diffuser

The curved diffuser is simply a straight diffuser with a bend. The curvature is usually circular or elliptical and has a cross-sectional area which usually diverges linearly when moving from the inlet to the outlet. Some important geometrical parameters [10] for a curved diffuser are listed below:

- $W_1$  and  $W_2$  are the widths of the inlet and outlet of the diffuser, respectively.
- $N$  is the length of the center-line.
- $L_{in}$  and  $L_{out}$  are the lengths of the inner wall, i.e. the convex wall, and the outer wall, i.e. the concave wall<sup>3</sup>.
- $\Delta\beta$  is the turning angle of the center-line from the inlet to the outlet.
- $b$  is the depth of the diffuser channel.

---

<sup>3</sup>The inner and outer wall are called the bottom and top wall in the experiment, respectively.

Certain non-dimensionalized parameters have been used in several papers [7] on design of curved diffusers:

- Diffuser area ratio,  $AR = W_2/W_1$ .
- Diffuser aspect ratio,  $AS = b/W_1$ .
- The non-dimensional length of the channel,  $N/W_1$ .
- Static pressure recovery coefficient,  $C_p = (p_2 - p_1)/(\frac{1}{2}\rho U_1^2)$ .
- Reynolds number based on the inlet area averaged velocity and the hydraulic diameter<sup>4</sup> of the inlet cross-section,  $Re = (U_1 D_h)/\nu$
- The diverging angle of the curved diffuser  $\theta_{eff} = \tan^{-1} \left( \frac{AR-1}{2(N/W_1)} \right)$

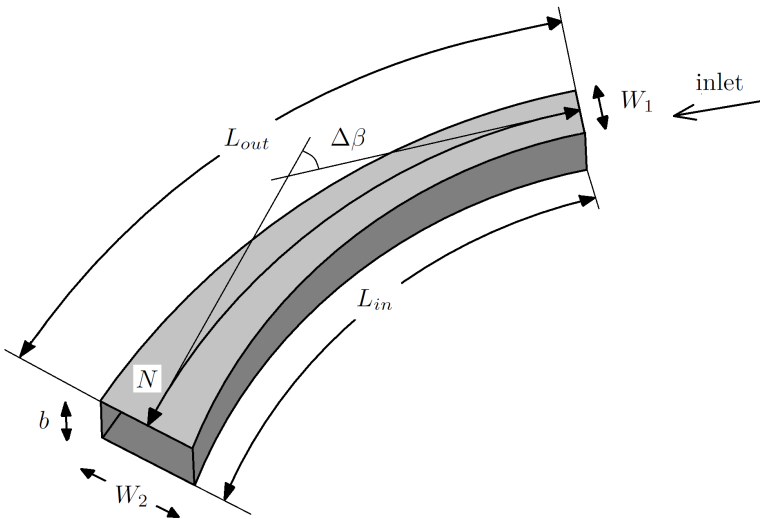


Figure 2.3: The dimensions of a curved diffuser.

The curved geometry of the diffuser induces a centrifugal force on the fluid as it flows through it. This introduces a non-symmetrical pressure distribution across the center-line. The pressure increases at the outer wall which gives rise to a radial pressure gradient, which in turn causes a pressure-driven secondary motion of the flow, e.g production of vortices. Majumdar [10] observed in 1998 large secondary motions produced at the inlet of a high aspect ratio diffuser because of a radial pressure difference. This caused the flow to go from being two-dimensional to three-dimensional downstream. The biggest challenge of the design of a curved diffuser is to prevent flow separation, as this might cause extensive losses. Moore [11] concluded in 1955 that the Reynolds number based on the inlet width  $W_1$  and the aspect ratio

<sup>4</sup>The hydraulic diameter of a rectangular duct:  $D_h = \frac{2ab}{a+b}$ , where  $a$  is the width/height and  $b$  is the height/width of the duct.

$AS$  has little or no effect on the flow regimes in a straight diffuser, making the other geometrical parameters dominant, i.e. diverging angle  $\theta_{eff}$ , center-line length to inlet width ratio  $N/W_1$ , area ratio  $AR$  and the turning angle  $\Delta\beta$ . Based on Moore's conclusion Fox and Kline did a similar study in 1962, but with curved diffusers. They discovered that the same flow regimes observed in a straight diffuser were present in a curved diffuser. The observed flow regimes were: a regime of well behaved, unseparated flow; a regime of large transitory stall; a regime of fully developed stall; and a jet flow regime, where the flow had entirely separated from the walls.

## 2.3 Laser Doppler Velocimetry

LDV is an optical technique for the investigation of fluid structures in a liquid or gas flow. It captures the velocity of a particle passing through a measurement volume with a high spatial and temporal resolution. The method is non-intrusive, which means that the probe does not disturb the flow. This is paramount when investigating flow phenomena such as flow separation and vortex structures, since a probe placed in the flow domain would affect the natural occurring phenomena. The first paper about LDV was released by Yeh and Cummins [12] in 1964 and LDV has ever since been widely used to investigate various fluid characteristics. Another great advantage of LDV is that it does not require any calibration, as the velocity data can be computed directly from the received signal without any input [13]. A frequency shift between the two crossing laser beams makes it possible to determine the direction of the fluid flow, something which enables LDV to capture unexpected back flow. By having three pairs of laser beams, LDV is able to simultaneously capture all the velocity components in a measurement volume.

### 2.3.1 Principles of LDV

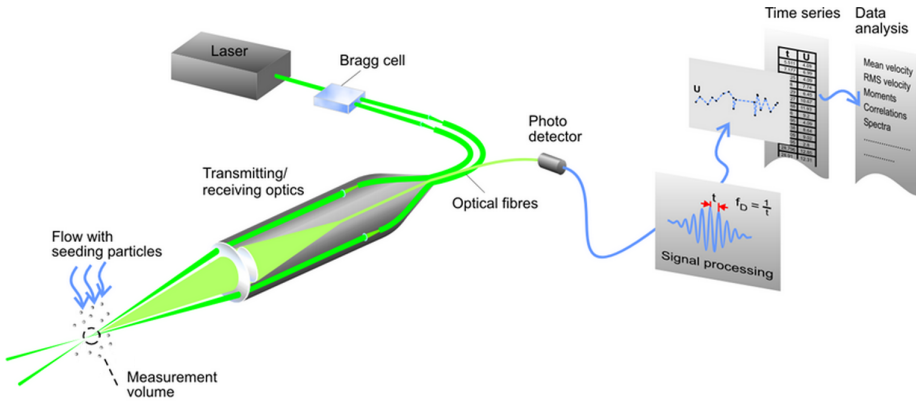


Figure 2.4: The principle of LDV [1].

### The Doppler effect

The principles behind LDV are closely related to the Doppler effect. A simplified case explains this. The objective of LDV is to determine the velocity  $\vec{U}$  of a particle following the flow. The particle passes through a laser beam with the direction<sup>5</sup>  $\vec{e}_i$ , the frequency  $f_i$  and the speed of light  $c$ . Light is scattered in all directions<sup>6</sup>,

<sup>5</sup>  $\vec{e}$  is the unit vector, i.e. it has the magnitude of one.

<sup>6</sup> According to the Lorenz-Mie scattering theory.

but we only consider the direction of the light received by the photodetector,  $\vec{e}_s$ . The photodetector observes the particle as a moving transmitter, the detected frequency  $f_s$  is therefore given a Doppler shift compared to the incoming frequency  $f_i$ . According to the Doppler effect, the frequency of the scattered light received by the photodetector can be calculated as:

$$f_s = f_i \frac{1 - \vec{e}_i \cdot (\vec{U}/c)}{1 - \vec{e}_s \cdot (\vec{U}/c)} \quad (2.9)$$

The speed of light  $c$  is always much larger than the particle velocity  $\vec{U}$ , i.e.  $\vec{U}/c \ll 1$ . Equation 2.9 can then be linearized to:

$$f_s \approx f_i \left[ 1 + \frac{\vec{U}}{c} \cdot (\vec{e}_s - \vec{e}_i) \right] = f_i + \Delta f \quad (2.10)$$

The only unknown parameter of equation 2.10 is  $\vec{U}$ . This approach is simplified compared to the real configuration. The velocity of the particle has to be very high in order to obtain a frequency shift which can be recorded by the photodetector, something which is not always practically convenient.

### Crossed beam configuration

LDV uses two laser beams originating from the same source, which cross each other in a measurement volume, measuring the velocity in only one dimension. A total of six beams, i.e. three beam pairs, is needed for acquiring the velocity in three dimensions. The directions of the two beams in the crossed beam configuration are  $\vec{e}_1$  and  $\vec{e}_2$ , both having the same frequency  $f_I$ . A particle passing through the measurement volume will scatter the light of both beams. The scattered light from both beams is detected by the photodetector in the direction  $\vec{e}_s$ , with the frequency of beam 1 and 2 as  $f_{s,1}$  and  $f_{s,2}$ , respectively. An illustration of the seeding particle can be seen in figure 2.5. The Doppler effect gives the frequencies:

$$f_{s,1} \approx f_I \left[ 1 + \frac{\vec{U}}{c} \cdot (\vec{e}_s - \vec{e}_1) \right] \quad (2.11)$$

$$f_{s,2} \approx f_I \left[ 1 + \frac{\vec{U}}{c} \cdot (\vec{e}_s - \vec{e}_2) \right] \quad (2.12)$$

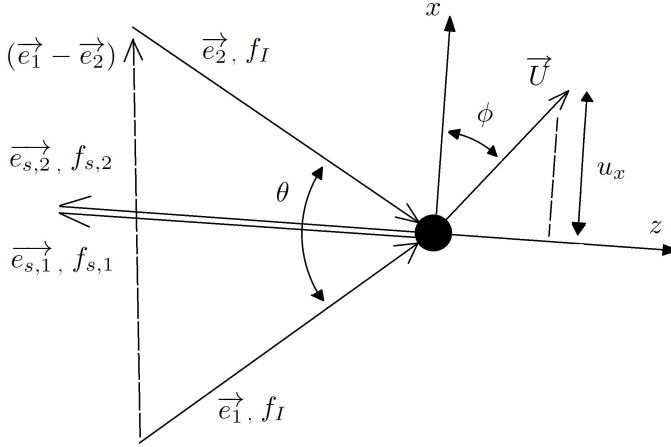


Figure 2.5: A seeding particle in the flow, which scatters the light received from the two laser beams.

By combining equation 2.11 and 2.12,  $\vec{e}_s$  can be eliminated, which means that the location of the photodetector is irrelevant<sup>7</sup> for the calculation of the particle velocity  $\vec{U}$ .

$$\Delta f_s = f_{s,2} - f_{s,1} = f_I \left[ \frac{|\vec{U}|}{c} \cdot (\vec{e}_1 - \vec{e}_2) \right] \quad (2.13)$$

The wave length of the incoming light is defined as  $\lambda = c/f_I$ . By applying the rule of scalar product between the vectors, equation 2.13 can be written as:

$$\Delta f_s = \frac{1}{\lambda} \left[ |(\vec{e}_1 - \vec{e}_2)| \cdot |\vec{U}| \cdot \cos(\phi) \right] = \frac{1}{\lambda} 2 \sin(\theta/2) \cdot u \quad (2.14)$$

$\phi$  is the angle between the direction of the  $x$ -axis and the velocity  $\vec{U}$ , and  $\theta$  is the angle between the two laser beams. From equation 2.14,  $u$  can be calculated by knowing  $\theta$ ,  $\lambda$  and detecting the frequency shift  $\Delta f_s$ .

<sup>7</sup>Not irrelevant when considering the intensity of the scattered light. Lorenz-Mie scattering theory explains that the direction of the received light has a large influence on the intensity, e.g. backscattering versus forward-scattering.



### 2.3.2 The fringe model

Equation 2.14 can also be derived by another more illustrative model called the fringe model. The two laser beams with the same wavelength  $\lambda$  cross each other in the measurement volume. The coherent beams form an interference pattern consisting of parallel planes with higher light intensity, also known as fringes. The light intensity between the fringes is lower. As seen from figure 2.6 the spacing between the maximum intensity planes  $\delta_f$  is constant.

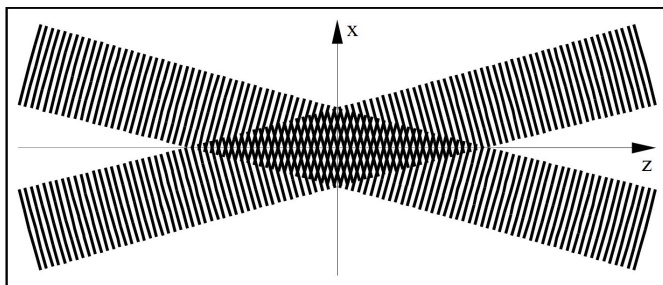


Figure 2.6: Intersection of the coherent laser beams forming fringes. [2]

The spacing between the fringes is defined as:

$$\delta_f = \frac{\lambda}{2 \sin(\theta/2)} \quad (2.15)$$

The fringes are normal to the direction of the measurement, i.e. the  $x$ -axis. As the particle passes through the fringes, it scatters light with the frequency,

$$\Delta f_s = \frac{u}{\delta_f} = \frac{2 \sin(\theta/2)}{\lambda} u \quad (2.16)$$

This corresponds to the result achieved in equation 2.14.

### 2.3.3 Frequency shift

LDV is able to measure positive and negative velocities. By looking at equation 2.16 one can see that if the velocity  $u$  becomes negative, the frequency shift also becomes negative. The photodetector is not able to distinguish between positive and negative frequencies. To cope with this problem a Bragg cell is used. The Bragg cell splits the incoming laser beam into two beams and adds a fixed frequency shift  $f_0$  to one of the beams. The beams travel to the intersection point, i.e. the measurement

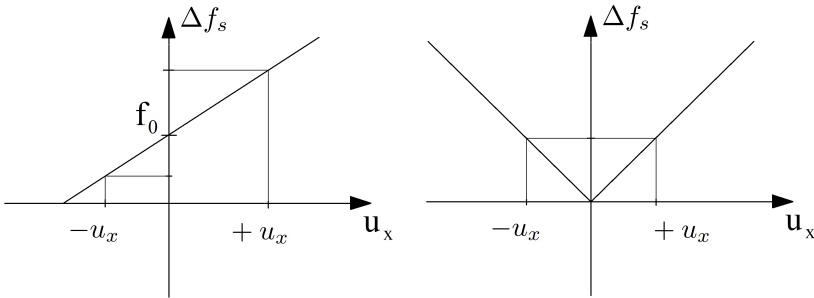


Figure 2.7: The graph to the left shows LDV with a frequency shift of  $f_0$ , while the graph to the right shows equation 2.16, which represents an ambiguity of the received frequency  $\Delta f_s$ .

volume, with the frequencies  $f_I$  and  $f_I + f_0$ . Replacing the incident frequencies in the equations 2.11 and 2.12, and substituting them into each other, yield:

$$\Delta f_s = f_0 + \frac{2 \sin(\theta/2)}{\lambda} u + f_0 |\vec{U}/c| \cdot |(\vec{e}_s - \vec{e}_2)| \cdot \cos(\phi) \quad (2.17)$$

The length of unit vectors are always 1, resulting in  $|(\vec{e}_s - \vec{e}_2)| \leq 2$ . Moreover,  $|\vec{U}/c| \ll 1$ , because the speed of light is always much larger than the particle speed, and  $\cos(\phi) \leq 1$ . From this it is assumed that the last term in equation 2.17 can be neglected, yielding:

$$\Delta f_s = f_0 + \frac{2 \sin(\theta/2)}{\lambda} u \quad (2.18)$$

### 2.3.4 Seeding particles

The velocity of the fluid flow obtained by LDV is in fact the velocity of the seeding particle present in the flow. It is therefore important that the particle is following the flow accurately and that it scatters enough light so that the photodetector can detect it. The choice of seeding particles for a fluid flow is therefore of utmost importance. There are several factors needing to be addressed:

- Shape of the particle.
- Size of the particle.
- Relative density of the particle and fluid.
- Concentration of particles in the fluid.
- Body forces acting on the particle.
- The particle's ability to scatter light.

The shape of the particle should optimally be spherical as this ensures that the light is scattered independently of its orientation in space, and that the drag force acting on the particle is working in a favorable manner. The relative density of the particle and the fluid should be equal to one in order to avoid buoyancy forces. The size of the particle affects its ability to scatter light and the body forces exerted on it. This is a trade-off because bigger particles scatter more light, but are at the same time heavier, which reduces their ability to follow the flow. In addition, the size can be optimized according to the fringe spacing to obtain a better signal. Moreover, if the concentration of particles in the fluid is high, the particles could interact with each other and result in undesirable motion. The concentration of seeding particles in the flow is usually too low for this to happen, so it can be neglected.

### 2.3.5 Dimensions of the measurement volume

The dimensions of the measurement volume can be calculated from the beam diameter  $d_I$ , the focal length of the front lens  $F$ , the wavelength of the light  $\lambda$  and the length between the beams on the front lens of the probe  $l$ . The angle  $\theta$  between the beams is calculated from the beam spacing  $l$  and the focal length  $F$ :

$$\theta = 2 \sin^{-1} \left( \frac{l/2}{F} \right) \quad (2.19)$$

The dimensions in the  $x$ -,  $y$ - and  $z$ -direction of the measurement volume are:

$$d_x = \frac{d_f}{\cos(\theta/2)}, \quad d_y = d_f, \quad d_z = \frac{d_f}{\sin(\theta/2)} \quad (2.20)$$

Where  $d_f$  is the beam waist diameter, which is the minimum diameter of the beam after the front lens. This is located at the measurement volume in order to maximize the spatial resolution of the equipment.  $d_f$  is calculated from:

$$d_f = \frac{4F\lambda}{\pi E d_I} \quad (2.21)$$

Now that the dimensions of the measurement volume are defined, i.e. equation 2.20, the number of fringes  $N_f$  can be calculated based on the fringe spacing from the equation 2.15. The fringes are always normal to the  $x$ -axis, see figure 2.6.

$$N_f = \frac{d_x}{\delta_f} = \frac{d_f}{\cos(\theta/2)} \frac{2 \sin(\theta/2)}{\lambda} = \frac{2d_f}{\lambda} \tan(\theta/2) \quad (2.22)$$



# Chapter 3

## Experimental Work

### 3.1 The Typhoon Pump

Typhonix has been researching on the optimal design for the growth of oil droplets in a multistage centrifugal pump named Typhoon. The working fluid consists of water and oil droplets. The growth of oil droplets increases the separation efficiency of hydrocyclones. Typhonix tested the Typhoon pump using various combinations of operating parameters, including flow rate, oil concentration, inlet oil droplet size and salt content in the water. One of the main findings of the research was that the growth of oil droplets increases for longer fluid residence time. Increased fluid residence time can be achieved by either having multiple pump stages, increased diffuser volume, increased return channel volume or a combination of these. The diffuser and the return channel of the pump is the part where the oil droplets are believed to have the opportunity to collide and grow. These volumes have consequently been increased as much as possible without affecting the hydraulic efficiency of the pump [3].

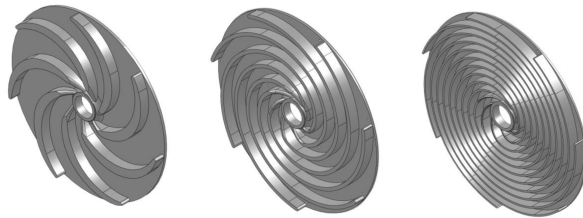


*Figure 3.1: The return vanes of Typhoon 1, 2 and 3, from left to right respectively. (Typhonix)*

In addition to the parameters mentioned above, Typhonix also experimented with three different designs of the return vanes on the back side of the diffuser, maintaining the original design of the diffuser on the front side for each of the three designs, i.e. Typhoon 1, 2 and 3 (figure 3.1). All the designs have the same fluid residence time,

flow volume and the number of return vanes. The difference between them is the curvature of the return vanes, where Typhoon 1, 2 and 3 have increasing curvature, respectively. The increase in curvature increases the velocity and the turbulence level in the return channels for Typhoon 3 compared to Typhoon 2, and similarly for Typhoon 2 compared to Typhoon 1. The hypothesis was that the increased velocity and turbulence level in the return channel could promote the growth of oil droplets. However, they concluded that it did not increase the outlet droplet size, but rather significantly decreased the hydraulic efficiency of the pump because of increased flow resistance. Typhoon 1 was therefore chosen as the optimal design.

### 3.2 The Single-stage Centrifugal Pump Test Rig

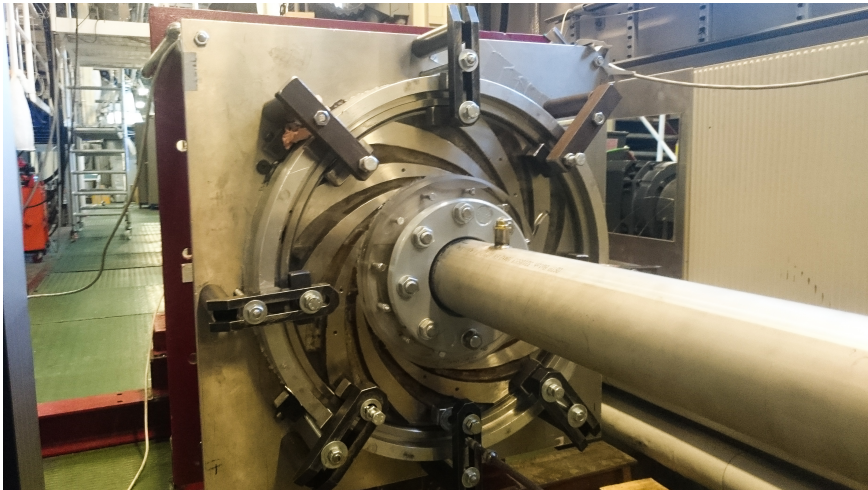


*Figure 3.2: The test rig.*

The design chosen for the test rig at NTNU was a single-stage version of Typhoon 1. The pump is connected to a closed water loop with a 12,000 liters water tank. The working fluid does not contain oil droplets since the oil-in-water emulsion is expected to behave as pure water. The water is pumped through a 4 meters long inlet pipe and returns back to the water tank through an outlet pipe. The inlet and outlet pipes are 100 mm in diameter. The inlet pipe has a gate valve (inlet valve) and a flow meter installed on it. The inlet valve is located close to the water tank, i.e. approximately 4 meters from the impeller. With a flow rate of 16.67 l/s and 20 °C water, the Reynolds number for the flow in the inlet pipe is calculated to be approximately 10,000. The flow in the pipe can consequently be characterized as turbulent. According to Blevins' Handbook for Applied Fluid Dynamics [8], fully developed flow in a pipe is obtained after 25 diameters for  $Re > 10,000$ .  $L/D$  for the inlet pipe is 40, meaning that the flow is fully developed when it reaches the pump

inlet. The outlet pipe has a butterfly valve (outlet valve) installed close to the water tank. The impeller is driven by an electric motor. The front cover of the pump is made of Plexiglas, providing optical access to the diffuser channels.

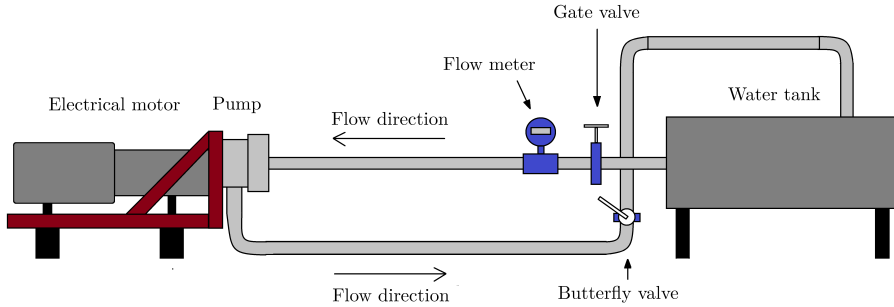


Figure 3.3: Layout drawing of the single-stage centrifugal pump test rig.

### 3.2.1 Sensors

Sensors that were used during operation of the test rig were a flow meter installed on the inlet pipe, a torque meter on the shaft connecting the motor and the impeller, a rotational speed sensor on the shaft and a differential pressure sensor measuring the static pressure build-up of the pump. These sensors were linked to a data acquisition board and the data were processed and logged by the software Labview. Data and routines for the calibration of the flow meter, torque meter and differential pressure sensor can be found in appendix A.

### 3.2.2 Operating the test rig

The rotational speed of the impeller was adjusted by turning a knob on the electrical motor control panel, situated between the water tank and the pump. When the desired rotational speed was set, the flow rate was set by adjusting the inlet and outlet valve. Initially the flow rate was adjusted solely by the inlet valve, but when the desired flow rate was reached, the pump experienced cavitation because of the low pressure induced by the inlet valve. The solution to this problem was to install a second valve on the outlet pipe, i.e. the outlet valve, consequently increasing the pressure in the pump and avoiding cavitation.

### 3.2.3 The characteristic curve

The characteristic curve of the pump was mapped during two measurements campaigns ranging from a flow rate of approximately  $8 \text{ l/s}$  to  $35 \text{ l/s}$ . Measurements with a lower flow rate than  $8 \text{ l/s}$  were not conducted because of the resulting high

pressure in the pump, which could break the front Plexiglas cover. The performance test of the Typhoon pump [14], provided by the manufacturer Standart, is plotted in figure 3.4 together with the performance of the test rig. The Standart performance report is based on a three-stage version of the pump, which is assumed to give approximately three times higher total head. The total head  $H$  on the characteristic curve provided by Standart was therefore divided by three. The rotational speed of the pump was kept constantly at 1480 *rpm*. The data acquired from the test rig show good agreement with Standart's data.

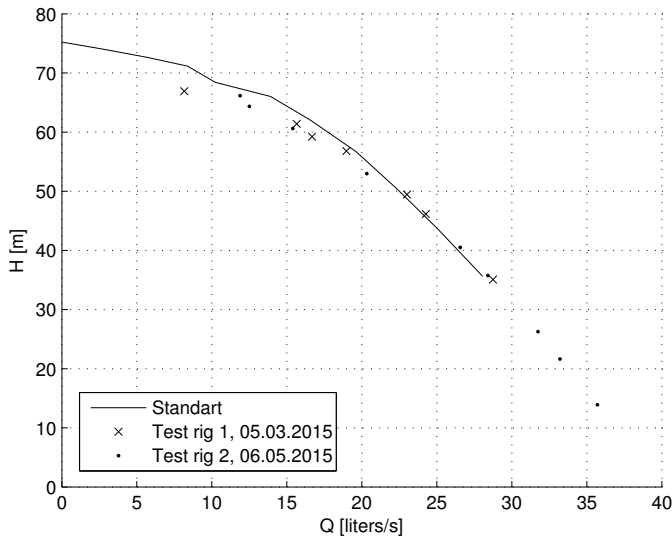


Figure 3.4: Characteristic curve of the single-stage centrifugal pump test rig.

### 3.2.4 Operating conditions

The bulk of the measurements were conducted at best efficiency point (BEP) based on the Standart performance report.  $Q_{BEP}$  is  $60 \text{ m}^3/h$ , i.e.  $16.67 \text{ l/s}$ . Two more operating points were chosen in order to investigate possible flow separation in the diffuser at  $12.5 \text{ l/s}$  and  $25 \text{ l/s}$ , i.e.  $0.75Q_{BEP}$  and  $1.5Q_{BEP}$  respectively. The rotational speed of the pump was 1480 *rpm* for all measurement campaigns.

The temperature of the water was initially not considered influential on the velocity measurements, but further investigation showed that the velocity distribution is temperature dependent, introducing a systematic error to the measurements, something which will be discussed later. The temperature of the circulating water was regularly measured during four measurement campaigns, on four different days. Figure 3.5 shows the temperature change over time for the four days and a linear regression



of the given data. The rate of change is approximately  $2.28^{\circ}\text{C}/\text{h}$ . The desired temperature of the water is  $20^{\circ}\text{C}$ , since that is the water temperature in the CFD simulation.

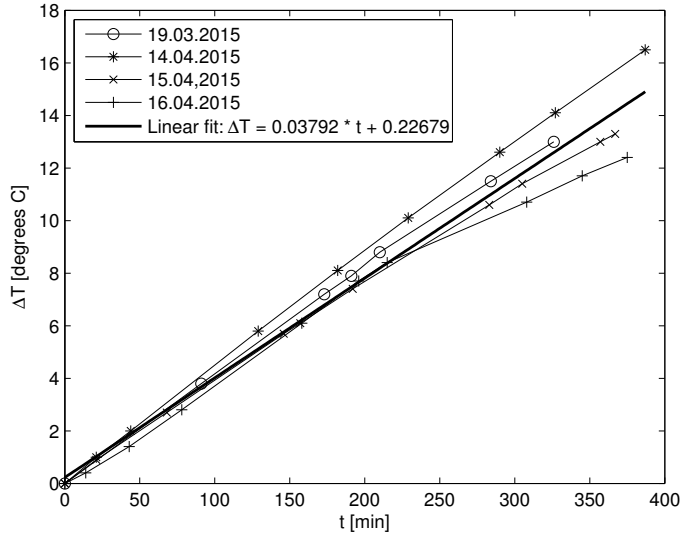


Figure 3.5: Temperature change of the water while running the pump.

### 3.2.5 Geometry of the diffuser

The geometry of the pump is described according to the parameters described in section 2.2.2. The diffuser channel geometry was not smooth. The inner surface was rough with many bumps. The top and bottom walls were not perfectly perpendicular in respect to the inner surface and the Plexiglas, giving the channel a near-trapezoidal cross-section. The depth  $b$  varied throughout the channel. The dimensions of the test rig diffuser channel are shown in table 3.1:

Parameter	Value	Unit
$W_1$	$12 \pm 1$	[mm]
$W_2$	$22 \pm 1$	[mm]
$L_{in}$	185	[mm]
$L_{out}$	226	[mm]
$N$	190	[mm]
$b$	$18 \pm 2$	[mm]
$\Delta\beta$	$35 \pm 3$	[°]
$AR$	$1.85 \pm 0.24$	[-]
$AS$	$1.52 \pm 0.29$	[-]
$N/W_1$	$15.94 \pm 1.33$	[-]

Table 3.1: The dimensions of the diffuser channel.

## 3.3 Laser Doppler Velocimetry System

The monochromatic light used in the LDV was produced from a Spectra Physics 177G high power air-cooled argon ion laser system, see technical specifications in table 3.2. The laser light is split into two beams with different wavelengths, i.e. 514.5 nm and 488 nm. These two beams are again diffracted into two beam pairs, where one beam in each pair goes through a Bragg cell<sup>1</sup> which gives it a frequency shift of 40 MHz. This is done in order to obtain directional unambiguity. The two beam pairs are directed into a probe through fiber-optical cables. The probe emits the laser beam pairs through a front lens which deflects the beams so that they intersect each other in a measurement volume 300 mm away. The probe has also a photodetector, also known as the photomultiplier (PM), which receives the back-scattered light as the seeding particles in the flow move through the measurement volume. The photodetector converts the optical signal into an analog signal and sends the information to a Burst Spectrum Analyzer (BSA) processor where the

---

<sup>1</sup>A Bragg cell is a acousto-optical modulator which uses sound waves to shift the frequency of light.

velocity data are calculated for each Doppler-burst<sup>2</sup>. The probe can measure the velocity in two dimensions at a point, a third probe is needed if three dimensions are desired. The probe was mounted on a three-axis traverse table controlled by a computer. The software for setting the LDV parameters, analyzing the data and controlling the traverse is BSA Flow Software, developed by Dantec Dynamics.

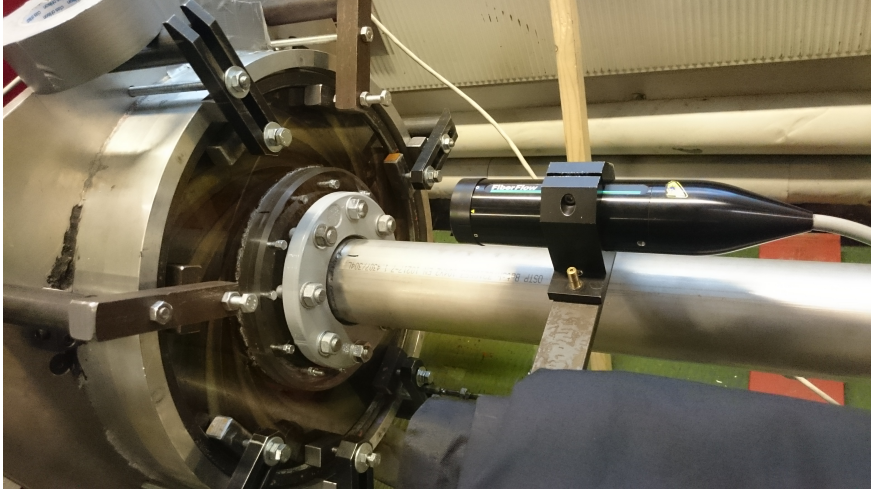


Figure 3.6: The LDV probe pointing toward the measurement domain.

System delivered by	Dantec Dynamics
Laser model	Spectra Physics 177-G0232
Type	Argon ion
Wave length, $\lambda_{blue}/\lambda_{green}$ [nm]	488/514.5
Beam diameter, $d_I$ [mm]	0.74
Beam spacing, $l$ [mm]	38
Focal length, $F$ [mm]	300
Expander ratio, $E$ [-]	1

Table 3.2: Technical specifications for the LDV system.

### 3.3.1 The measurement volume

The measurement volume is defined as the volume formed by the intersection of the laser beams. See section 2.3.5 for the equations used to calculate the dimensions shown in table 3.3. The size of the measurement volume also represents the spatial resolution of the measurements performed by the LDV.

<sup>2</sup>A Doppler-burst is a burst of light originating from the scattered light of a passing seeding particle.

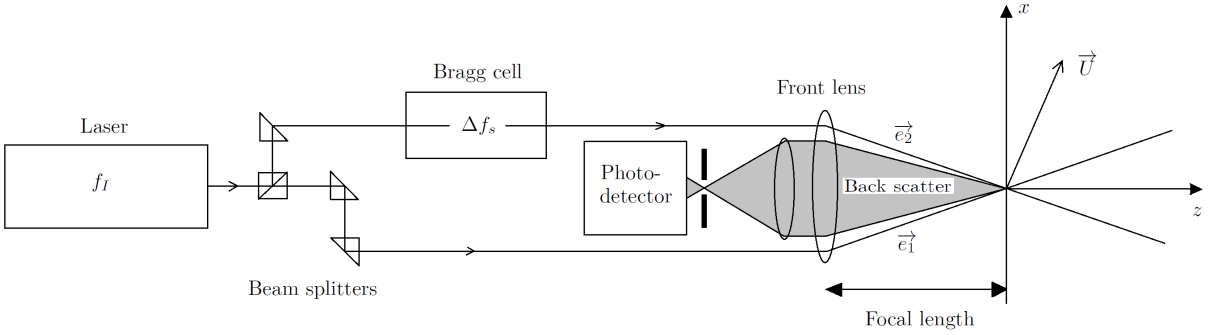


Figure 3.7: Schematic drawing of the LDV system.

Dimension	Blue laser	Green laser	Unit
$d_f$	0.252	0.266	[mm]
$d_x$	0.252	0.266	[mm]
$d_y$	0.252	0.266	[mm]
$d_z$	4.000	4.200	[mm]
$N_f$	$\approx 66$	$\approx 66$	[-]

Table 3.3: Calculated dimensions of the measurement volume.

### 3.3.2 Operating the LDV system

The LDV system and the traverse were controlled by BSA Flow Software. The probe was mounted on the traverse and placed normal to the front Plexiglas cover, which gave it optical access to the internals of the pump. The desired coordinates for the measurement points, i.e.  $(x, y, z)$ , were generated in Matlab and imported to BSA Flow Software as a text file. The measurement grid of points was divided into regions which made it possible to specify sampling and fine-tuning parameters for different parts of the diffuser channel. When the settings were set for all regions, a measurement campaign could be conducted. The traverse automatically positioned itself in the given grid points while BSA Flow Software acquired velocity data at each point with the predetermined settings for the region. The velocity data acquired were processed in real-time and displayed as a histogram for each point. Also real-time data rate, validation level, sample time and the number of samples acquired at the current point were displayed. Another useful tool was the system monitor in BSA Flow Software where the Doppler bursts for each of the beam pairs were plotted. This information was very useful when fine-tuning the LDV system. Important parameters for the fine-tuning and the sampling are listed below:

- Maximum samples [-]: If the predefined maximum acquisition time is not reached, the LDV system acquires this number of samples at each point before moving to the next point.
- Maximum acquisition time [s]: If the predefined maximum number of samples is not acquired, the LDV system acquires for this amount of time at each point before moving to the next point.
- Center frequency [m/s]: The expected average velocity of the flow.
- Bandwidth [m/s]: The expected velocity variation of the flow.
- Record length [-]: The record length of the Doppler-burst.
- High voltage level [V]: The high voltage level of the photodetector.
- Signal gain [dB]: The gain of the photodetector signal amplifier.
- Burst detector SNR level [dB]: Sets the signal-to-noise ratio threshold level of the burst detector. High values reject bursts with too much noise, giving a lower data rate and higher validation rate, and vice versa.

### Fine-tuning

The fine-tuning of the LDV system appeared to be very important. After fine-tuning the system for the first time, the data rate became 10 times higher, which enabled us to acquire 10 times larger sample sizes in each measurement point. The fine-tuning is dependent on the condition of the flow that the LDV system is measuring. Low velocities are usually harder to measure than high velocities since less information is received by the photodetector, i.e. fewer seeding particles passing through the measurement volume per time unit, this requires the LDV system to be more sensitive.

The first step is to set the center frequency, i.e. the expected average velocity of the flow, and then set the expected velocity fluctuation range. It is better to set the range to be too wide, than too narrow. The following procedure should be performed while looking at the system monitor on the LDV computer. As mentioned earlier, a trade-off between the data rate and the validation level has to be made, since these balance each other. If reliable and accurate data are desired, the validation rate should be above 80% for all points, which will make the data rate low compared to the maximum achievable data rate. The advantage of having a high validation level is that the data have less noise, which was desired in this experiment. This can be achieved by making the LDV system less sensitive. What seemed to be a good approach was to start with the default settings and decreasing the record length until the validation level became unstable, then either decreasing the high level voltage, decreasing the signal gain or increasing the burst SNR level so that it became stable again. The objective is to maximize the data rate while having the desired validation level. If the flow condition in the measurement domain varies considerably, the measurement domain should be divided into regions and then fine-tuned individually.

### 3.3.3 Seeding particles

The seeding chosen for the test rig was Polyamid Seeding Particles (PSP) from Dantec Dynamics with a diameter of  $5\ \mu\text{m}$ . The particles have a density of  $1030\ \text{kg}/\text{m}^3$ , which make them neutrally buoyant in water flows. The amount of particles in the water was in the order of one or two small spoons of particles in 12,000 liters of water.

## 3.4 Preparation

### 3.4.1 Health, safety and environment

Health, safety and environment (HSE) assessments were conducted for the single-stage centrifugal pump test rig and the LDV system. The assessments can be found in appendix C. Operators of the LDV system had to wear protective glasses which filtered out the laser light. When using the LDV system, it was important to cover the probe so that high power light could not damage anyone in the vicinity of the test rig. Warning signs and light on the test rig and the doors leading in to the laboratory were used.

### 3.4.2 Coordinate system

A Cartesian coordinate system, i.e.  $(x, y, z)$ , was chosen for the test rig. The  $(x, y)$ -origin was chosen to be a randomly marked point on the outer steel ring of the front side of the pump. The mark was a well-defined permanent point, i.e. approximately  $0.1\ \text{mm}$  in diameter. The  $z$ -coordinate of the origin was chosen to be  $7\ \text{mm}$  from the inner Plexiglas surface, meaning that it was located approximately  $11\ \text{mm}$  from the inner surface of the diffuser channel. The measurement domain is displayed in figure 3.8. The origin is located inside the red circle on the left side of the figure.

### 3.4.3 Measurement points

The chosen measurement points were based on the diffuser walls. The coordinates for the walls were found by using the LDV system and the traverse. The LDV measurement volume is a well-defined point. By pointing the measurement volume along the wall edges, the  $(x, y)$ -coordinates for the walls were noted. A Matlab routine was made in order to generate a grid with a desired density of points. By specifying the constant spacing between the points in the  $x$ - and  $y$ -direction, the grid was automatically generated in the most efficient order and was ready to be exported directly to BSA Flow Software. All points were measured in the  $z = 0$  plane. The reason for choosing this plane and not the middle plane was to maximize the backscatter of the laser, hence increasing the data rate. The velocity profile in the  $z$ -direction was initially thought to have thin boundary layers and to be relatively



Figure 3.8: The diffuser domain. The origin is inside the red circle.

flat, so that an offset of a couple of millimeters would not differ from the middle plane. This is further discussed later on.

#### 3.4.4 Alignment of the traverse table

The alignment of the probe in respect to the pump front cover is important. The measured velocities in the  $x$ - and  $y$ -directions, i.e.  $u$  and  $v$  respectively, were desired to be parallel to the Plexiglas cover and inner surface of the diffuser channel. This was assured by checking that the probe was attached perpendicularly to the  $x$ - and  $y$ -axis of the traverse. The  $x$ - and  $y$ -axis of the traverse was then aligned with the Plexiglas. This was done by attaching a fine distance measuring tool beside the probe on the traverse and measuring the change in distance as it moved along the  $x$ - and  $y$ -axis. By adjusting the orientation of the traverse iteratively until the change in distance was zero, after moving the traverse along the axes, the traverse table was assured to be aligned. Also the rotational orientation of the probe was adjusted so that the probe measured  $u$  and  $v$  parallel to their respective axes on the traverse. This was assured by pointing the laser pairs at a wall far away and moving the probe along the  $x$ - and  $y$ -axis, and making sure that one of the laser points in a laser pair overlapped with the previous position of the other laser point as the probe moved along its axis.

#### 3.4.5 Number of samples

The objective of the measurements on the test rig was to obtain the steady velocity field in the diffuser channel. A test to check the steadiness of the flow was conducted close to the inlet of the diffuser. This region was expected to have the most unsteady velocity distribution in the channel, meaning that this region needed a larger number

of samples in order to obtain the steady velocity. The result of the test is shown in figure 3.9. The velocities stabilize for sample sizes above 10,000. The  $v$  velocity seems to slightly decay as the sample size increases. This might be due to unstable operating conditions of the pump.

In order to acquire 10,000 or more samples in the downstream part of the diffuser ( $x = [20 \text{ mm}, 60 \text{ mm}]$ ), 30 seconds of sampling time in each point was required, while it was set to be 10 seconds for the rest. The downstream part needed a higher sampling time because the data rate was lower.

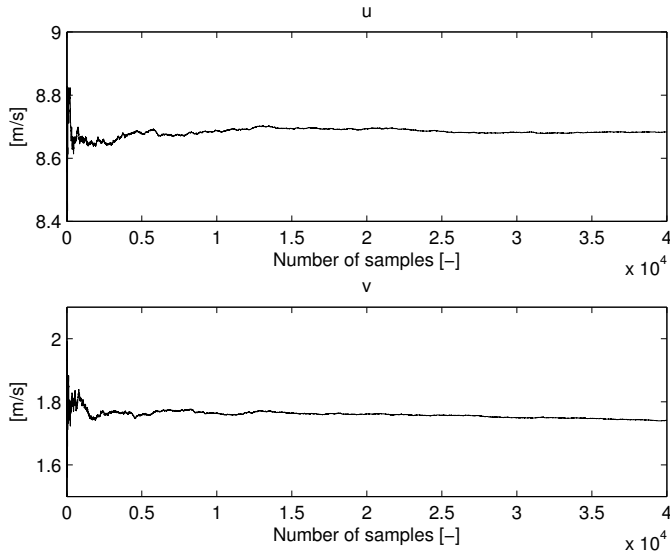


Figure 3.9: Steadiness of  $u$  and  $v$  at  $(x, y) = (140 \text{ mm}, 49.2 \text{ mm})$ .

### 3.5 Procedures

To start a measurement campaign, seeding particles had to be added to the water. This was done by installing a valve on the inlet pipe with a tube on it. The seeding particles were mixed and stirred with water in a small bucket until the mixture was homogeneous. The mixture was then injected to the flow through the valve. This ensured that the seeding particles were immediately exposed to a turbulent flow, rapidly mixing it with the water.

The measurement grid was imported into BSA Flow Software and split into seven regions. The fine-tuning of the LDV system and sample specifications were defined in each region since the flow characteristics change throughout the diffuser channel.



This was done by adjusting the previously mentioned parameters so that the data rate and validation level were optimized.

The traverse table with the probe was adjusted to its origin. This was simply done by first pointing the measurement volume at the  $(x, y)$ -origin mark, thereafter pointing the measurement volume at the inner Plexiglas surface and moving it  $7\text{ mm}$  in the positive  $z$ -direction, lastly moving it back to the  $(x, y)$ -origin mark without changing the  $z$ -coordinate and zeroing it.

The test rig was set to the operating conditions by turning the pump on and setting the right rotational speed with the knob located on the control panel, and thereafter adjusting the inlet and outlet valve iteratively so that the correct flow rate was achieved. This was continuously logged and monitored with a Labview program. Since the flow meter was installed downstream and close to the inlet valve, the flow rate signal was fluctuating a lot, making it hard to set the correct flow rate.

The measurement campaign was initiated in BSA Flow Software. The LDV signals were monitored on the computer in real-time.

### 3.5.1 Measurement campaigns

The measurement campaigns conducted are listed in table 3.4. Measurement campaigns M1 to M6 were conducted for the the whole diffuser domain. M7 and M8 were conducted on a confined domain in order to possibly detect a back flow along the bottom diffuser wall. The confined domain was centered where flow separation was expected to appear.  $\Delta x$  and  $\Delta y$  are distances between the measurement points in the  $x$ - and  $y$ -direction respectively. The number of points for the measurements with equal  $x$ - and  $y$ -spacing, e.g M1 and M2, varies because the LDV system only acquires velocity data that are validated by BSA Flow Software. The validation level varies according to the flow conditions in the measurement point and the LDV parameters set in the region. M5 and M6 were omitted from the results because of poor data, the reason for this is unknown.

Measurement	Flow rate	Number of points	$\Delta x$ [mm]	$\Delta y$ [mm]	Date
M1	$Q_{BEP}$	676	5	1	24.02.2015
M2	$Q_{BEP}$	673	5	1	27.02.2015
M3	$Q_{BEP}$	890	2	2	17.03.2015
M4	$Q_{BEP}$	893	2	2	19.03.2015
M5*	$Q_{BEP}$	922	2	2	14.04.2015
M6*	$Q_{BEP}$	879	2	2	15.04.2015
M7	$1.5Q_{BEP}$	350	2	2	16.04.2015
M8	$0.75Q_{BEP}$	357	2	2	16.04.2015

Table 3.4: The measurement campaigns (\* means that the measurement is omitted).

# Chapter 4

## Data Analysis

### 4.1 BSA Flow Software Raw Data

The velocity data received from BSA Flow Software were processed using Matlab.

Each measurement campaign is stored in a folder by BSA Flow Software. The folder contains a number of raw files which correspond to the number of grid points for the total measurement campaign, e.g. M1 has 676 files. Each of these files contain all the velocity samples acquired in a point, which for some points were as many as 20,000. The header of the text file has information about the traversing coordinates for the measured point, acquisition date and time and the directory of the LDV project on the LDV computer. The raw data are organized in five columns as shown in table 4.1.

Row#	AT [ms]	TT [ $\mu$ s]	LDA1 [m/s]	LDA2 [m/s]
------	---------	---------------	------------	------------

Table 4.1: The columns in the BSA Flow Software raw file.

AT is the arrival time in milliseconds, which represents the elapsed time between the start of the sample acquisition in a point and the moment when acquiring the  $n$ 'th sample. The samples were captured randomly in time. TT is the transit time in microseconds, which represents the acquisition time of the velocity sample. LDA1 and LDA2 are the velocities  $u$  and  $v$  in meter per second in the  $x$ - and  $y$ -direction, respectively. The transit time of each velocity sample is in the order of  $10 \mu$ s, which is so small that it approximately gives the instant velocity in the point.

## 4.2 Statistical Analysis

The true statistical mean of the velocity in the flow domain  $(x, y, t)$  is defined as the ensemble-average of infinite samples:

$$\langle u(x, y, t) \rangle = \lim_{N \rightarrow \infty} \frac{1}{N} \sum_{n=1}^N u_n(x, y, t) \quad (4.1)$$

Where  $n = 1, 2, \dots, N$ ,  $N$  is the number of samples and all the samples are acquired from independent events.  $\langle u(x, y, t) \rangle$  corresponds to the steady velocity distribution and  $u_n(x, y, t)$  corresponds to the  $n$ 'th unsteady velocity distribution. The statistical characteristics of the velocity mean are considered to be stationary, i.e. they are independent of time,  $\langle u(x, y, t) \rangle = \langle u(x, y) \rangle$ . Likewise, the statistical characteristics of the time-averaged velocity over the time period  $T$ ,

$$\overline{u_n(x, y)} = \lim_{T \rightarrow \infty} \frac{1}{T} \int_0^T u_n(x, y, t) dt, \quad (4.2)$$

can be considered to be independent of the samples  $n$ , i.e.  $\overline{u_n(x, y)} = \overline{u(x, y)}$ . This implies that the time-averaged velocity and ensemble-averaged velocity both provide the true statistical mean velocity, thus meaning that both are independent of time and sample.

$$U(x, y) = \langle u(x, y, t) \rangle = \overline{u_n(x, y)} \quad (4.3)$$

By the Reynolds decomposition technique the unsteady velocity can be presented as the sum of the mean velocity  $U(x, y)$  and the random fluctuating velocity  $u'_n(x, y, t)$ .

$$u_n(x, y, t) = U(x, y) + u'_n(x, y, t) \quad (4.4)$$

This illustrates that the unsteady velocity is a random variable fluctuating about the mean velocity. By substituting equation 4.4 into the ensemble-averaged and the time-averaged velocity equation, i.e. 4.1 and 4.2 respectively, they yield:

$$\langle u'_n(x, y, t) \rangle = \overline{u'_n(x, y, t)} = 0 \quad (4.5)$$

This shows that the statistical properties of the random velocity fluctuations can not be quantified by averaging; instead the standard deviation, also known as the

root-mean-square (RMS), can be used. The standard deviation  $\sigma$  is defined as the square root of the variance of the random variable:

$$u'_{RMS}(x, y, t) = \sigma_{u'}(x, y, t) = \sqrt{\text{var}[u'_n(x, y, t)]} = \sqrt{\langle (u'_n(x, y, t))^2 \rangle} \quad (4.6)$$

The RMS of the velocity fluctuations can also be considered to be statistically stationary, i.e.  $u'_{RMS}(x, y, t) = u'_{RMS}(x, y)$ .

### 4.3 Post-processing the Raw Data

The procedures described below can be applied for the measured velocities in the  $x$ ,  $y$  and  $z$  directions, i.e.  $u$ ,  $v$  and  $w$  respectively<sup>1</sup>. The streamwise velocity vector is defined as:

$$\vec{U} = [u, v, w] \quad (4.7)$$

#### 4.3.1 Steady velocity distribution

The steady velocity distribution of the diffuser channel was calculated by ensemble-averaging the unsteady velocity samples,  $u_n(x, y, t)$ , acquired in each point. Equation 4.1 requires an infinite number of samples to obtain the true statistical mean, which is impossible in a physical experiment. Instead an estimate is calculated from:

$$U(x, y) = \frac{1}{N} \sum_{n=1}^N u_n(x, y, t), \quad (4.8)$$

The choice of  $N$  in each point was a trade-off between laboratory time and acceptable statistical error. A test of the steadiness of the flow based on sample size  $N$  is presented in section 3.4.5. By doing the same in the  $x$ -,  $y$ - and  $z$ -direction the streamwise mean velocity vector is found. Since  $w$  was not measured, the mean velocity vector in the  $(x, y)$ -plane is considered. The mean velocity magnitude is calculated by:

$$\left| \vec{U}(x, y) \right| = \sqrt{U(x, y)^2 + V(x, y)^2} \quad (4.9)$$

---

<sup>1</sup>The velocity in the  $z$ -direction  $w$  was not measured

### 4.3.2 Turbulence

In turbo machinery the random fluctuating velocity  $u'_n(x, y, t)$  is composed by a random part and a periodic part, i.e.  $u'_{n,random}(x, y, t)$  and  $u'_{n,periodic}(x, y, t)$  respectively. The periodic part can be an accumulation of several periodic sources, such as vibration or pressure pulsations caused by the passing of the rotor blades or an off-centered shaft, while the random part is the turbulence in the flow. The velocity fluctuations calculated from the LDV velocity data, correspond to the sum of random and periodic velocity fluctuations,  $u'_n(x, y, t)$ . If the turbulence of the flow is wanted, a complete understanding of the periodic part of the fluctuating velocity is needed so that the random part can be unveiled.

$$u'_n(x, y, t) = u'_{n,random}(x, y, t) + u'_{n,periodic}(x, y, t) \quad (4.10)$$

However, the periodic velocity fluctuations were not mapped in this experiment, which prevented us from describing the true turbulence in the flow. Moreover, only  $u$  and  $v$  were measured by the LDV system which restricts us to two-dimensional turbulence.

The turbulence can be quantified in several ways. Turbulent kinetic energy  $k$  and turbulence intensity  $I$  are two quantities that are commonly used. The kinetic energy in a flow is the mean kinetic energy per unit mass associated to the eddies in a turbulent flow. It is calculated from the RMS of the random velocity fluctuations in all directions:

$$k(x, y) = \frac{1}{2} (u'_{RMS,random}(x, y)^2 + v'_{RMS,random}(x, y)^2 + w'_{RMS,random}(x, y)^2) \quad (4.11)$$

The turbulence intensity  $I$  is the ratio between the RMS of the random total velocity fluctuation and the magnitude of the mean velocity:

$$I = \frac{U'_{RMS,random}(x, y)}{|\vec{U}(x, y)|} \quad (4.12)$$

The RMS of the total velocity fluctuation is defined as:

$$U'_{RMS}(x, y) = \sqrt{\frac{1}{3} (u'_{RMS}(x, y)^2 + v'_{RMS}(x, y)^2 + w'_{RMS}(x, y)^2)} \quad (4.13)$$

Since  $w'_{RMS}$  and  $U'_{RMS,periodic}$  are not known, the velocity fluctuations in the flow are presented as the approximate RMS of the total velocity fluctuation:

$$U'_{RMS}(x, y) \approx \sqrt{\frac{1}{2} (u'_{RMS}(x, y)^2 + v'_{RMS}(x, y)^2)} \quad (4.14)$$

## 4.4 Evaluation of the Raw Data

### 4.4.1 Skewness

There are four parameters which are calculated from the raw data, i.e. the velocity means  $U$  and  $V$ , and the RMS velocity fluctuations  $u'_{RMS}$  and  $v'_{RMS}$ . The unsteady velocity data acquired in each point were theoretically expected to be normally distributed around the velocity mean  $U$  with a standard deviation of  $u'_{RMS}$ . The normal distribution curve appears because of the random nature of the turbulence. This could be approximated by having a sufficiently large sample size in each point. Since some periodic fluctuations were expected in the flow, some measurement points showed a biased normal distribution, also known as skew normal distribution, see figure 4.1. The skewed distribution shows the sample distribution for the  $u$ -velocity in a measured point during M4 with a total of 12,736 samples. The histogram seems to have periodic velocity fluctuations that are concentrated below the mean.

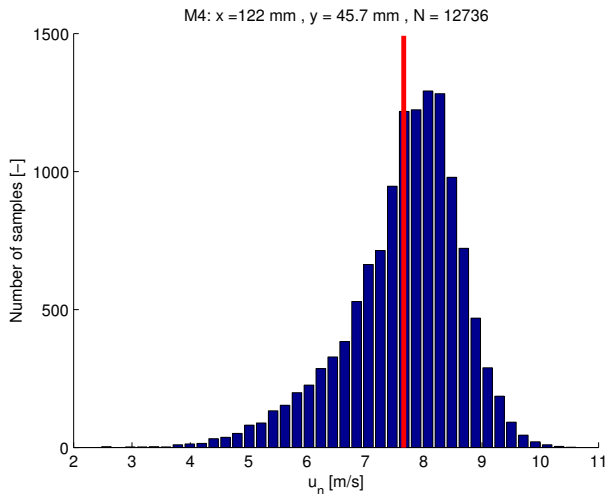


Figure 4.1: Histogram of the velocities in the point  $(x, y) = (122 \text{ mm}, 45.7 \text{ mm})$ , which is approximately skew normally distributed. The red line represents the velocity mean.

#### 4.4.2 Filtering the data

The LDV system produces noise in addition to the true velocity data. After studying the histograms, two types of noise were identified: Tail-noise and zero-noise. Causes for the noise will be discussed later on. Tail-noise is characterized as velocity measurements that are acquired beyond the expected edge of the approximate normal distribution. These velocity readings are also known as outliers. Zero-noise is characterized as noise velocity measurements that gather around zero velocity. If the mean velocity is far from zero, it results in two peaks. For both cases, the noise causes the calculated velocity mean to differ from the true mean velocity of the flow. Furthermore, the RMS velocity fluctuation of the flow has a larger value than expected because of the outliers.

By examining the histograms for a measurement campaign and identifying the points with noise, certain trends were noted. The points with tail-noise and zero-noise had an unexpectedly high RMS velocity fluctuation compared to the noiseless points. A filter based on experience made sure to identify all points with a RMS velocity fluctuation higher than  $1.5\text{ m/s}$ . Also points with less than 4000 samples and more than 20,000 samples were identified. The points with a too low number of samples were usually data which were not acceptably close of being normally distributed histograms. The points with a too high number of samples were usually data containing pure noise. The identified points were neglected. The neglected points for M3, M4, M5 and M6 are displayed in figure 4.2. The green points have a RMS velocity fluctuation higher than  $1.5\text{ m/s}$ , the red points have a sample size that is outside the interval 4000 to 20,000 and the black points fulfill both criteria. The measurement campaigns M1 and M2 were not filtered at all because of a relatively low sample size in each point, making M1 and M2 less reliable than M3, M4, M5 and M6, this is discussed later. The reason for omitting M5 and M6 from the results was because the applied filter resulted in approximately one third of the data being neglected, meaning that the data contained a lot of noise.



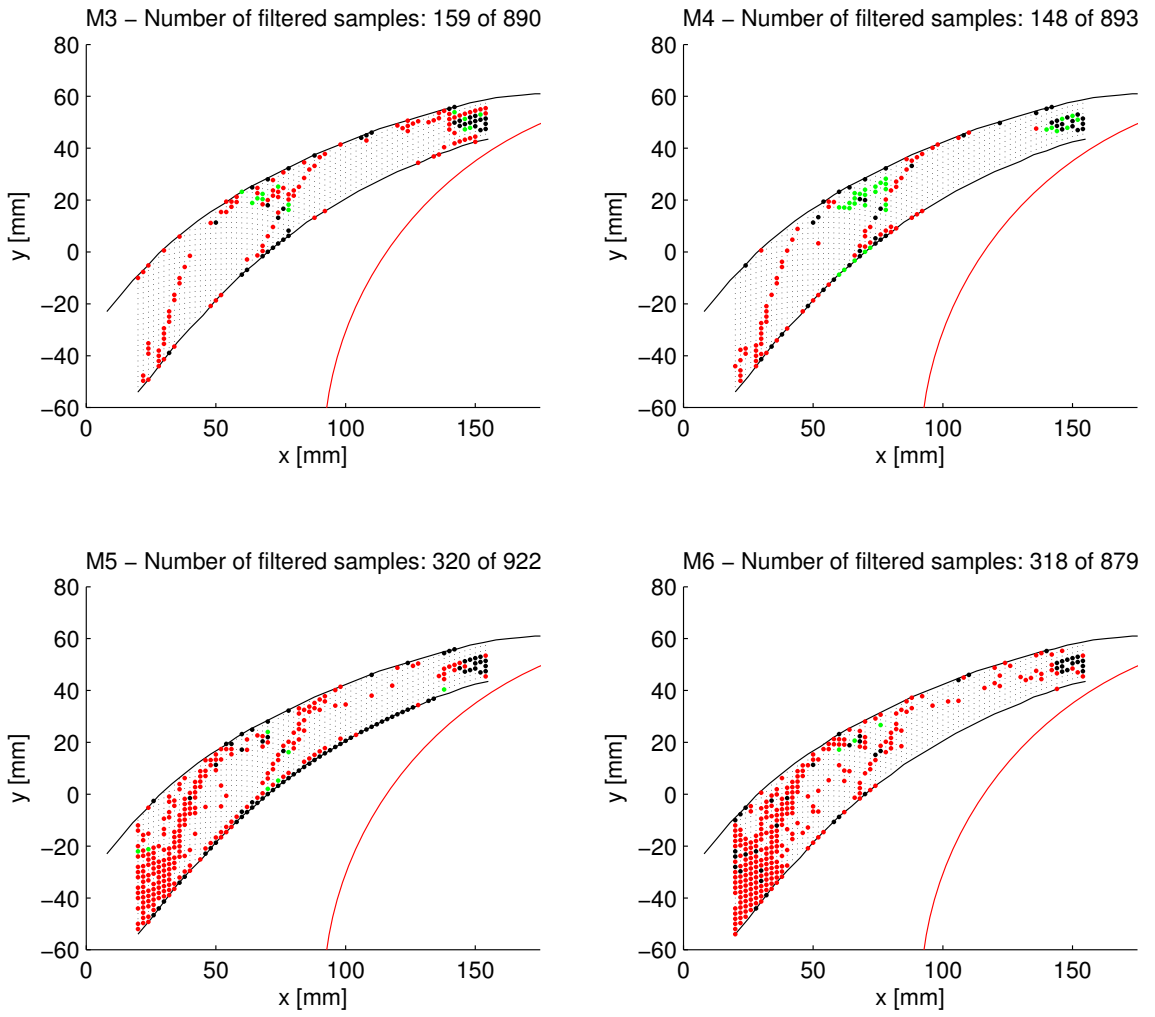


Figure 4.2: The neglected points.

## 4.5 Plotting Routines

### 4.5.1 Velocity vector plot

The post-processed data are represented in several types of plots, such as vector plot, three-dimensional (3d) plot, contour plot and widthwise cross-sectional plot. The velocity vector plot displays the velocity vectors with the mean velocity magnitude and the flow angle  $\psi$  with respect to the  $x$ -axis.  $\psi$  in degrees is defined as:

$$\psi = \arctan \left( \frac{V(x, y)}{U(x, y)} \right) \quad (4.15)$$

### 4.5.2 Three-dimensional plot

The 3d plot is basically a filled contour plot with a small interval between the contours and where the contour lines are removed. The measured data points are non-uniformly distributed in the  $(x, y)$ -plane because of having a non-uniform grid and neglected data points. In order to obtain a complete plot of the diffuser channel, a surface defined on a dense uniform grid in the  $(x, y)$ -plane is interpolated cubically to fit the measured data values. An essential part of the Matlab script for the 3d plot is displayed below. The calculated mean velocities are stored in the vector `magnitude` with the corresponding  $(x, y)$ -coordinates in the vectors `x` and `y`. The function `linspace` creates the vectors `xlin` and `ylin` consisting of `gridsize` number of elements, which are uniformly distributed and span from the minimum to the maximum of the  $x$ - and  $y$ -positions in the measurement domain. Based on these vectors the matrices `X` and `Y` (`gridsize x gridsize`) are computed. They contain the  $x$ - and  $y$ -coordinates for the uniform grid respectively. The function `griddata` interpolates the measured values `magnitude` onto `X` and `Y` and stores it in the matrix `VEL` (`gridsize x gridsize`).

The interpolated surface passes through all the measured points. The value of `gridsize` was set to 1000, giving a 1000 by 1000 elements uniform grid.

```
xlin = linspace(min(x),max(x),gridsize);
ylin = linspace(min(y),max(y),gridsize);
[X,Y] = meshgrid(xlin,ylin);
VEL = griddata(x,y,magnitude,X,Y,'cubic');
contourf(X,Y,VEL,contourlevels);
```

### 4.5.3 Widthwise cross-sectional plot

The widthwise cross-sectional plot uses the interpolated data values from the 3d plot. The cross-sections of the diffuser channel, which give the minimum channel width, are calculated. The data values from the 3d plot, which overlap with the widthwise cross-section lines, are found and stored. The widthwise cross-sectional profile now contains the data values from a point on the bottom wall of the diffuser, to the point on the top wall which gives the smallest distance. The distance measured from the bottom wall is normalized with the total width of the corresponding widthwise cross-section. Figure 4.3 shows the widthwise cross-sectional profiles. This type of plot is used in chapter 7.

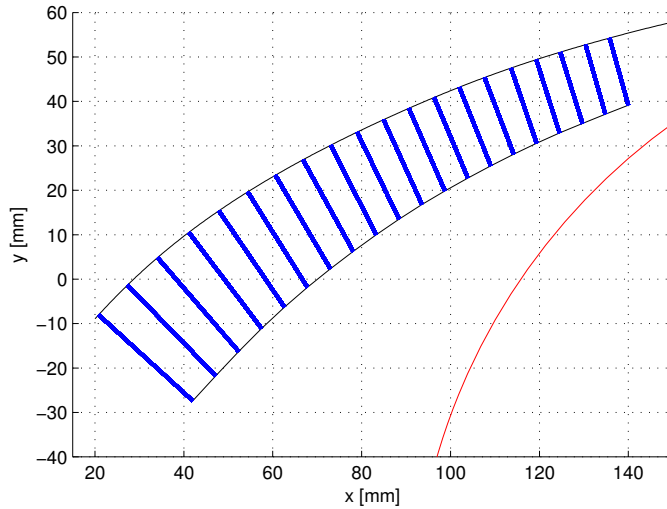


Figure 4.3: The widthwise cross-sectional profiles.



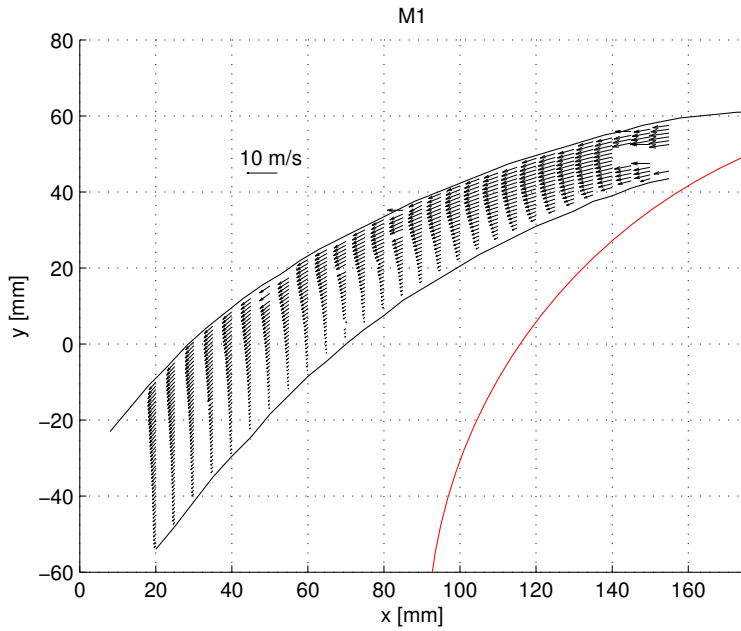
# Chapter 5

## Results

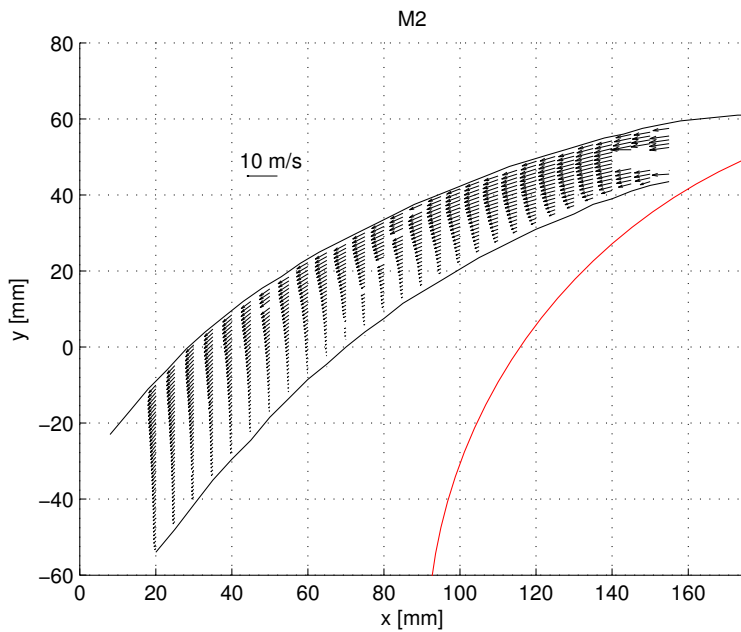
The results from the measurement campaigns listed in table 3.4 are displayed in this chapter. The velocity data acquired from the LDV system was post-processed according to chapter 4. All data are plotted according to the  $(x, y, z)$ -coordinate system explained in section 3.4.2.



## 5.1 Steady Velocity Distribution

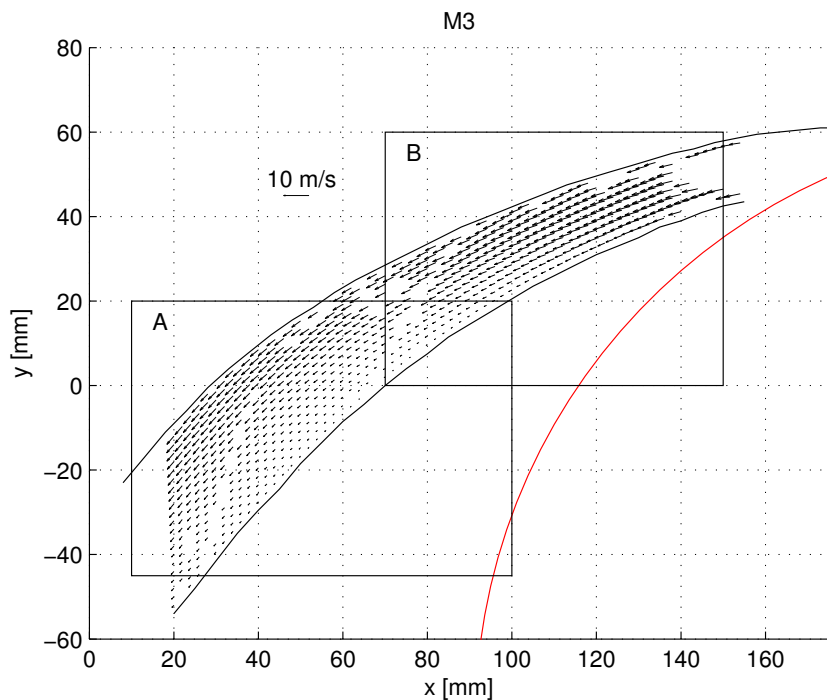


(a) M1

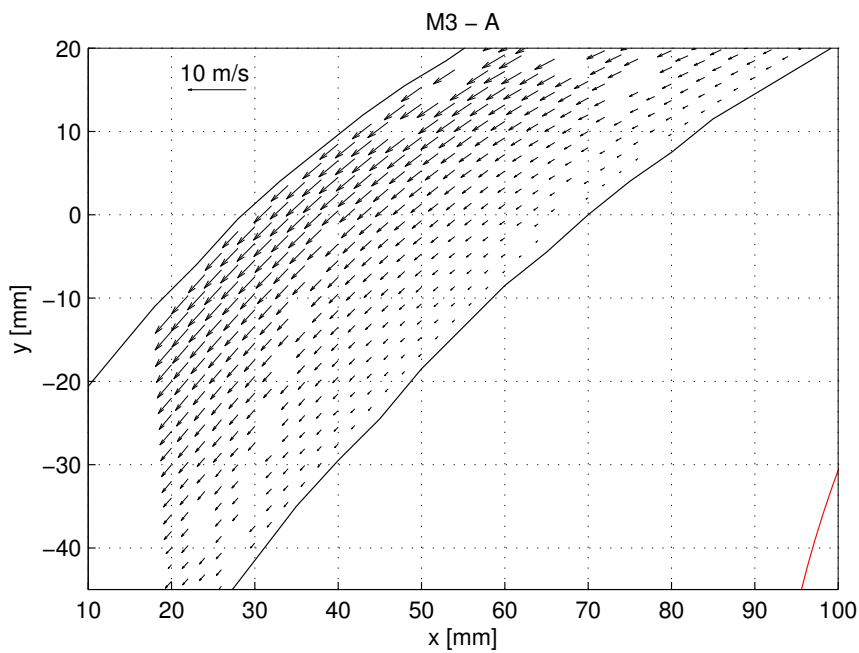


(b) M2

Figure 5.1: Steady velocity vector plots in the diffuser.



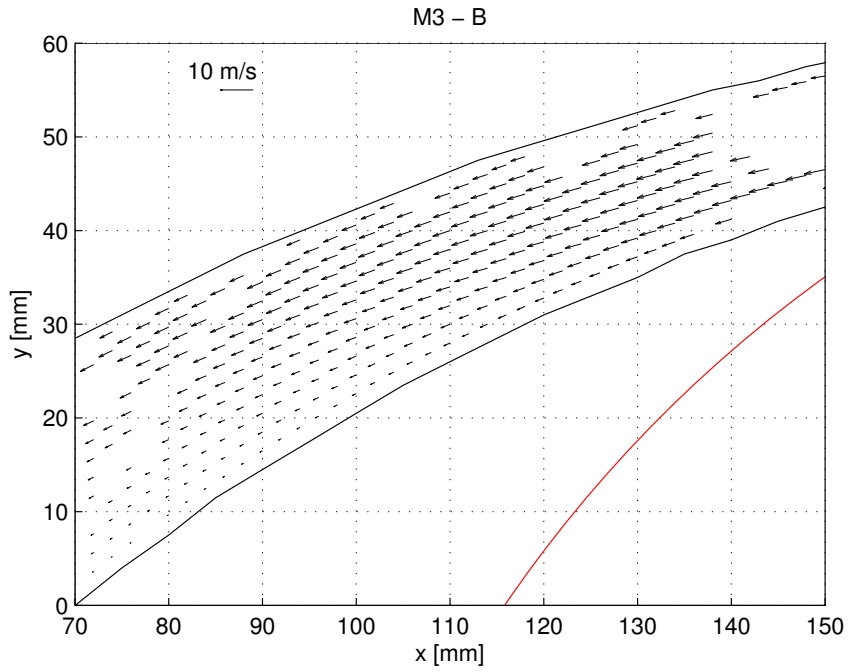
(a) M3



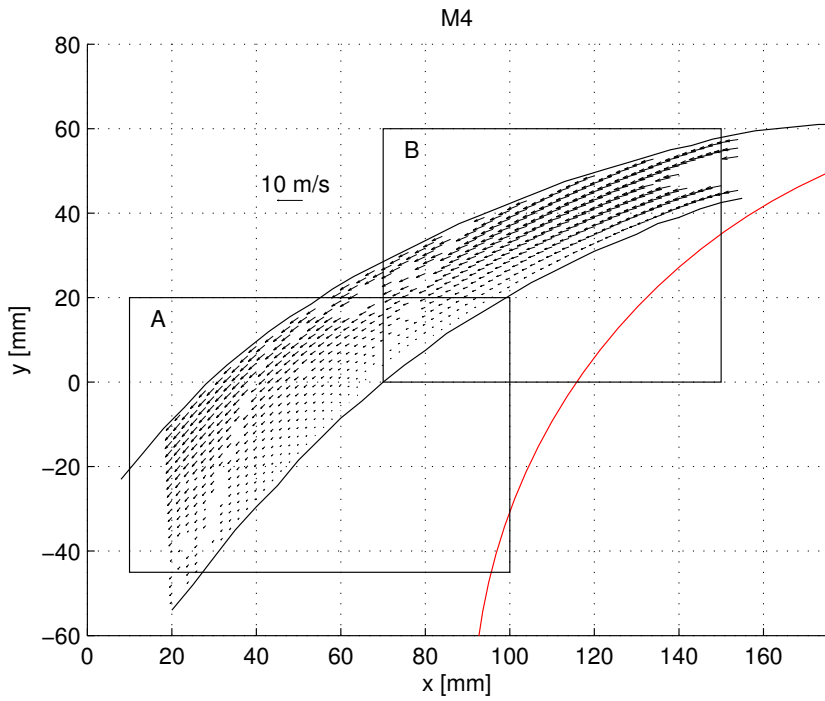
(b) M3 - A

Figure 5.2: Steady velocity vector plots in the diffuser.



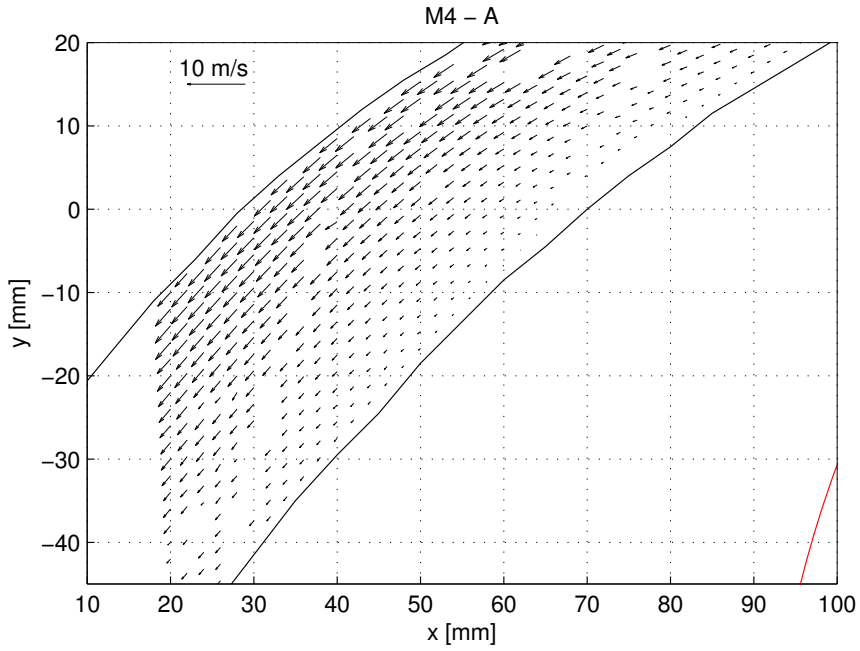


(a) M3 - B

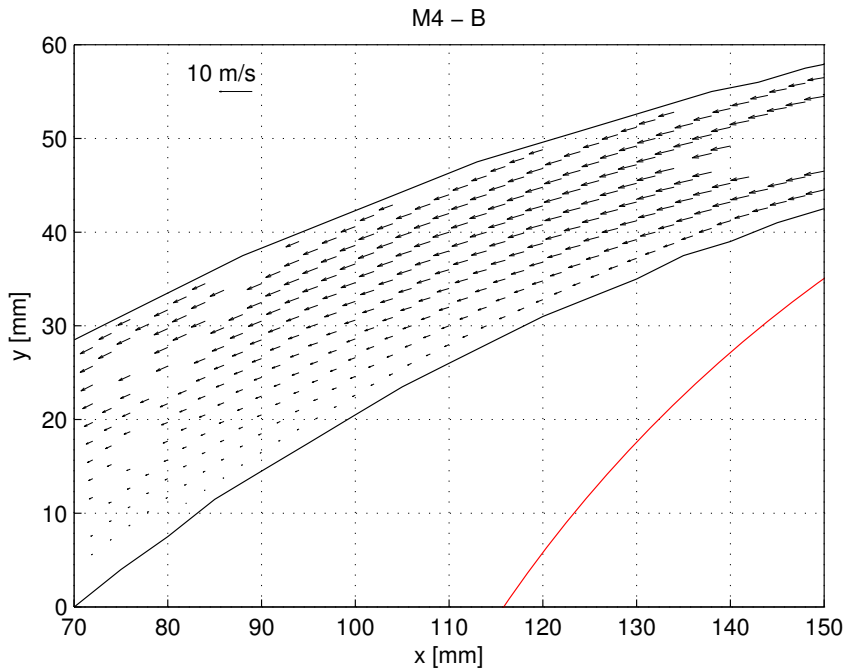


(b) M4

Figure 5.3: Steady velocity vector plots in the diffuser.

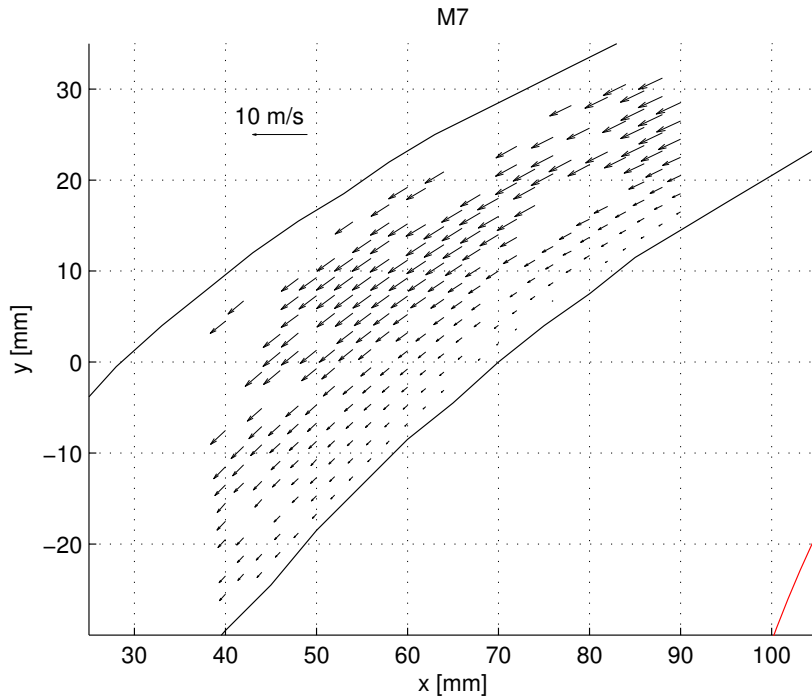


(a) M4 - A

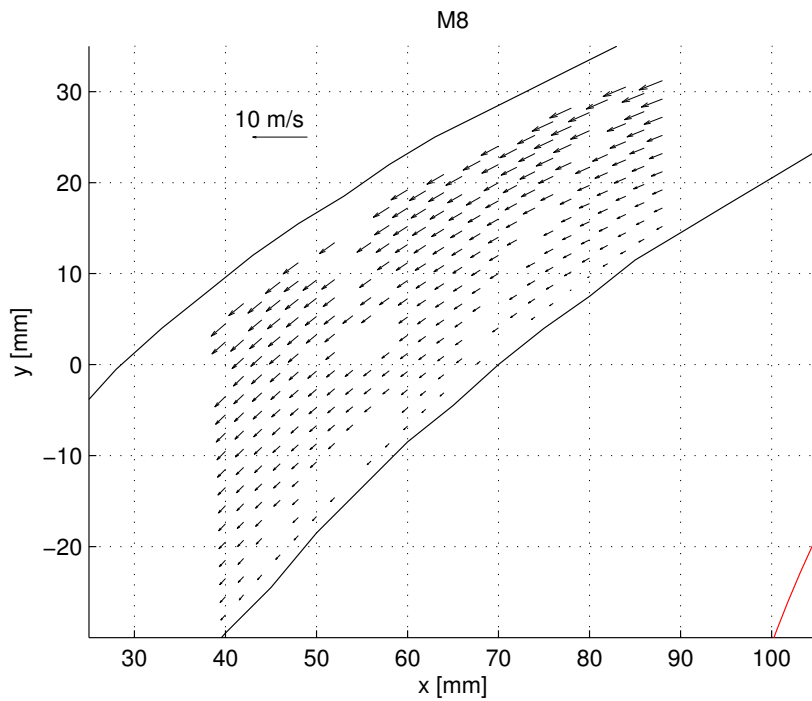


(b) M4 - B

Figure 5.4: Steady velocity vector plots in the diffuser.

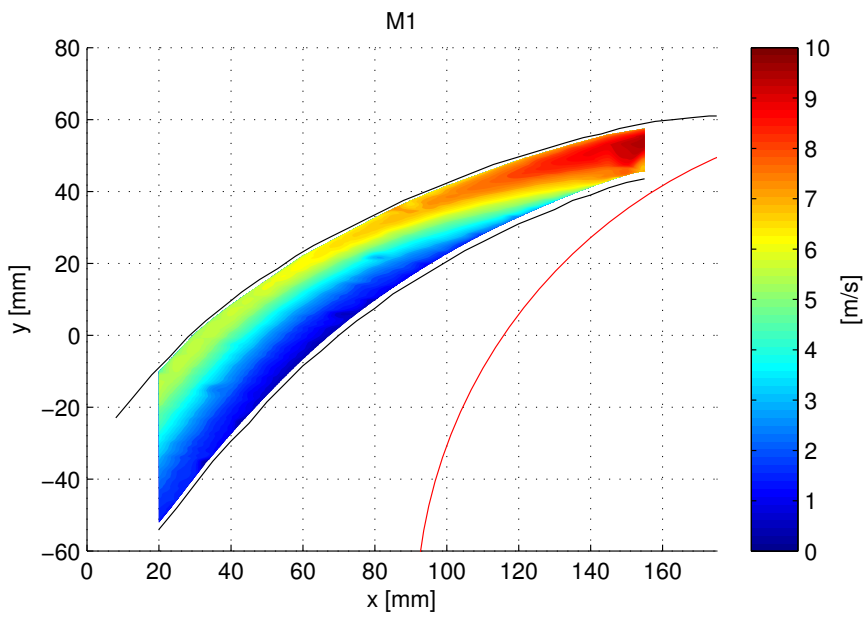


(a) M7

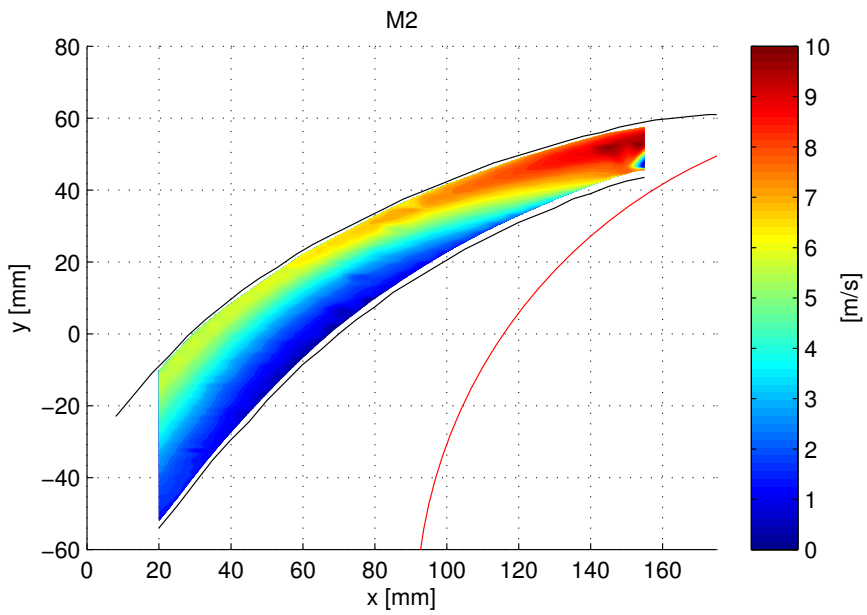


(b) M8

Figure 5.5: Steady velocity vector plots in the diffuser for a)  $1.5Q_{BEP}$  and b)  $0.75Q_{BEP}$ .

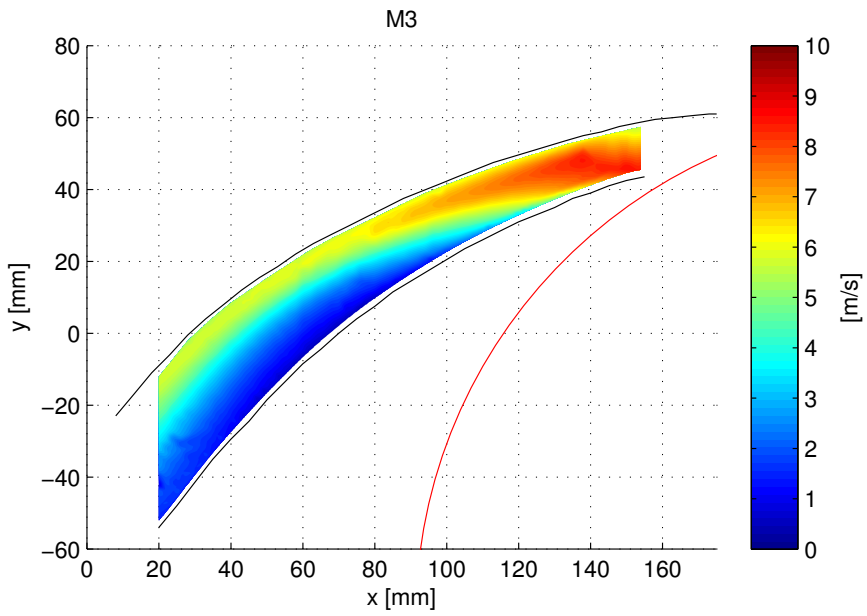


(a) M1

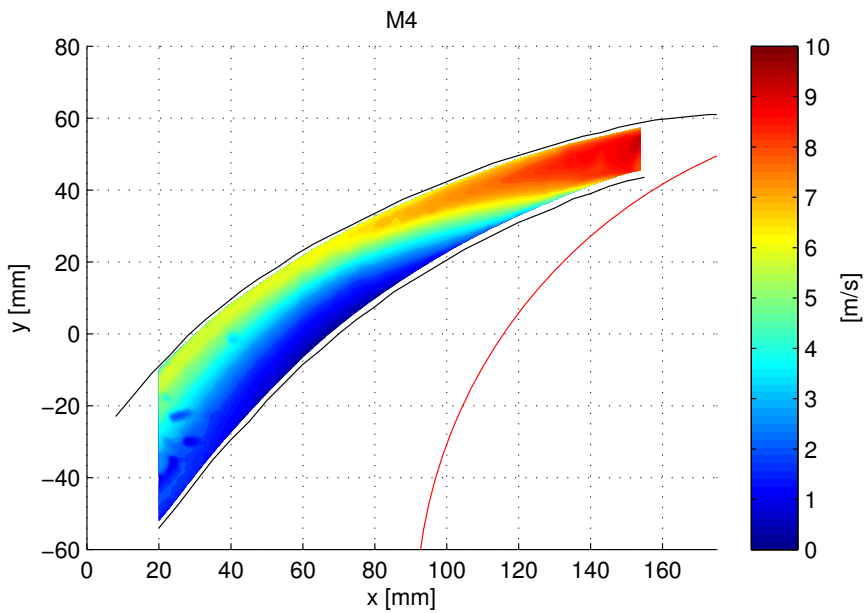


(b) M2

Figure 5.6: 3d plots of the steady velocity magnitude in the diffuser.

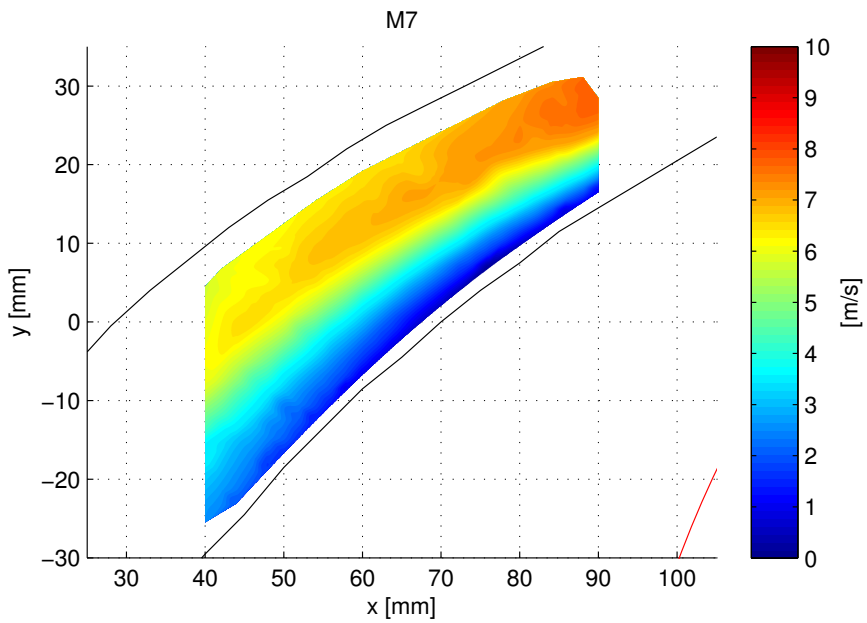


(a) M3

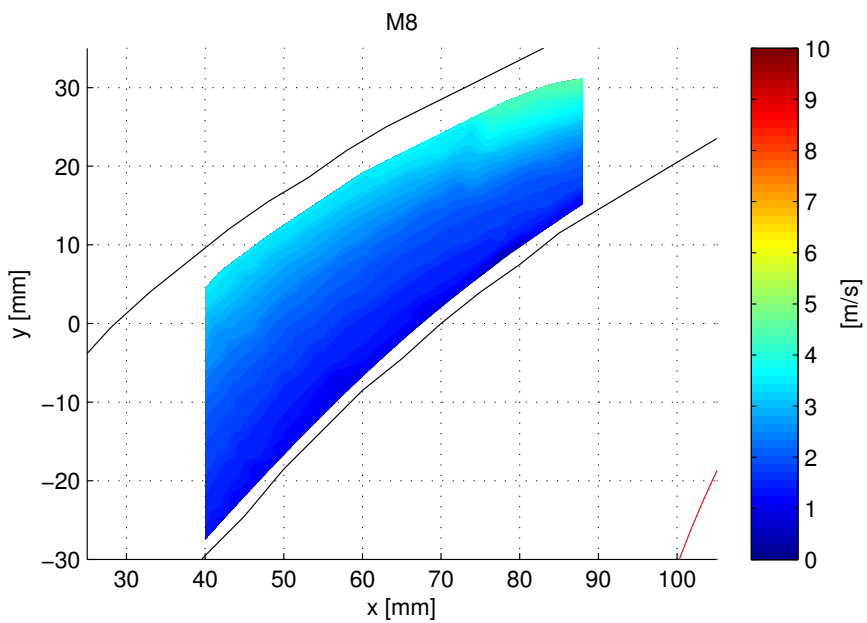


(b) M4

Figure 5.7: 3d plots of the steady velocity magnitude in the diffuser.



(a) M7

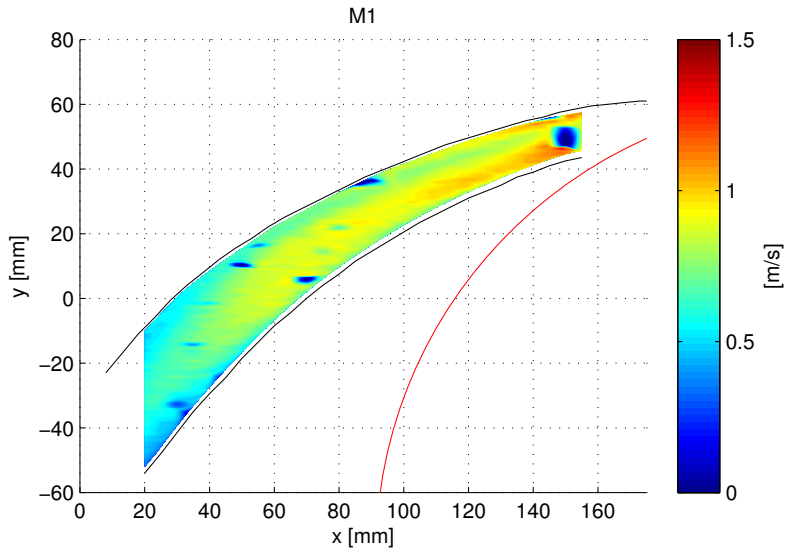


(b) M8

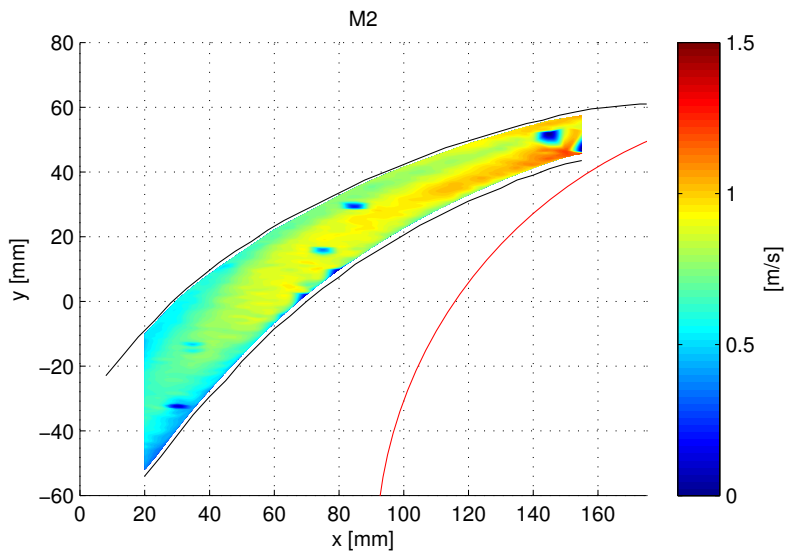
Figure 5.8: 3d plots of the steady velocity magnitude in the diffuser for a)  $1.5Q_{BEP}$  and b)  $0.75Q_{BEP}$ .



## 5.2 RMS of the Total Velocity Fluctuation Distribution



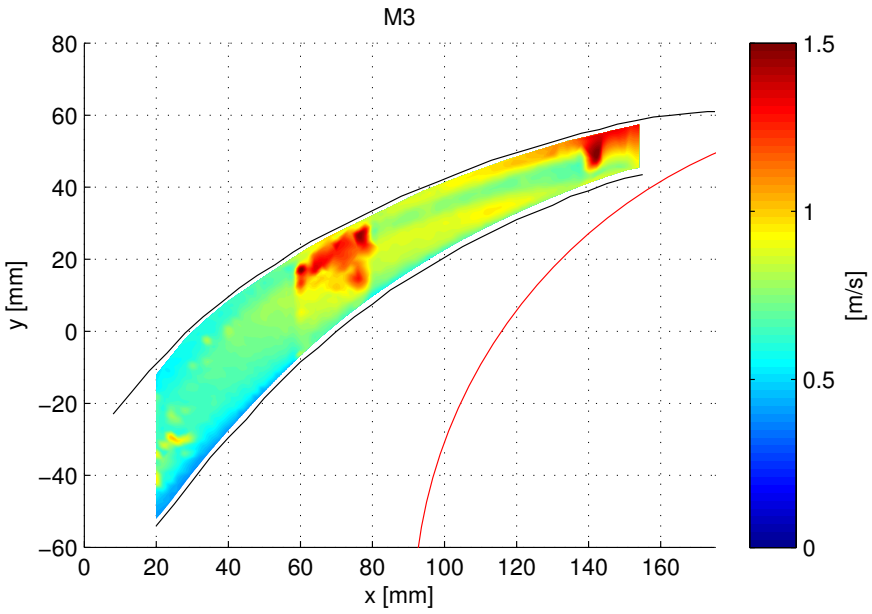
(a) M1



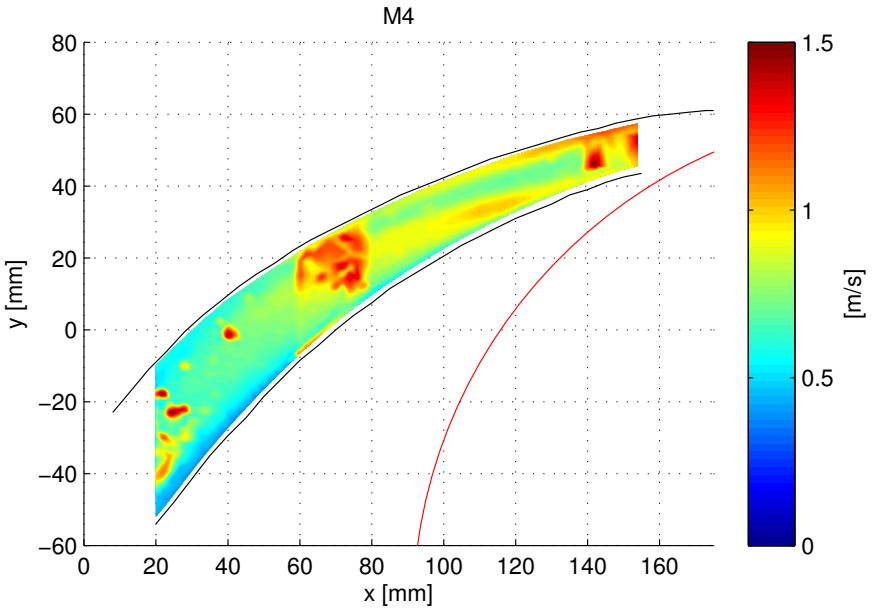
(b) M2

Figure 5.9: 3d plots of the RMS of the total velocity fluctuation in the diffuser.





(a) M3



(b) M4

Figure 5.10: 3d plots of the RMS of the total velocity fluctuation in the diffuser.



# Chapter 6

## Evaluation of the Experiment

### 6.1 The Test Rig

The purpose of the test rig is to compare the internal velocity conditions with a CFD simulation of the Typhoon pump, thus the desired operating conditions of the pump need to be correct and stable.

#### 6.1.1 Water temperature change

The reason for the water temperature increase is because of viscous dissipation of energy from the turbulent flow. Eddies in the Kolmogorov length scale range are known to dissipate the kinetic energy as heat. The water is consequently heated, and this happens wherever the flow is turbulent. For the test rig, the highest rate of viscous dissipation of kinetic energy happens particularly where the flow is most turbulent, e.g. in the flow after the valves, inside the pump casing or in pipe bends.

The effect of the temperature increase on the velocity in the diffuser channel was investigated. A velocity profile at  $x = 130 \text{ mm}$  was acquired for five different water temperatures, see figure 6.1. The graph indicates that the velocity profile in the diffuser channel changes as the water temperature varies. From the graph it can be observed that the velocity is higher for colder water in the upper part of the diffuser cross-section. In the lower part the opposite occurs, but with a lower scattering. This cross-section is very close to the diffuser inlet, which might give the largest effect of temperature change. The effect is thought to diffuse as the flow moves further downstream, since other forces, such as centrifugal forces, become dominant.

In section 3.2.4 the temperature rise rate was found to be about  $2.28 \text{ }^\circ\text{C}/\text{h}$  as the pump was running. The increase in water temperature decreases the viscosity of the water, meaning that friction losses, due to viscous shear stress in the impeller and in the pipes, decrease. Since the impeller has a constant rotational speed, the pump consumes less power since the torque decreases. The total head and flow rate of the

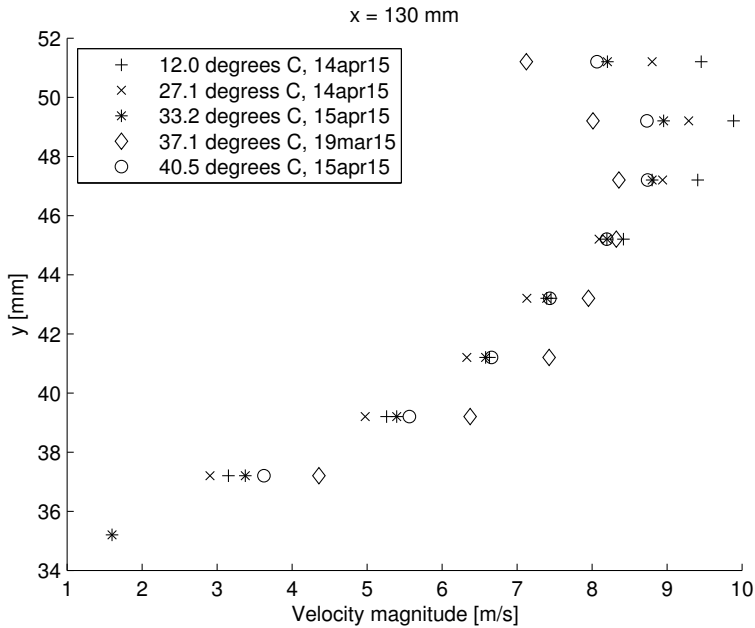


Figure 6.1: Investigation of the effect of temperature change on the velocity profile close to the diffuser inlet.

pump also increases because of the decreased friction loss. This was observed during measurement. Figure 6.2 shows flow rate, pressure difference (total head), shaft torque and rotational speed of the test rig during execution of M2. The rotational speed of the impeller is kept constant by the electrical drive of the motor, the shaft torque decreases, the flow rate and the pressure difference increase throughout the measurement campaign. The change of operating conditions over time is assumed to be affected by the change of viscosity, but also other unknown phenomena can be influential. Testing with a constant temperature of the working fluid should be conducted in order to possibly rule out other unknown effects.

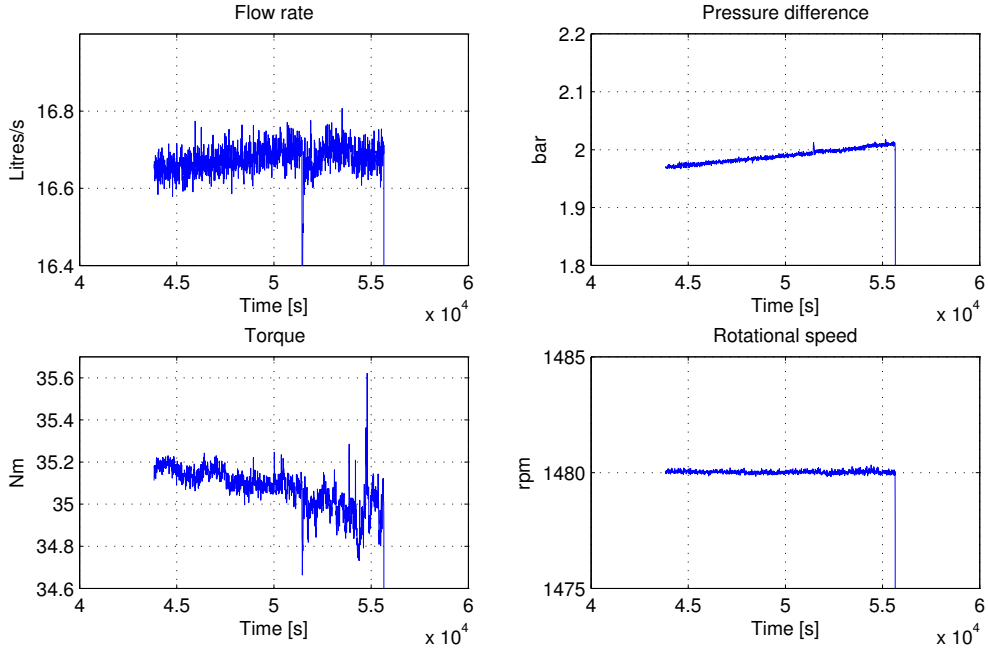


Figure 6.2: Operating conditions of the pump during M2.

### 6.1.2 The geometry of the diffuser

The geometry of the diffuser has some differences compared to the computer-aided design (CAD) model, from which the numerical grid is based on. The inner surface contains bumps, which possibly can introduce an increased level of disturbance to the flow. The top and bottom walls are not completely perpendicular to the inner surface, i.e. the width of the diffuser channel varies in the  $z$ -direction. This might have introduced some unexpected flow structures in the diffuser.

The steady velocity magnitude profile was measured in the  $z$ -direction at two  $(x, y)$ -positions, the result is shown in figure 6.3.  $z = 0 \text{ mm}$  represents the plane on which all measurements were conducted. The slope at  $z = 0 \text{ mm}$  introduces an error of the measured velocity for an offset of the  $z$ -position. The optimal condition of the velocity magnitude variation in the  $z$ -direction is a flat velocity profile near the  $z = 0 \text{ mm}$  plane, which would eliminate the mentioned velocity error. Based on these results, the diffuser channel can be concluded to have a three-dimensional velocity distribution.

An explanation for this can be the inlet conditions, e.g. a non-uniform inlet velocity distribution in the  $z$ -direction affects the three-dimensional flow in the diffuser.

Another explanation can be three-dimensional flow characteristics appearing naturally in a curved diffuser, due to a radial pressure gradient.

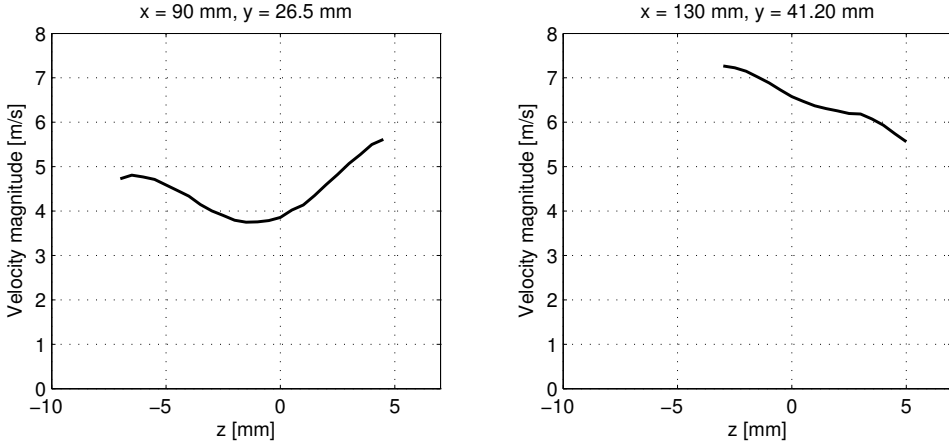


Figure 6.3: Velocity magnitude profile along  $z$ , at  $(x, y) = (90 \text{ mm}, 26.5 \text{ mm})$  and  $(x, y) = (130 \text{ mm}, 41.5 \text{ mm})$ .

### 6.1.3 Other factors

The flow rate in the test rig circuit is measured by a flow meter mounted on the inlet pipe. Any leakage occurring between the flow meter and the diffuser will affect the flow rate in the diffuser channels, where the velocity measurements are conducted. Leakage should therefore be minimized. The pump was leaking water from several places. The amount of leakage was considered to be much lower than the BEP flow rate of  $16.67 \text{ l/s}$ , and was therefore neglected.

The test rig experienced some vibrations while running at BEP, this was not considered to be influential on the mean velocity measurements nor the position of the LDV measurement volume with respect to the diffuser. However, the velocity fluctuations might have been influenced, giving the RMS velocity fluctuations a false rise.

## 6.2 The LDV System

A well-behaving LDV system is desired. This can be defined as a system that provides reliable and accurate velocity data of a flow with a sufficiently high data rate and with an acceptable signal-to-noise ratio.

The mean data rate in a point is defined as:

$$\text{Data rate} = \frac{\text{Number of samples}}{\text{Total sampling time}} \quad (6.1)$$

The quality of the velocity data acquired in a point by the LDV system is dependent on the number of samples acquired and the signal-to-noise ratio. The number of samples acquired is dependent on the sampling time and the data rate in each point. The data rate in the measurement campaigns conducted varied from 0 Hz to 17,000 Hz, where the bulk of the measurement points had a data rate of about 500-2000 Hz. The points which had data rates much higher than 2000 Hz, were usually giving signal with a lot of noise and were consequently filtered out. According to Scarano [13], the data rate of the LDV system is limited by the concentration of the seeding particles in the flow and the velocity of the flow, the maximum achievable data rate is often in the range of 1000 Hz to 10,000 Hz for a experimental setup. Eisele et al. [5] had data rates between 600 Hz and 2000 Hz and was acquiring the unsteady velocity in the outlet of an impeller. This region is known to be highly fluctuating. This indicates that the achieved data rate for the LDV system used in this experiment was relatively high and definitely sufficient for the purpose of this project, i.e. measuring the steady velocity distribution.

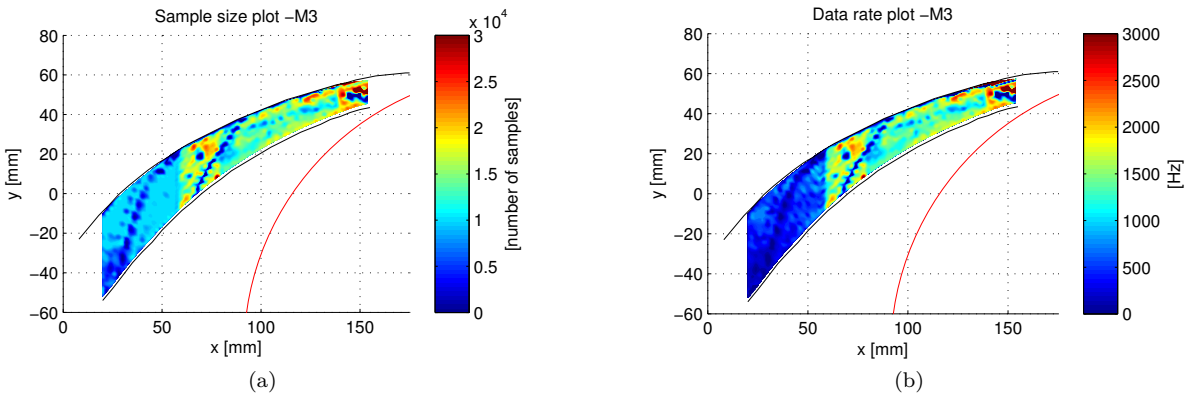
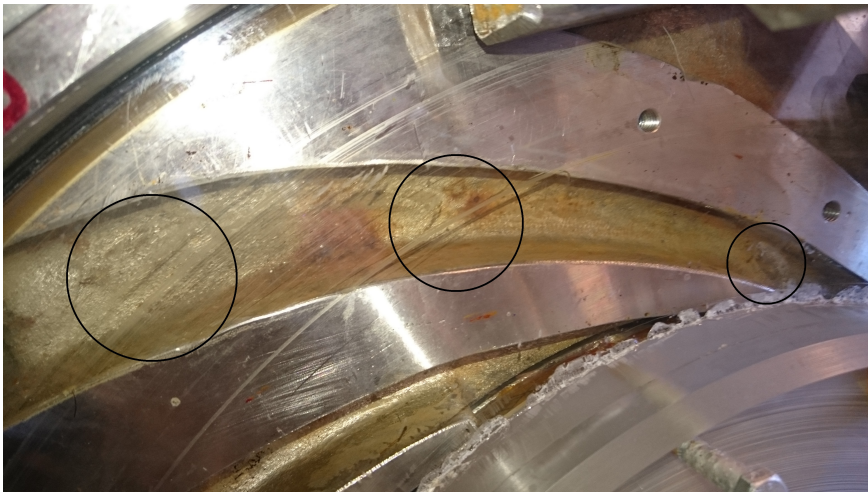


Figure 6.4: Sample size and data rate plot of M3.

A plot of the sample size and data rate achieved in each point during M3 is shown in figure 6.4 as a 3d plot. By looking at the data rate plot it can be concluded that the data rate for the downstream part is much lower than for the upstream part. This is mainly because the velocity of the water is lower for this part, i.e. fewer seeding particles pass through the measurement volume per time unit. In the region confined by  $x = [60 \text{ mm}, 80 \text{ mm}]$  there is a clear change in data rate and sample

size, this is due to predefined settings for the LDV system. For unknown reasons it was challenging to obtain good velocity data for this region, and the solution was to make the LDV system more sensitive, resulting in a lower signal-to-noise ratio of the acquired signal. The increased noise consequently increases the calculated RMS velocity fluctuations in this region. This can be observed in the RMS velocity fluctuation plots in section 5.2.

By examining the data rate plot, a small region close to the inlet and two lines in the downstream part of the diffuser can be observed to have a low data rate. This is a direct consequence of having a damaged Plexiglas cover on the test rig. Figure 6.5 shows that the location and shape of the scratches match the low data rate regions in the data rate plot. This illustrates the importance of having a clear Plexiglas cover. The surface of the Plexiglas cover should also be as smooth as possible, as bumps deflect the laser light and prevent the LDV measurement volume to be formed or appear in the wanted location.



*Figure 6.5: The scratches on the Plexiglas cover of the pump.*

The LDV system detects the backscattered light from the seeding particles. Backscattered light has a lower intensity than forward-scattered light, it is therefore particularly important that refraction of the laser light is minimized so that the data rate is maximized. Dirt on the Plexiglas or on the probe lens decreases the data rate. Also dirty water decreases the intensity of the backscattered light.



## 6.3 Uncertainty Analysis

Experimental work always includes errors to the acquired data. It is statistically impossible to obtain the exact physical value. Important questions all experimentalists should ask themselves are: How reliable are the results? What is the maximum expected deviation from the physical value? The LDV system and the test rig have many potential sources of error. These are discussed here.

### 6.3.1 Sources of error

Kline and McClintock [15] describe different types of error which can appear during an experiment: systematic errors, random errors and mistakes. Systematic errors are errors that have a fixed value or a fixed trend which persist when repeating the experiment. Examples of this type of error can be a poorly calibrated sensor or an offset on the position of the sensor. Random errors are errors which cause a repeated reading to differ when measuring the same physical quantity. An example of this can be inbuilt uncertainty of the equipment. Mistakes are completely erroneous readings, e.g. a data logging mistake or a human mistake. Systematic errors can be corrected for during measurement by eliminating the source of error. It can also be corrected for after an experiment, if the source of error is identified and quantified. Random errors are not possible to correct for, but they can be statistically quantified and included in the uncertainty analysis. The expected value of the random error is zero, meaning that by repeating a measurement several times under the same conditions and averaging the acquired data, will decrease the random error. The uncorrected systematic error however can not be averaged out since it is constant. If a value is identified as a mistake, it can be neglected. If the mistake is close to the expected physical value, it is hard to detect, i.e. it is not an outlier. An outlier is defined as a value which clearly deviates from the expected value.

### Unstable operating condition

The unstable operating conditions of the test rig caused errors. The temperature change during the measurements discussed in the previous section showed an apparent trend in the measured velocities. Even though this is a systematic error, it can not be corrected for since the temperature was not continuously logged for all measurement campaigns. Furthermore, the increase in flow rate during measurements is thought to be caused by the temperature increase. This could explain why the velocity profile changes for different temperatures, however this can be counter-argued by the fact that we monitored and regulated the flow rate manually by adjusting the valves to a certain extent. The change of the velocity profile may also be attributed to the fact that the viscosity of the water decreases, something that might affect the behavior of the fluid flow inside the diffuser.

The opening position of the butterfly valve on the outlet valve, might have been affected by the pressure exerted on it by the flow. This might have slightly opened it during measurements, consequently increasing the flow rate.

An overview of the unstable flow rate for a selection of measurement campaigns is displayed in table 6.1.

Measurement	Flow rate range [l/s]	Deviation from $Q_{BEP}$ [l/s]
M2	16.65 – 16.70	–0.02, +0.03
M3	16.65 – 16.77	–0.02, +0.10
M4	16.64 – 16.71	–0.03, +0.04
M5	16.64 – 16.70	–0.03, +0.03

Table 6.1: Flow rate deviation from  $Q_{BEP} = 16.67$  l/s.

Based on table above, the flow rate is estimated to be within the range  $Q = 16.67 \pm 0.10$  l/s. The effect of this deviation on the cross-sectional mean velocity measured at the inlet of one of the ten diffusers can be estimated to be:

$$U_{mean} \pm \Delta U = \frac{1}{10 \cdot W_1 b} (Q_{BEP} \pm \Delta Q) = 7.72 \pm 0.02 \text{ m/s} \quad (6.2)$$

For the rest of the channel it corresponds to  $\Delta U/U_{mean} = \Delta Q/Q_{BEP} \approx 0.26\%$  deviation from the mean velocity. In reality a deviation of 0.26% can be larger because this calculation assumes the velocity profile to be uniform, which is not true. The purpose of this calculation is to illustrate the impact of having a varying flow rate on the test rig.

### Measurement position

Another source of error is the position of the LDV measurement volume. This error is the sum of the errors emerging from the pinpointing of the  $(x, y, z)$ -origin, aligning of the traverse table and the accuracy of the moving traverse table. The pinpointing of the origin adds a systematic error to a single measurement campaign, while the alignment adds a systematic error to all measurement campaigns. The deviation of the position after locating the origin is estimated to be  $\pm 0.2$  mm in the  $(x, y)$ -plane, and  $\pm 0.5$  mm the  $z$ -direction. The movement of the traverse adds a random error to the position and is estimated to move to a position within  $\pm 0.2$  mm of its target, independent of the traveled distance. This gives a maximum estimated error on the position for each measurement of  $\pm 0.4$  mm in the  $(x, y)$ -plane and  $\pm 0.7$  mm in the  $z$ -direction.

The location of the  $z$ -coordinate of the origin decides which  $z$ -plane is being measured. The velocity profiles in the  $z$ -direction displayed in figure 6.3 show that there is a slope at  $z = 0$ . Based on the velocity slope in the  $z$ -direction, an offset of  $\pm 0.7 \text{ mm}$  on the  $z$ -coordinate of the origin gives an estimated error on the velocity of  $\pm 0.2 \text{ m/s}$ , which is 5.19% of the measured velocity in  $z = 0$  for that point. This error might be larger in regions of the diffuser where the velocity change in the  $z$ -direction is larger. This was not further investigated and an error of  $\pm 0.2 \text{ m/s}$  is assumed.

### LDV system

The manufacturer of the LDV probe, Dantec Dynamics, states that a calibration of the fringe spacing in the LDV measurement volume can be performed in order to minimize any systematic errors. This calibration is assumed to be a part of the manufacturing process. The calibration uncertainty is given by Dantec Dynamics to be 0.04% of the reference velocity used in the calibration with a coverage factor<sup>1</sup> of 2 [16]. For the highest velocities measured in the diffuser of about  $10 \text{ m/s}$ , this corresponds to an uncertainty of  $10.000 \pm 0.004 \text{ m/s}$ . This is so small compared to the uncertainties mentioned above that it is neglected.

The accuracy of the velocity data is also dependent on the amount of noise produced. The noise adds an error to the calculated velocity mean compared to the true mean. Examples of the mentioned tail-noise and zero-noise from section 4.4 are shown in figure 6.6.

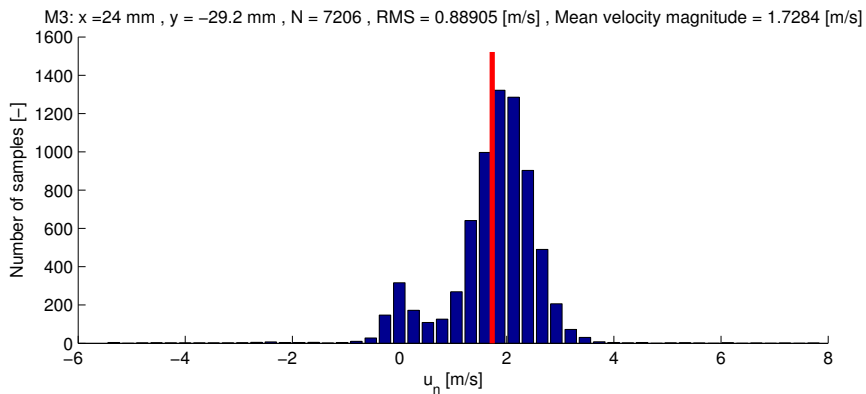
Based on the filtering criteria mentioned in section 4.4, the velocity data in figure 6.6b were omitted from M3 because of the high level of RMS velocity fluctuation caused by the tail-noise. However the velocity data in figure 6.6a with the zero-noise were not filtered out. The zero-noise figure shows an offset from the true mean of about  $0.2 \text{ m/s}$ . Luckily most of the points having tail-noise and zero-noise were filtered out, leaving only a few points with a maximum velocity offset of about  $0.2 \text{ m/s}$  in the results. This estimated error has been confirmed by investigating velocity histograms with the same type of noise.

A solution to further filter the data would be to calculate a confidence interval based on a confidence level, e.g. 95%<sup>2</sup>. This means that there is a 95% probability that a randomly acquired velocity sample has a value within the calculated confidence interval. The velocity data which have values outside this interval, i.e. 5%, can be identified as outliers or noise. A method used for identifying the outliers is the generalized studentized deviate test (generalized ESD test), described by Rosner [17] in 1975. This method detects outliers for a predefined confidence level by performing

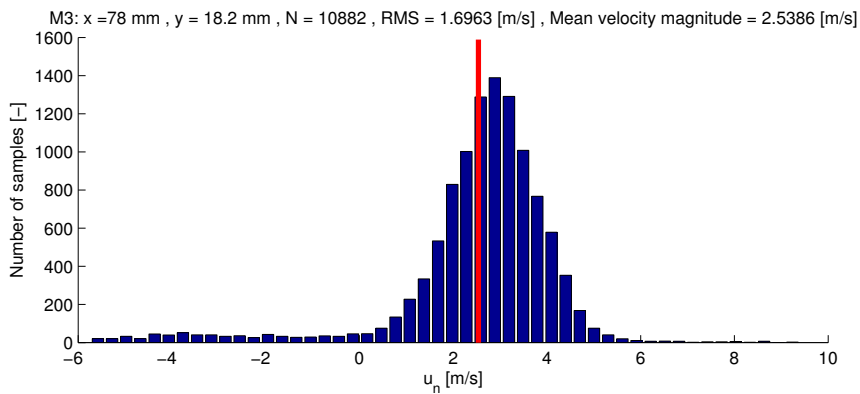
---

<sup>1</sup>A coverage factor of 2 gives a 95% level of confidence on a normal distribution, which means that the measured velocities are within two standard deviations from the mean.

<sup>2</sup>Significant level of  $\alpha = 5\%$



(a) Zero-noise



(b) Tail-noise

*Figure 6.6: Data with noise from the LDV system.*

Grubbs' test<sup>3</sup> iteratively and removing the detected outlier from the data set for each iteration. An attempt on implementing this method on the acquired data was done, but the attempt was unsuccessful and therefore rejected.

<sup>3</sup>Grubbs' test is described in Rosner's paper and is used to detect a single outlier.

### 6.3.2 Repeatability

The sum of all errors discussed above and undiscovered errors represent the total known uncertainty of the velocity measurements performed in the diffuser. The effect of the uncertainty on the velocity can be observed by comparing the measurement campaigns with each other. The total uncertainty is represented as the scattering of data around the mean. Figures 6.7a to 6.9b show a selection of the filtered data represented as the mean velocity magnitudes for the measurement campaigns, the average of the mean velocity magnitudes for the data acquired at the same points and the RMS of the mean velocity magnitude deviations (RMS deviations). The piecewise linear red line passes through the average of the mean velocity magnitudes, and the green dotted line represents the RMS deviations. The RMS deviation represents the uncertainty of the mean velocity magnitude. The maximum RMS deviation for the upstream part, i.e.  $x = 140 \text{ mm}$  and  $x = 120 \text{ mm}$ , is  $0.63 \text{ m/s}$ . The downstream part, i.e.  $x = 60 \text{ mm}$  and  $x = 40 \text{ mm}$ , has a maximum RMS deviation of  $0.26 \text{ m/s}$ .

The upstream part of the diffuser has a larger uncertainty on the measurements performed. The reason for this might be that the inlet condition of the diffuser is more sensitive to changes of operating conditions, such as temperature change or a varying flow rate. The deviation is also thought to be larger for the upstream measurements, simply because the velocities are higher here. The magnitude of the disturbances which originate from sources of error affecting the flow inside the impeller and the inlet pipe, e.g. change in viscosity or flow rate, are thought to be larger close to the inlet of the diffuser than further downstream. The disturbance at the inlet diffuses as the flow is affected by the expanding channel area and strong centrifugal forces from the top wall. This means that the flow downstream is more predictable than the upstream flow.

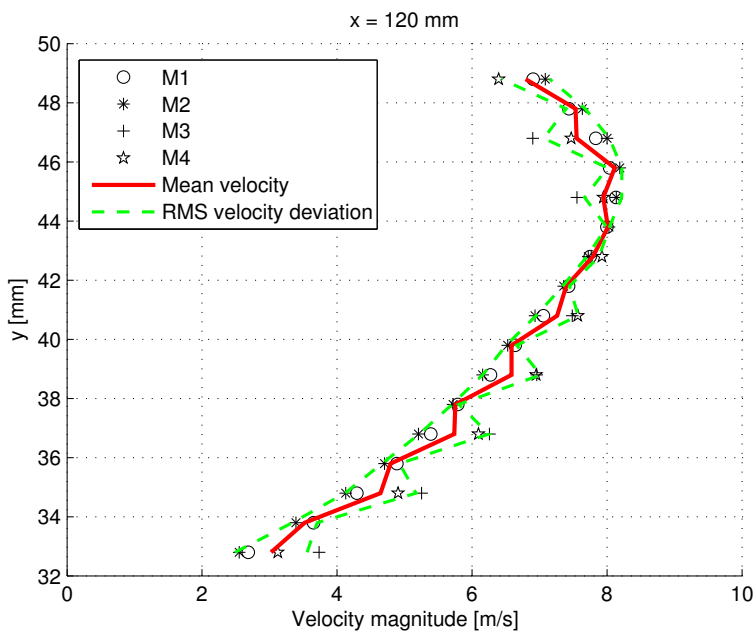
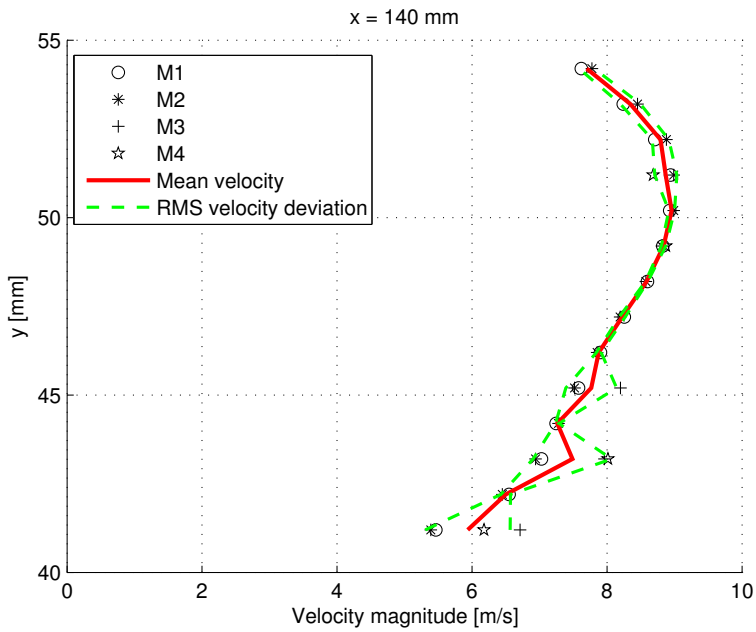


Figure 6.7: The mean velocity magnitudes of the measurement campaigns at  $Q_{BEP}$  (points), the average of the mean velocity magnitudes (red line) and the RMS of the deviation (green dotted line).

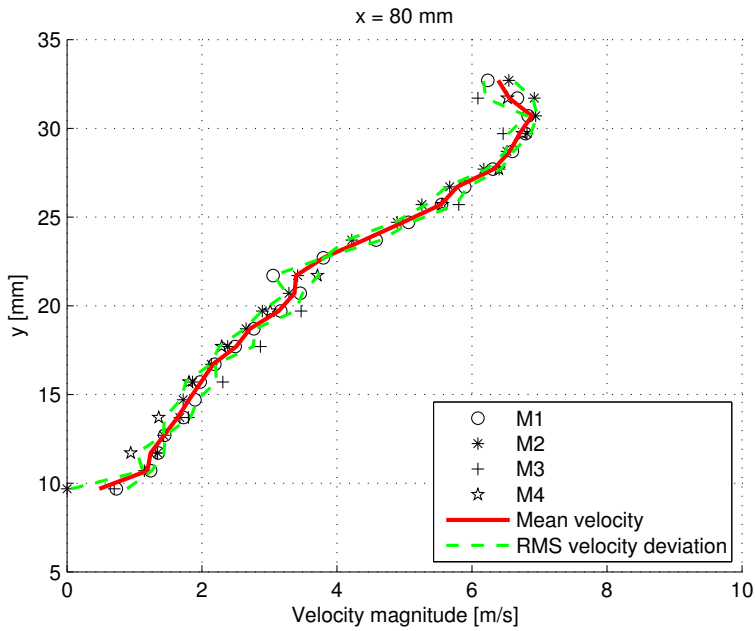
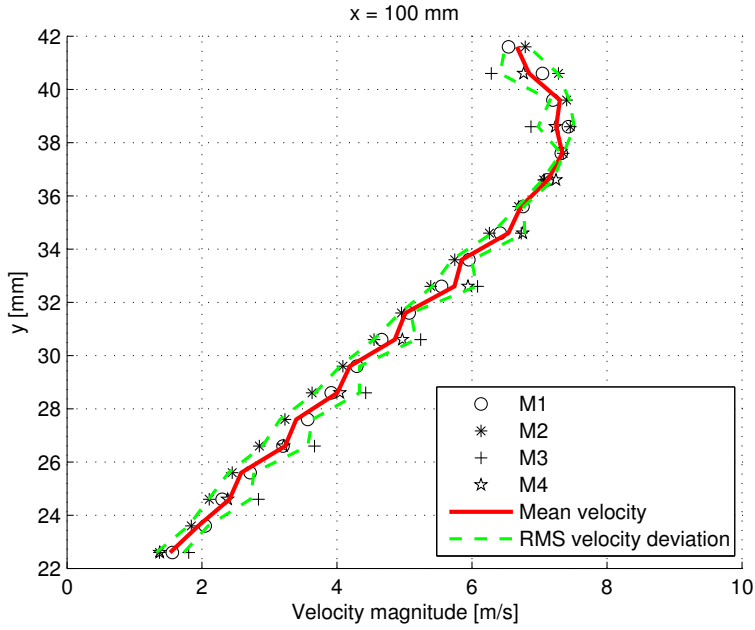


Figure 6.8: The mean velocity magnitudes of the measurement campaigns at  $Q_{BEP}$  (points), the average of the mean velocity magnitudes (red line) and the RMS of the deviation (green dotted line).

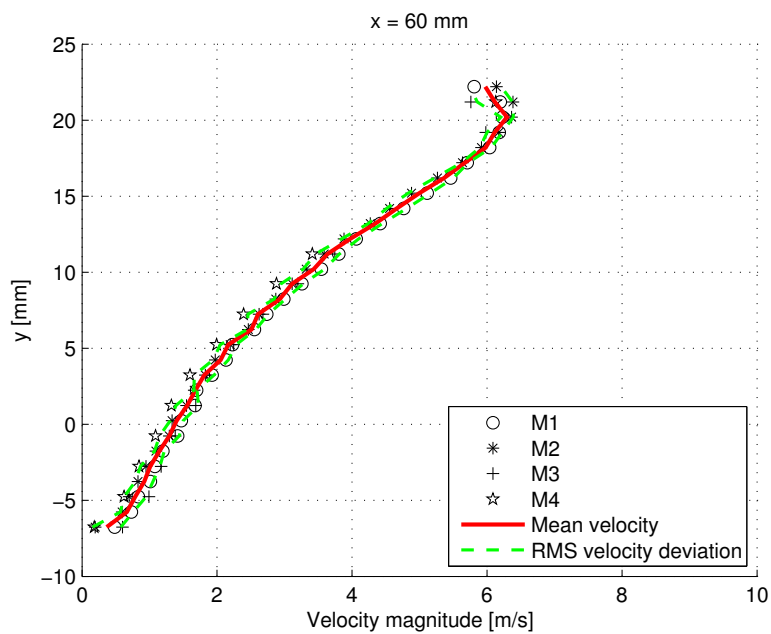
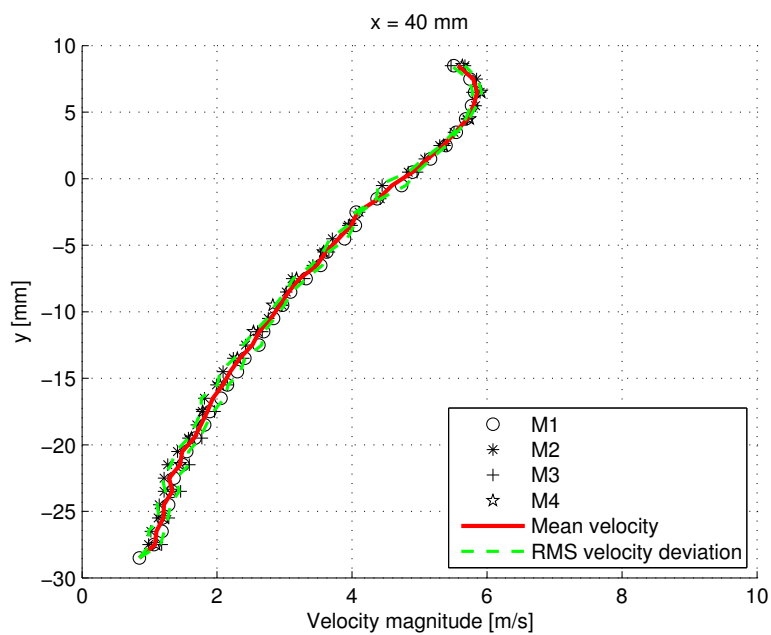
(a)  $x = 60 \text{ mm}$ (b)  $x = 40 \text{ mm}$ 

Figure 6.9: The mean velocity magnitudes of the measurement campaigns at  $Q_{BEP}$  (points), the average of the mean velocity magnitudes (red line) and the RMS of the deviation (green dotted line).



# Chapter 7

## Discussion

### 7.1 Flow Characteristics

The velocity measurements displayed in chapter 5 are discussed here. Measurement campaign M3 is considered to be the most successful measurement conducted because of relatively large sample sizes obtained in each measurement point and an overall low level of noise. M3 will therefore be the center of attention in the discussion.

#### 7.1.1 Flow direction

The velocity vector plot of M3 can be seen in figure 5.2a with a close-up look in figure 5.2b and 5.3a. Some velocity vectors are neglected due to the applied filter explained in section 4.4. The red circle on the right-hand side of the plot represents the approximate edge of the impeller and gives a sense of where the inlet of the diffuser is. The velocity vector plot shows that the steady flow is following the curved walls of the diffuser quite nicely.

Figure 7.1 is a contour plot of the flow angle  $\psi$ . If  $\psi = 0$  the flow is heading in the negative  $x$ -direction and if  $\psi = 90^\circ$  it is heading in the negative  $y$ -direction. The angle of the wall tangent for a point on the wall is represented as the color of the thick lines over and under the diffuser. This theoretically represents the flow angle near the walls. The plot has two distinct regions, namely  $x = [20 \text{ mm}, 60 \text{ mm}]$  and  $x = [80 \text{ mm}, 150 \text{ mm}]$ , i.e. downstream and upstream respectively. When looking at cross-sections, which are defined between two points that amount to the minimum channel width between the bottom and the top wall in the mentioned regions, some characteristics can be observed.

In the downstream region the flow angle is near-constant along the widthwise cross-section. This can be observed from the constant contour lines which are straight and perpendicular with respect to the wall.

In the upstream region the widthwise cross-sectional profiles are non-uniform. When

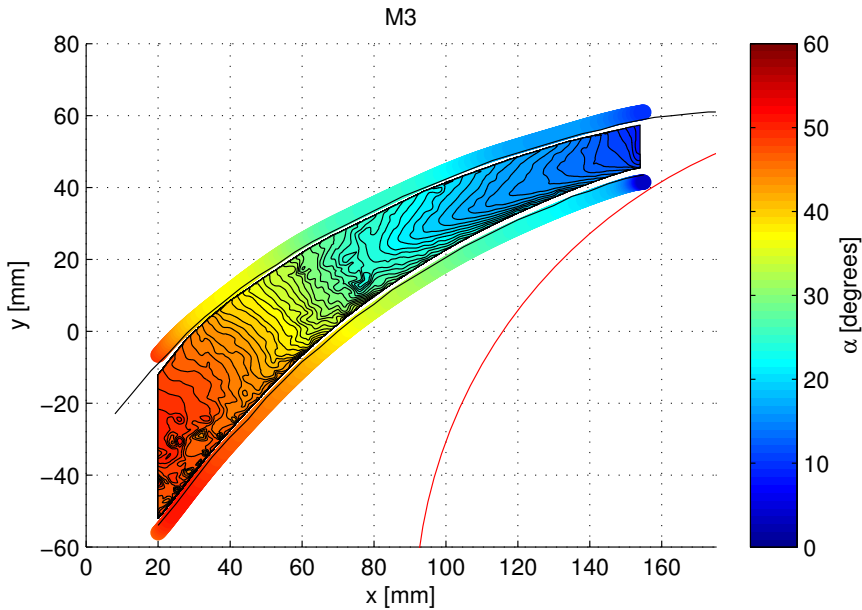


Figure 7.1: Flow angle contour plot for M3.

observing how the flow angle varies in the streamwise direction, the velocity vectors near the top and bottom wall follow the curvature nicely, while the flow angle in the middle of the channel changes much slower. This suggests that the flow in middle does not follow the curvature of the diffuser walls until the flow has reached the downstream region, i.e. they are non-parallel with respect to the wall upstream. This can also be observed by closely investigating the velocity vectors in the close-up figure B of M3, i.e. figure 5.3a.

This phenomenon can have several explanations. The flow entering the diffuser from the impeller has to flow over the leading edge of the diffuser vanes. The leading edge has a rounded tip which deflects the flow coming from the impeller into the diffuser channel. This deflection might give the flow a non-parallel inlet velocity, which persists in the channel until it is straightened by the curved top wall. Another explanation for this might be because of the geometry of the impeller blades. The absolute velocity vector in the velocity triangle of the impeller is not designed properly so that it matches to the diffuser channel inlet angle. If this is true, the design of the pump is not optimal. The cause of the non-parallel steady flow in the upstream part can also be a combination of these hypotheses, or other unknown causes.

The vector velocity plot shows no back flow in the diffuser under the ideal operation conditions ( $Q_{BEP}$ ). This was expected because flow separation at the walls would lead to a low static pressure recovery, thus a low total head. Flow separation and vortices might occur periodically in the diffuser. This is not possible to acquire with a steady velocity measurement since the unsteady characteristics will be averaged out.

### 7.1.2 Velocity magnitude

The velocity magnitude plot for M3 is displayed in figure 5.7a. By studying the 3d plot, a small low velocity region between  $x = 140 \text{ mm}$  and the diffuser inlet, close to the top wall in the M3 domain, can be seen. This is because of a poor data rate in this region, caused by damages on the Plexiglas and is disregarded from the discussion.

A widthwise cross-sectional plot of the velocity magnitude for M3 is displayed in figure 7.2 in order to visualize the development of the velocity magnitude through the diffuser. The vertical axis in this plot is a normalized channel width scale ( $d/W$ ), where  $d$  is the distance from the bottom wall and  $W$  is the corresponding channel width to the location of the cross-section.

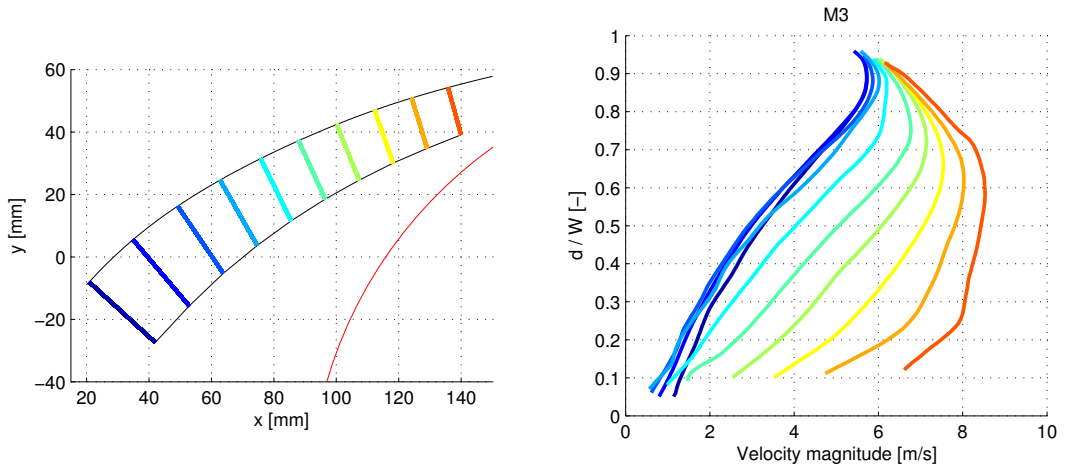


Figure 7.2: Widthwise cross-sectional plot of the velocity magnitude for M3.

The magnitude of the velocity is approximately  $8.5 \text{ m/s}$  at its maximum at the inlet. The shape of the velocity profile for the widthwise cross-section is near-uniform at the inlet, but changes shape as the channel area diverges downstream. The peak velocity magnitude moves from about  $d/W = 0.6$  to  $d/W = 0.9$  as the flow moves downstream. The top part of the velocity field slowly decelerates down to about  $5.5 \text{ m/s}$  and has the same shape from around  $x = 60 \text{ mm}$  to the outlet of the

measurement domain. The bottom part of the velocity field decelerates quickly after the inlet of the diffuser. It continues to decelerate until the lowest measured velocity is reached at around  $x = 70 \text{ mm}$ , i.e. almost stagnation with a magnitude of  $0.6 \text{ m/s}$ . The flow slightly accelerates after the point of minimum velocity magnitude for the bottom part, while the top part slightly decelerates.

The main characteristic to be concluded from this, is that the high velocity flow core in the top part persists through the entire diffuser. The effect of the diverging channel area is strongest in the bottom part of the channel where the flow almost stagnates. The velocity decelerates strongly in the upstream part and stabilizes in the downstream part. A hypothesis for this can be as follows. The high velocity core has the bulk of the total momentum in the flow, i.e. it has the highest flow velocity. At the inlet, the total of the momentum is uniformly distributed across the channel width. As the fluid moves downstream in the diffuser channel, it experiences two changes due to the surrounding geometry: the redirection caused by the top wall and the diverging cross-sectional area. The direction of the inlet flow and the curvature of the top wall forces the bulk of momentum to be concentrated on the top part of the channel, shifting the bulk of momentum away from the bottom part. As the fluid moves downstream it is also affected by the diverging cross-sectional area. As a consequence of the persistence of the high velocity core in the top part, the bottom part is strongly decelerated in order to satisfy the mass conservation law, hence the low velocity region in the bottom part is created.

### 7.1.3 Turbulence

The turbulence in a flow is related to the RMS of the total velocity fluctuation (RMS velocity fluctuation), as described in section 4.3.2. Figure 5.10a shows the RMS velocity fluctuation distribution throughout the diffuser channel, while figure 7.3 shows the widthwise cross-sectional plot of the RMS velocity fluctuation.

By looking at figure 5.10a, the RMS velocity fluctuation in the region located in the interval  $x = [60 \text{ mm}, 80 \text{ mm}]$  and  $x = [140 \text{ mm}, 155 \text{ mm}]$  deviates heavily from the other values in the plot. This is due to signals with a lot of noise. Figure 7.3 therefore focuses on the good signals acquired in  $x = [80 \text{ mm}, 140 \text{ mm}]$ .

The RMS velocity fluctuation in the well-behaving region has a characteristic shape with two peaks (S-shape). The peak closest to the bottom wall, i.e. the bottom peak, emerges right after the inlet of the diffuser and grows in magnitude until it reaches its maximum,  $U'_{RMS} = 0.95 \text{ m/s}$  for  $x = 115 \text{ mm}$  and  $d/W = 0.3$  and starts decaying while expanding in width. In the downstream part of the diffuser, the bottom peak is expanded to almost the total channel width and has a value of approximately  $U'_{RMS} = 0.70 \text{ m/s}$ . The second peak, i.e. the top peak, is located close to the top wall and has its maximum value at the inlet,  $U'_{RMS} = 1.05 \text{ m/s}$ , and diffuses as

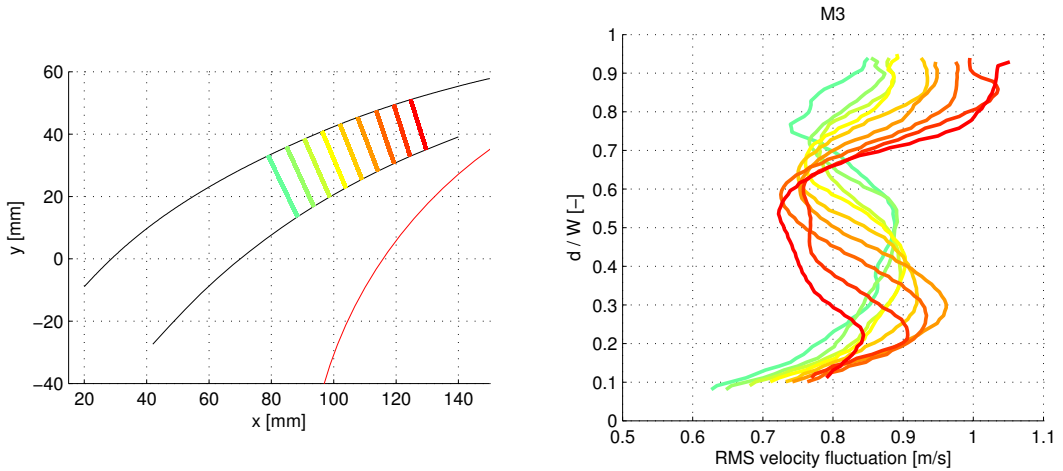


Figure 7.3: Widthwise cross-sectional plot of the RMS of the total velocity fluctuations for M3.

the flow moves downstream. The top peak vanishes in the downstream part of the diffuser. In between the peaks, the point with the minimum value moves toward the top wall, as the flow moves downstream.

The RMS velocity fluctuation is closely related to the behavior of the mean velocity magnitude. The streamwise velocity variation in the widthwise direction<sup>1</sup> is proportional to the viscous shear stress in the fluid flow. Viscous shear stress causes mixing of the fluid and produces vortices. Vortices are known to cause velocity fluctuations. This implies that a higher widthwise variation of velocity causes higher velocity fluctuations because of higher viscous shear stress. This also implies that where there is no widthwise velocity variation, e.g. a point with maximum or minimum velocity, no fluctuations caused by viscous shear stress can exist.

By comparing the widthwise cross-sectional plot for the mean velocity magnitude and the RMS velocity fluctuations, i.e. figure 7.2 and 7.3 respectively, coinciding characteristics in accordance with the viscous shear stress theory can be observed. The bottom peak in the RMS velocity fluctuation plot follows the steepest part of the bottom velocity magnitude curves. The same is observed for the top peak. Also the change in magnitude of the RMS velocity fluctuation happens in accordance to the steepness of the curve at the same position, where larger velocity variations cause higher values of the RMS velocity fluctuation. The location of the minimum RMS velocity fluctuation corresponds to the location of the maximum velocity in

<sup>1</sup>The streamwise mean velocity vector  $\vec{U}$  is in the sake of this argument assumed to be perpendicular to the width of the diffuser.

the velocity magnitude plot. This is also in accordance with the mentioned theory.

#### 7.1.4 Off-design points

Measurement campaigns M7 and M8 were conducted in order to possibly observe flow separation. The vector plots for M7 and M8 are displayed in figure 5.5a and 5.5b respectively. When considering the flow direction, no flow separation was observed for either  $0.75Q_{BEP}$  or  $1.5Q_{BEP}$ . The vectors seem to follow the geometry of the diffuser nicely.

The velocity magnitude plots for M7 and M8 are displayed in figure 5.8a and 5.8b, respectively. M7 shows a high velocity core on the top part of the diffuser and a low velocity region close to the bottom wall. The high velocity core decays from just below  $8\text{ m/s}$  to about  $6\text{ m/s}$ . The low velocity region shows velocities down to about  $0.5\text{ m/s}$ . The velocity distribution in M8 is more uniform than compared to M3 and M7. This indicates that the flow did not initially have enough momentum to keep the high velocity core for long, obtaining a uniform velocity distribution at an early point.

## 7.2 Comparison Between Experimental and Numerical Results

The numerical model for the centrifugal pump was constructed by PhD candidate Alessandro Nocente et al. at NTNU [18]<sup>2</sup>. The single-stage version of the Typhoon pump described in section 3.1 was used as the geometry for the model. The simulation was solved for the same operating conditions as described in section 3.2.4. The commercial software Ansys Fluent was used to solve the Reynolds-averaged Navier-Stokes (RANS) equations. An unsteady solver with a sliding mesh for the impeller was used. The realizable  $k\text{-}\epsilon$  turbulence model was used for the RANS equations. The mean velocity magnitude distribution of the simulation is displayed in figure 7.4.

A confined domain representing the diffuser channel in the total numerical grid was chosen, rotated and translated in order to fit the coordinates of the test rig. This was done by making sure the diffuser walls of the numerical grid overlapped with the walls of the test rig. Moreover, the location of the leading edge of the diffuser vane was adjusted so that it matched the test rig. The location of the leading edge in the plot can be identified as the high velocity region near the inlet. The fitting was done iteratively by means of visual estimate in Matlab, resulting in a very approximate comparison. The velocity magnitude is plotted in the simulation coordinate system, thus the  $x$ - and  $y$ -values are not comparable to other plots.

---

<sup>2</sup>Will be published in August 2015.

The simulation shows similar velocity characteristics when compared to M3. The inlet of the diffuser has a near-uniform velocity profile with a peak velocity of about 7-8  $m/s$ . The flow is decelerated on the bottom part of the channel down to about 1.8  $m/s$ . The top part is also decelerated down to about 5  $m/s$ . The characteristic high velocity core on the top part is recognized and behaves in the same manner as in M3. However, the low velocity region in the bottom part of the channel is thinner and has a higher minimum velocity magnitude. Also the velocity magnitudes of the high velocity core decelerate faster in the simulation.

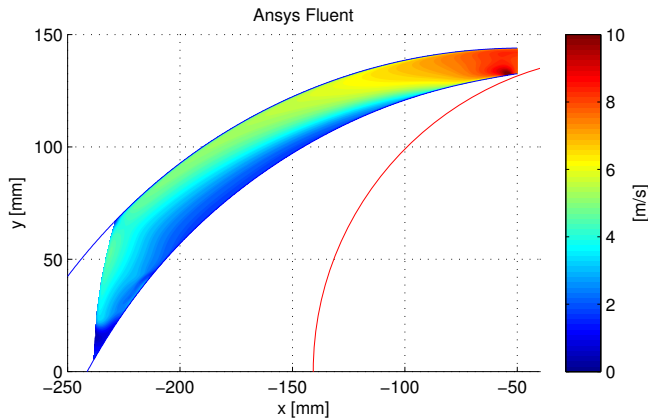


Figure 7.4: Steady velocity magnitude plot of the CFD simulation from Ansys Fluent.

In figures 7.5a to 7.7b the velocity magnitude through constant  $x$ -profiles was plotted for all measurement campaigns and the simulation. The simulation data are represented as the red line. The measurement data coincide quite well and form a well-defined behavior of the flow. The development of the measured velocity profiles are similar for the simulation. By observing how the shape of the velocity profile changes through the diffuser, it can be concluded that the simulation is showing a similar flow behavior. The velocity magnitude deviates quite a lot for certain regions. For the bottom part of the velocity profile, the simulation velocity profile coincides well with the measurements in the upstream part of the diffuser, but for the downstream part it gives approximately the double of the measured value. The high velocity core in the simulation is approximately 15-20% lower than for the measurements throughout the diffuser.

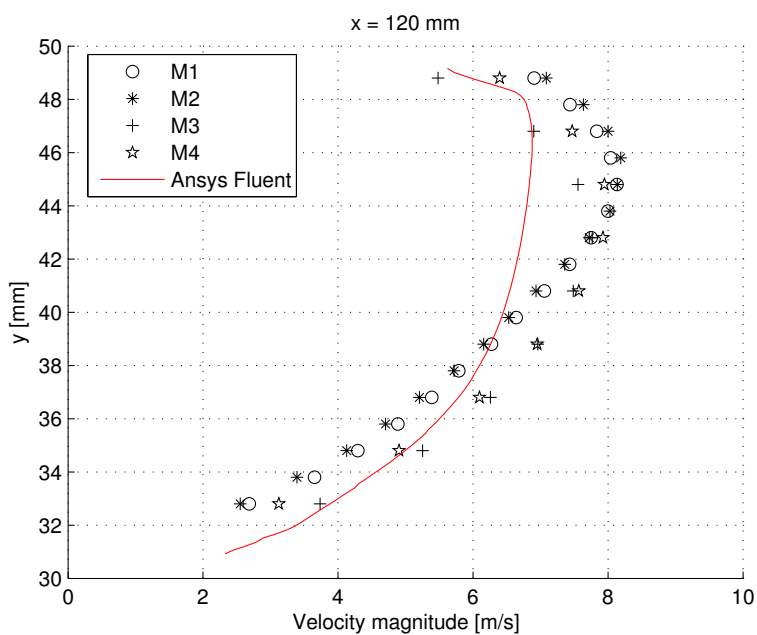
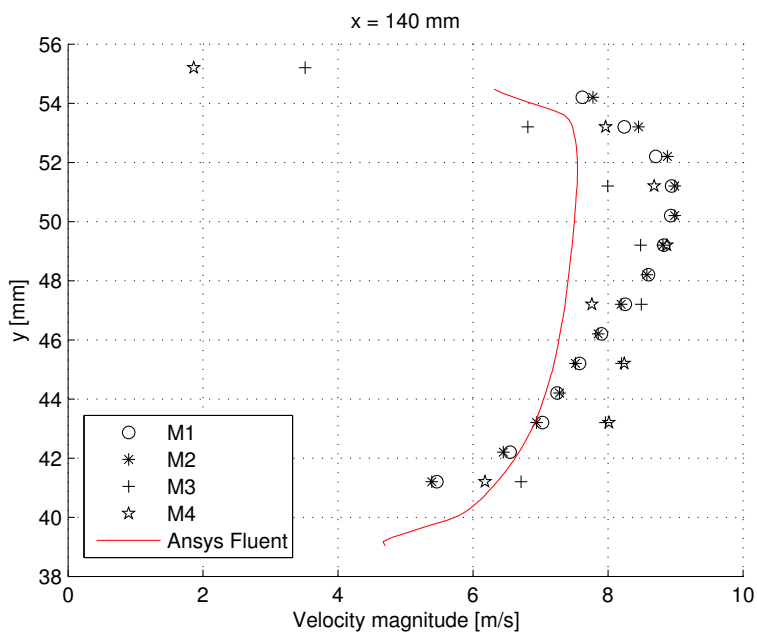
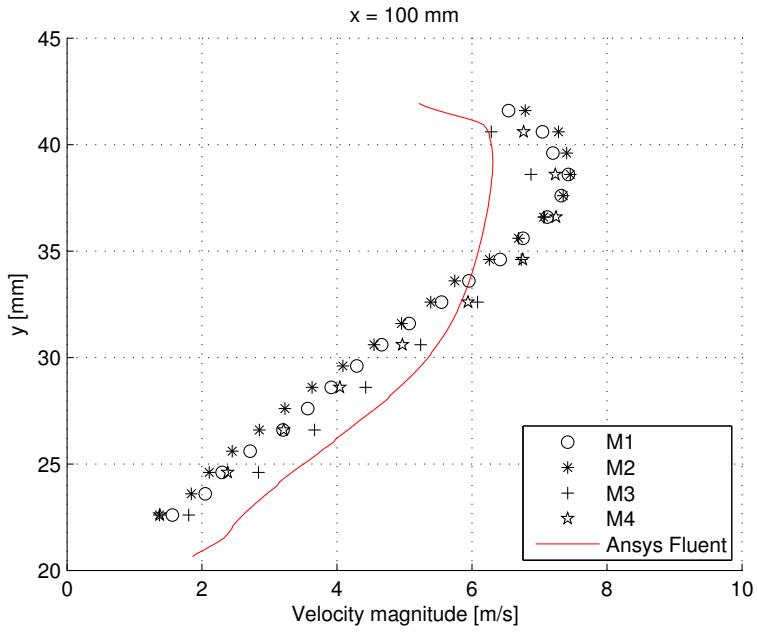
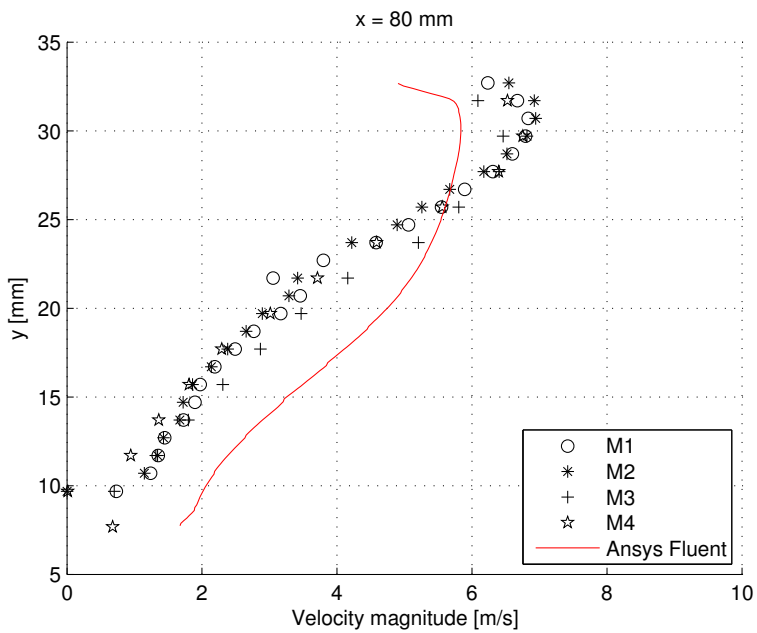


Figure 7.5: Velocity profiles for all measurement campaigns at  $Q_{BEP}$  compared to the numerical model performed in Ansys Fluent.





(a) x = 100 mm



(b) x = 80 mm

Figure 7.6: Velocity profiles for all measurement campaigns at  $Q_{BEP}$  compared to the numerical model performed in Ansys Fluent.

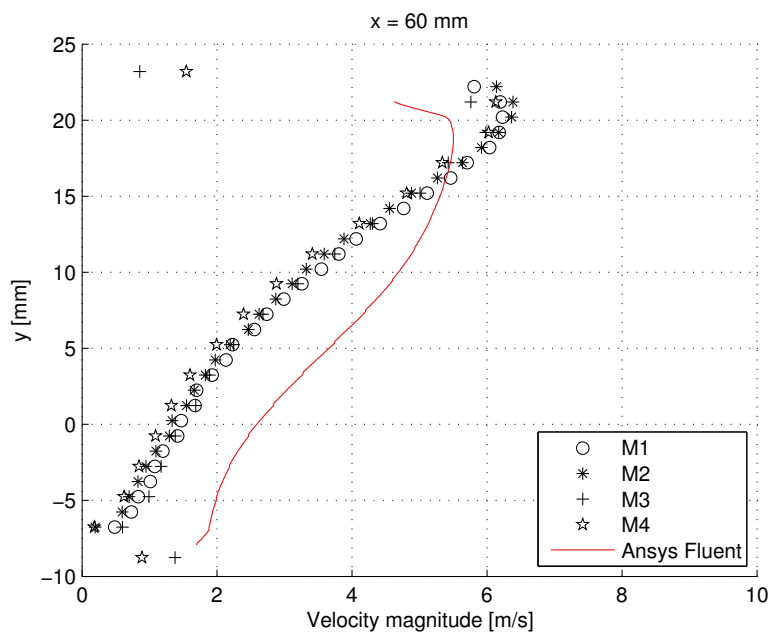
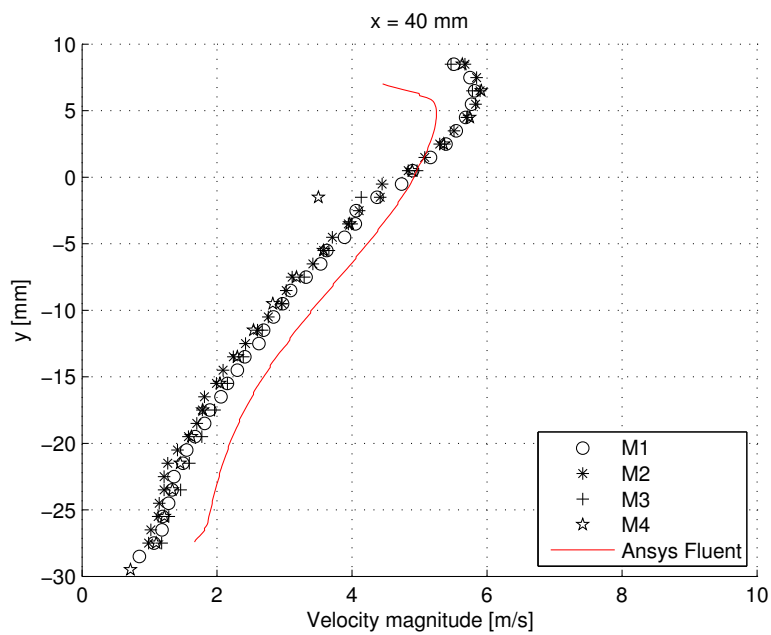
(a)  $x = 60 \text{ mm}$ (b)  $x = 40 \text{ mm}$ 

Figure 7.7: Velocity profiles for all measurement campaigns at  $Q_{BEP}$  compared to the numerical model performed in Ansys Fluent.

# Chapter 8

## Conclusions

Measurements of the the two-dimensional steady velocity distribution and velocity fluctuations inside a diffuser channel of a single-stage version of the Typhoon centrifugal pump have been successfully performed. The data acquired by the LDV system are accurate, reliable and show good repeatability. The stability of the test rig operating conditions are satisfactory for the intended purpose of this thesis, and an overall evaluation and uncertainty analysis for the experiment have been performed. Based on this, the acquired data are well-suited for validation of the CFD simulation performed by Nocente et al. [18].

The LDV system is a complex technique which requires patience and experience in order to obtain reliable and accurate results, and this has been accomplished during this thesis. Also Matlab routines have been made in order to properly visualize the flow characteristics of the diffuser. Procedures for running the test rig and operating the LDV system have been described, benefiting future work on the test rig or LDV flow measurements in general.

The measured steady velocity distribution in the diffuser channel shows a well-behaved flow without flow separation at the walls for the best efficiency point  $Q_{BEP}$ . The main flow characteristics observed in the curved diffuser at BEP are:

- Non-parallel inlet conditions, i.e. the direction of the steady velocity vectors measured in the mid-width channel at the inlet are not strictly parallel to the walls.
- A high velocity core persists throughout the entire top part of the diffuser channel, with a maximum velocity of approximately  $8.5 \text{ m/s}$  and a minimum velocity of  $5.5 \text{ m/s}$ .
- A large low velocity region appears in the bottom part of the channel and has a minimum velocity magnitude of approximately  $0.6 \text{ m/s}$ .
- The steady velocity magnitude develops from being near uniformly distributed in the widthwise direction at the inlet, to non-uniformly distributed at the

outlet of the diffuser channel.

- The RMS of the total velocity fluctuation distribution in the widthwise direction has a characteristic S-shape in the upstream part of the diffuser channel, with peak values corresponding to high viscous shear stress zones. In the downstream part it is uniformly distributed in the widthwise direction.

The measurements conducted at  $0.75Q_{BEP}$  and  $1.5Q_{BEP}$  also show a well-behaved flow with no flow separation occurring.

A comparison between the steady velocity magnitude distribution in the CFD simulation and the measurements showed good agreement when considering the development of the flow through the diffuser. However, the steady velocity magnitudes showed large discrepancies.

# Chapter 9

## Further Work

Further experimental work will be done on the test rig at the Water Power Laboratory at NTNU. The operating conditions of the test rig should be improved. The temperature of the working fluid should be constantly monitored and regulated with used of a cooling system during measurements. This will diminish the effect of decreased viscosity and possibly give a stable flow rate. The flow meter should be moved to a location were it is not measuring a highly unsteady flow, this will give a more stable flow rate signal, making it easier to set the correct flow rate. In order to obtain a more comparable result to the CFD simulation, a diffuser which is geometrically equal to the numerical model should be made and installed.

A complete three-dimensional measurement of the steady velocity distribution of the diffuser channel can be performed by using LDV. This requires a second LDV probe, so that the  $w$ -velocity in the  $z$ -direction can be measured. The Plexiglas should be as clear and smooth as possible so that rarefaction of the laser light is minimized.

In order to investigate the coalescence of oil droplets in the diffuser, plastic particles having the same density and size as the oil droplets can be injected into the water. By illuminating the diffuser channel, the colliding particles can be observed by using a high speed camera.

Another technique for measuring the velocity can be used in order to validate the results presented in this thesis. Also static pressure measurements in the diffuser channel can be performed and compared to the CFD simulation.



# References

- [1] Dantec Dynamics, “LDA Slide Show, URL: <http://www.dantecdynamics.com/docs/support-and-download/research-and-education/lda.zip>,” 2015.
- [2] *BSA Flow Software Installation & User’s guide - Dantec Dynamics A/S*. Dantec Dynamics A/S, 2002.
- [3] T. Husveg and O. Austbø, “Typhoon Pump Laboratory Test Report - doc no.: 131101-04,” tech. rep., Typhonix, Aug. 2012.
- [4] S. S. Foslie, “Design of Centrifugal Pump for Produced Water,” 2013.
- [5] K. Eisele, Z. Zhang, M. V. Casey, J. Gulich, and A. Schachenmann, “Flow analysis in a pump diffuser—part 1: LDA and PTV measurements of the unsteady flow,” *Journal of fluids engineering*, vol. 119, no. 4, pp. 968–977, 1997.
- [6] N. Pedersen, P. S. Larsen, and C. B. Jacobsen, “Flow in a centrifugal pump impeller at design and off-design conditions—part I: particle image velocimetry (PIV) and laser Doppler velocimetry (LDV) measurements,” *Journal of Fluids Engineering*, vol. 125, no. 1, pp. 61–72, 2003.
- [7] R. W. Fox and S. J. Kline, “Flow regimes in curved subsonic diffusers,” *Journal of Fluids Engineering*, vol. 84, no. 3, pp. 303–312, 1962.
- [8] R. D. Blevins, “Applied fluid dynamics handbook,” *New York, Van Nostrand Reinhold Co., 1984, 568 p.*, vol. 1, pp. 144–157, 1984.
- [9] J. D. Anderson and J. F. Wendt, *Computational fluid dynamics*, vol. 206. Springer, 1995.
- [10] B. Majumdar, R. Mohan, S. N. Singh, and D. P. Agrawal, “Experimental study of flow in a high aspect ratio 90 deg curved diffuser,” *Journal of fluids engineering*, vol. 120, no. 1, pp. 83–89, 1998.
- [11] C. A. Moore, *Some Effects of Vanes and of Turbulence on Two-dimensional Wide-angle Subsonic Diffusers*. Department of Mechanical Engineering, Stanford University., 1955.

- [12] Y. Yeh and H. Z. Cummins, “Localized fluid flow measurements with an He–Ne laser spectrometer,” *Applied Physics Letters*, vol. 4, no. 10, pp. 176–178, 1964.
- [13] F. Scarano, *Reader in AE4-180 Experimental Aerodynamics**Reader in AE4-180 Experimental Aerodynamics*. Delft, The Netherlands: TU Delft, 2013.
- [14] Standart Pompa ve Makina San. Tic. A.Ş., “Pump Test Report - Typhonix,” performance report, Istanbul, Aug. 2013.
- [15] S. J. Kline and F. A. McClintock, “Describing uncertainties in single-sample experiments,” *Mechanical engineering*, vol. 75, no. 1, pp. 3–8, 1953.
- [16] Dantec Dynamics, “Calibrated LDA/PDA probes, URL: [www.dantecdynamics.com/docs/products-and-services/service-and-calibration/PI\\_calibrated\\_lda\\_pda\\_probe\\_183v6.pdf](http://www.dantecdynamics.com/docs/products-and-services/service-and-calibration/PI_calibrated_lda_pda_probe_183v6.pdf).”
- [17] B. Rosner, “On the detection of many outliers,” *Technometrics*, vol. 17, no. 2, pp. 221–227, 1975.
- [18] A. Nocente, T. Arslan, and T. K. Nielsen, “Numerical Simulation of Flow Inside Centrifugal Pump by Two Different Solvers,” *MekIT15, NTNU*, 2015.
- [19] S. M. Skodje, *Real Time Modelling of Flow Systems*. PhD thesis, NTNU, Trondheim, 2013.
- [20] H. Perlman, *Water Density, USGS*, <http://water.usgs.gov/edu/density.html>. 2014.



# Appendix

# Calibration



## A.1 Calibration of the Pressure Transducer

The differential pressure transducer on the test rig was calibrated. This sensor consists of four tubes. Two tubes measure the difference in pressure between the inlet and outlet pipe of the pump, i.e. low pressure and high pressure respectively. The remaining two tubes are there for letting air out of the pressurized tubes. The equipment used for calibrating the transducer was a sensor which measured pressure difference. The calibration procedure is described as the following. The low pressure tube of the transducer was not connected to the sensor, i.e. it was constantly measuring the atmospheric pressure. The high pressure tube was initially not connected to the sensor, which corresponded to zero bar difference, which gave the voltage output from the transducer at zero bar difference. By attaching the high pressure tube to the sensor and increasing the pressure inside iteratively, the sensor showed an increasing pressure difference. The transducer was connected to a data acquisition hardware, which was connected to a computer. A Labview program was used in order to obtain a time-averaged voltage output from the transducer. The voltage output could then be correlated to the pressure output of the sensor. The chosen range was between zero bar and four bar. An increasing and decreasing measurement campaign were conducted in order to reduce the effects of hysteresis. The calibration values and the fitted calibration curve can be seen in the following calibration report.

The calibration equation for the differential pressure transducer is given as equation A.1, where  $X$  is the voltage output in *volt* and  $Y$  is the corresponding pressure in *bar*.

$$Y = 0.5013554X - 0.9657302 \tag{A.1}$$

# CALIBRATION REPORT

---

## **CALIBRATION PROPERTIES**

Calibrated by: Karl Oskar Pires Bjørgen  
Type/Producer: FKKW37V1AKCWWAE / Fuji Electric  
SN: N1H5376F  
Range: 0-4 bar  
Unit: bar

## **CALIBRATION SOURCE PROPERTIES**

Type/Producer: Pressurements deadweight tester P3223-1  
SN: 66256  
Uncertainty [%]: 0,01

## **POLY FIT EQUATION:**

$Y = -965.73025300E-3X^0 + 501.35543986E-3X^1$

## **CALIBRATION SUMMARY:**

Max Uncertainty : 17.987391 [%]  
Max Uncertainty : 0.000647 [bar]  
RSQ : 1.000000  
Calibration points : 22

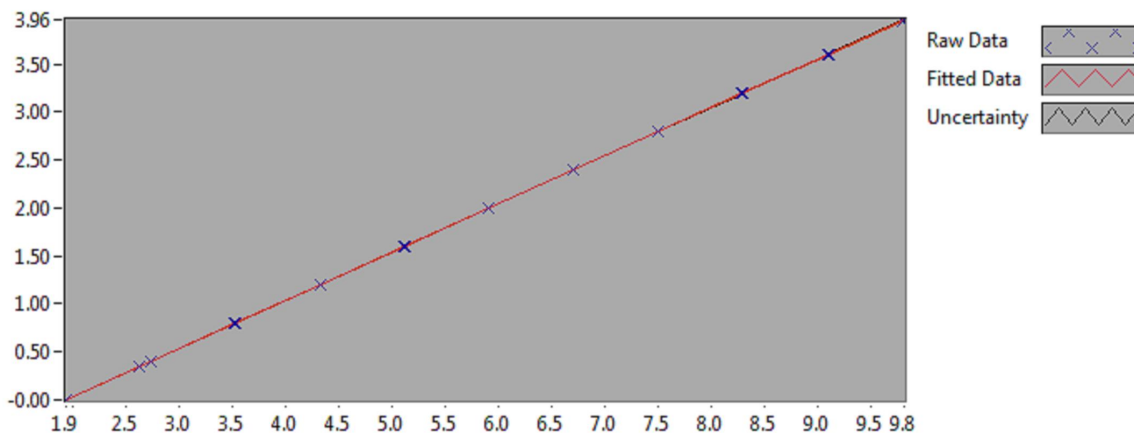


Figure 1 : Calibration chart (The uncertainty band is multiplied by 10 )

---

Karl Oskar Pires Bjørgen

---

**CALIBRATION VALUES**

<b>Value [bar]</b>	<b>Voltage [V]</b>	<b>Best Poly Fit [bar]</b>	<b>Deviation [bar]</b>	<b>Uncertainty [%]</b>	<b>Uncertainty [bar]</b>
0.002000	1.930193	0.001983	0.000017	17.985991	0.000360
0.398000	2.721554	0.398736	-0.000736	0.083693	0.000333
0.799000	3.518616	0.798347	0.000653	0.038635	0.000309
1.199000	4.318252	1.199249	-0.000249	0.021993	0.000264
1.598000	5.113460	1.597931	0.000069	0.015450	0.000247
1.998000	5.912037	1.998302	-0.000302	0.013999	0.000280
2.399000	6.711800	2.399267	-0.000267	0.011989	0.000288
2.799000	7.509199	2.799047	-0.000047	0.011247	0.000315
3.191000	8.293113	3.192067	-0.001067	0.012325	0.000393
3.597000	9.100745	3.596978	0.000022	0.011862	0.000427
3.957000	9.819870	3.957515	-0.000515	0.011980	0.000474
3.952000	9.807698	3.951412	0.000588	0.016359	0.000647
3.601000	9.108242	3.600737	0.000263	0.016062	0.000578
3.199000	8.306753	3.198905	0.000095	0.011968	0.000383
2.800000	7.510682	2.799791	0.000209	0.016413	0.000460
2.399000	6.710007	2.398368	0.000632	0.013034	0.000313
1.999000	5.913135	1.998852	0.000148	0.016332	0.000326
1.600000	5.116265	1.599337	0.000663	0.023721	0.000380
1.200000	4.320434	1.200343	-0.000343	0.026858	0.000322
0.800000	3.521451	0.799768	0.000232	0.042038	0.000336
0.350000	2.624935	0.350295	-0.000295	0.095036	0.000333
0.002000	1.929770	0.001770	0.000230	17.987391	0.000360

**COMMENTS:**


---

The uncertainty is calculated with 95% confidence. The uncertainty includes the randomness in the calibrated instrument during the calibration, systematic uncertainty in the instrument or property which the instrument under calibration is compared with (dead weight manometer, calibrated weights etc.), and due to regression analysis to fit the calibration points to a linear calibration equation. The calculated uncertainty can be used as the total systematic uncertainty of the calibrated instrument with the given calibration equation.

## A.2 Calibration of the Flow Meter

Flow meter	Serial number	Alias
Optiflux 2300 C	A07 00945	Swirl Flowmeter
Optiflux 2000 F	A05 1090	Pelton Flowmeter

Table A.1: The flow meters that were involved in the calibration procedure.

In order to calibrate the flow meter connected to the swirl rig the calibration was performed in two steps:

In the first step, the Pelton flow meter was calibrated by the calibrating tank, where the mass flow rate was measured directly. From this the voltage output from the Pelton flow meter could be correlated with the mass flow rate.

The calibration tank is placed on a scale. The water coming from the loop can be redirected to flow into the tank instead of flowing into the Francis basin. This redirection can be programmed for a desired time interval. The exact filling time can be read from the calibration tank computer. The mass before and after the filling is also registered there, in this way the mass flow rate was obtained. The data obtained in step one are shown in table A.2.

In the second step the voltage output from the Swirl flow meter and the Pelton flow meter was acquired in the same loop. They have the same mass flow rate. In this way it was possible to correlate the voltage output of the Pelton flow meter with the voltage output of the swirl flow meter. The procedures to set the valves correctly and for operating the pumps for step one and two are explained in Skodje's master thesis [19]. The data obtained in step two are listed in table A.3.

From the data obtained in the first step a linear function was fitted to the data set  $(Q_{calc}, E_{pelton})$  and the coefficients  $a_0$  and  $b_0$  were found. In order to correlate the voltage output of the Pelton flow meter with the voltage output of the Swirl flow meter from step two, a linear function was fitted to the data set obtained  $(E_{swirl}, E_{pelton})$ , and the coefficients  $a_1$  and  $b_1$  were found.

$$Q_{calc} = a_0 E_{pelton} + b_0 \quad (\text{A.2})$$

$$E_{swirl} = a_1 E_{pelton} + b_1 \quad (\text{A.3})$$

Since it is the volume flow rate, i.e.  $Q_{calc}$ , as a function of  $E_{swirl}$  that is interesting, we can combine equation A.2 and A.3 and obtain:

$$Q_{calc} = A E_{swirl} + B \quad (\text{A.4})$$

Where  $A$  and  $B$  are defined as  $A = \frac{a_0}{a_1}$  and  $B = -\frac{a_0 b_1}{a_1} + b_0$

The conversion from mass flow rate [ $kg/s$ ] to volume flow rate [ $m^3/s$ ] is based on the density of water (see table A.4), which is obtained by interpolating the water temperature from the USGS table [20].

$$Q_{calc} = 0.0062330536 E_{swirl} - 0.0124427393 \quad (\text{A.5})$$

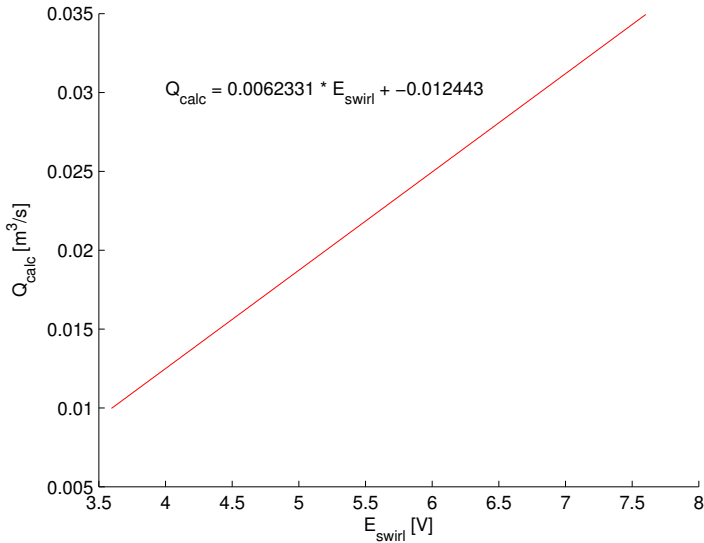


Figure A.1: Calibration curve for the Swirl flow meter.

$E_{pelton}$ [V]	Exact time [s]	Mass difference [kg]	$Q_{calc}$ [ $m^3/s$ ]
2.802594	150.098	1455.8	0.0097109396
3.032932	120.1	1508.1	0.0125724734
3.272918	100.099	1550.6	0.0155097084
3.51804	100.1	1857.1	0.0185752559
3.83062	70.101	1568.1	0.0223966537
4.281886	70.1	1960.8	0.0280057476
4.715604	50.101	1667.5	0.0333236866
5.104014	50.1	1909.4	0.0381585562
5.383265	40.101	1661.9	0.0414938066
5.780775	40.101	1856.5	0.0463527919
6.031529	40.1	1985.6	0.049577279
6.275424	40.101	2104.5	0.0525448158
6.270481	40.101	2104.2	0.0525372225
6.079192	40.101	2003.4	0.0500205673
5.833707	40.101	1886.7	0.0471068206
5.438399	40.1	1687.3	0.0421292016
5.083067	50.1	1897.4	0.0379188156
4.709345	50.1	1661.5	0.0332043789
4.330514	70.099	1969.1	0.0281248065
3.789973	70.101	1535.4	0.0219295674
3.481041	100.1	1814.1	0.0181450862
3.279659	100.1	1569.3	0.0156965964
2.99777	120.099	1463.8	0.0122033101
2.838548	150.098	1533.6	0.0102298858

Table A.2: Calibration data from step one.

$E_{pelton}$ [V]	$E_{swirl}$ [V]
2.840171	3.63565
2.993949	3.940329
3.134438	4.219083
3.328544	4.590513
3.493492	4.92029
3.630218	5.19433
3.876031	5.684003
4.032697	5.988848
4.284571	6.488569
4.52329	6.952287
4.662096	7.232838
4.84617	7.59911
4.84863	7.602899
4.707944	7.329809
4.550302	7.007543
4.290472	6.498814
4.054645	6.033737
3.901849	5.733141
3.654908	5.240339
3.465846	4.871222
3.324294	4.584688
3.155626	4.255415
3.000259	3.953358
2.820739	3.595131

*Table A.3: Calibration data from step two.*

$T_{water}$ [ $^{\circ}C$ ]	Density of Water [ $kg/m^3$ ]
16.81	972.6802618519
16.8	978.5520925926
16.8	982.4671031482
16.8	982.4669074074
16.8	988.3389338889
16.78	988.3391296296
16.8	992.2537487037
16.79	992.2539444444
16.8	994.2111561111
16.83	994.2111561111
16.82	994.2113518519
16.83	994.2111561111
16.82	994.2111561111
16.83	994.2111561111
16.83	994.2111561111
16.82	994.2113518519
16.8	992.2539444444
16.79	992.2539444444
16.8	988.3393253704
16.79	988.3389338889
16.78	982.4669074074
16.8	982.4669074074
16.82	978.5522883333
16.8	972.6802618519

Table A.4: Calibration data from step one, the temperature ( $T_{water}$ ), and the density of the water.



### A.3 Calibration of the Torque Meter

The torque sensor T10FS from HBM mounted on the shaft between the electrical motor and the impeller was calibrated. A one-meter long lever was attached to the shaft on one side of the torque meter. By keeping the other side fixed, weights were added to the lever. The lever was mounted in such way that a half-meter arm was present on each side of the shaft, allowing us to measure the voltage output of the torque meter for both directions. The weights were added in such way that a concentrated load was assumed. The force was transferred to the shaft as torque and the torque sensor registered it as a voltage output. By varying the added weight, a calibration curve was obtained by linear regression through the data points. The local gravitational acceleration<sup>1</sup> was used.

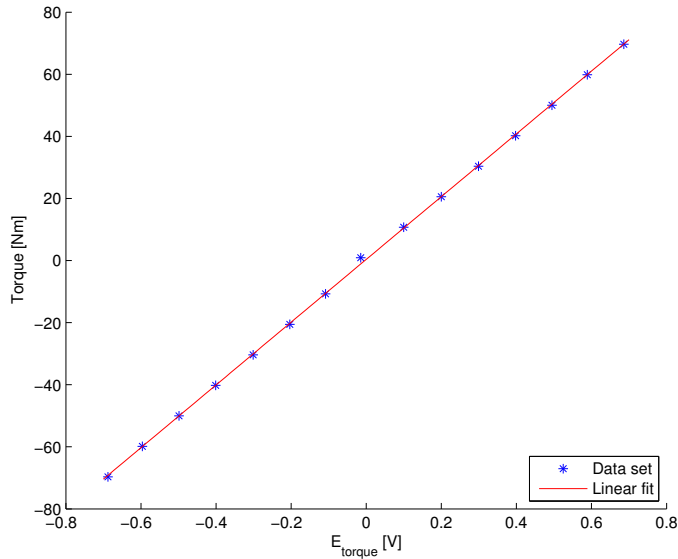


Figure A.2: Calibration curve for the torque meter.

$$\text{Torque} = 101.0954993876E_{\text{torque}} - 0.3676100894 \quad (\text{A.6})$$

<sup>1</sup>The local gravitational acceleration was measured by NGU in 2006,  $g = 9.82146516 \text{ m/s}^2$ .

<i>Mass</i> [kg]	<i>Torque</i> [Nm]	<i>E<sub>torque</sub></i> [V]
14	-69.6636523799	-0.68803
12	-59.8421872199	-0.596211
10	-50.0207220599	-0.498684
8	-40.1992568999	-0.400855
6	-30.3777917399	-0.301249
4	-20.5563265799	-0.203373
2	-10.7348614199	-0.108501
0	0.9133962599	-0.014438
2	10.7348614199	0.09971
4	20.5563265799	0.199791
6	30.3777917399	0.29907
8	40.1992568999	0.39779
10	50.0207220599	0.494624
12	59.8421872199	0.588658
14	69.6636523799	0.686189

*Table A.5: Calibration data for the torque meter.*

# Appendix **B**

## **Typhoon Performance Report**

The performance report from the manufacturer of the Typhoon pump is displayed here.

## Pompa Deneş Raporu / Pump Test Report

Müşteri / Customer : TYPHONIX

Proj. :

### Pompa Bilgileri / Pump Data

Tip / Type : SK-ME 150/3

D<sub>çark/İmp</sub> : 264 mm

DNe : 125 mm

Seri / Serial : 1

Tasarım / Design :

DNb : 150 mm

### Ölçme Sistemi / Measurement System

Man. (Emme/Suct.) : 0-3 bar (mutlak)

Debi / Flow : DN 300

D<sub>1</sub> : 125 mm

Man. (Basma/Disch.) : 0-10 bar

Δ z : 0.85 m

D<sub>2</sub> : 158 mm

T<sub>ort/amb</sub> : 29.4 °C

P<sub>atm</sub> : 998.8 mbar

T<sub>Su / Liq.</sub> : 28.2 °C

Test Sıvısı / Liquid : Su

ρ : 1.00 kg/dm<sup>3</sup>

P<sub>buh / vap</sub> : 0.390 m

### Motor Bilgileri / Motor Data

Üret./ Manuf. : WAT

P : 30 kW

Volt : 380 V

cos ϕ : 0.86

Tip / Type : QH 200L4C

n : 1465 rpm

I : 57.3 A

Seri / Serial : 30774

Fre. : 50 Hz

η<sub>m</sub> : 92.3 %

### Çalışma Noktası Bilgileri / Operating Conditions

Sıvı / Liquid : Su

ρ : 1.000 kg/dm<sup>3</sup>

Sıcaklık / Temp. : 20.0 °C

	n		Q		H		η <sub>p</sub>		η <sub>s</sub>	
	rpm	m <sup>3</sup> /h	m <sup>3</sup> /h	m	%	%	rpm	m <sup>3</sup> /h	m	%
Anma / Rated	1480	60.0	60.0	58.0	-	-	-	-	-	-
Deneş / Test		0.0	0.0	0.0	-	-	-	-	-	-

### Ölçümler / Measurements

No	n	Q	P <sub>giriş/suct</sub>	P <sub>çıkış/disch</sub>	v <sup>2</sup> /2g	H	P <sub>1</sub>	η <sub>m</sub>	P <sub>2</sub>	η <sub>p</sub>
	rpm	m <sup>3</sup> /h	barA	bar	m	m	kW	%	kW	%
1	1488.7	101.6	0.78	3.24	-0.16	36.04	19.55	91.4	17.88	55.6
2	1489.2	90.8	0.79	4.05	-0.13	44.19	19.25	91.4	17.57	62.0
3	1489.2	80.7	0.80	4.74	-0.10	51.17	18.61	91.2	16.97	66.1
4	1489.4	71.0	0.81	5.35	-0.08	57.43	17.78	91.1	16.19	68.4
5	1490.4	60.1	0.82	5.89	-0.06	62.86	16.67	90.9	15.15	67.7
6	1490.8	50.5	0.82	6.29	-0.04	66.99	15.50	90.7	14.05	65.3
7	1492.0	40.2	0.83	6.54	-0.03	69.51	14.07	90.4	12.72	59.7
8	1492.9	30.4	0.83	6.83	-0.02	72.40	12.56	90.1	11.32	52.9
9	1493.4	20.5	0.83	6.99	-0.01	74.00	10.99	89.8	9.83	41.9
10	1494.6	10.0	0.83	7.13	0.00	75.50	9.41	89.5	8.43	24.4
11	1495.6	0.0	0.84	7.26	0.00	76.82	8.18	89.3	7.30	0.0
12										
13										
14										
15										

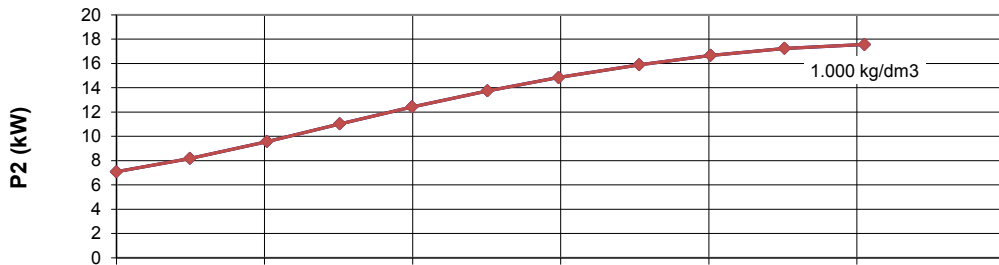
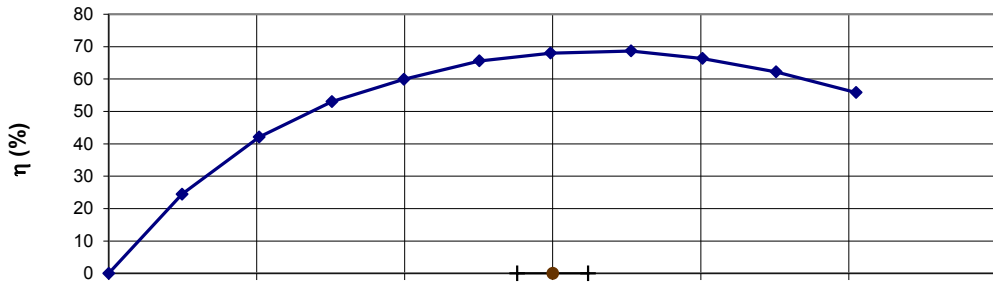
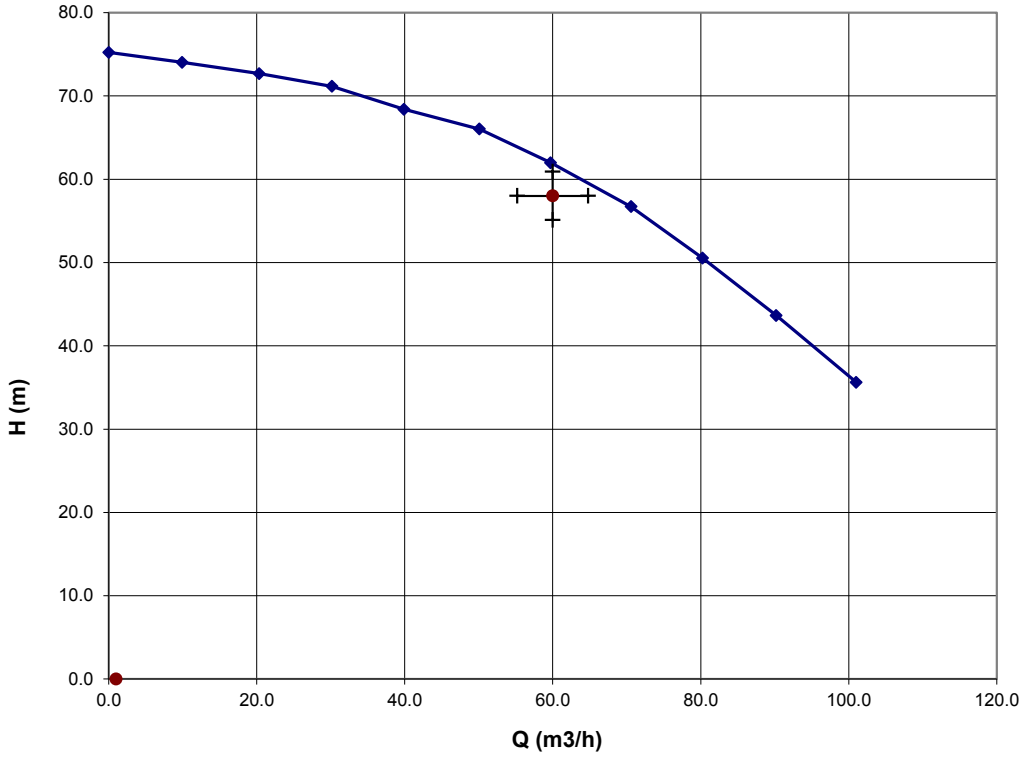
### Anma Şartlarında / Rated Conditions

No	n	Q	H	P <sub>2</sub> kW	P <sub>2</sub> kW	η <sub>p</sub>
	rpm	m <sup>3</sup> /h	m	@ 1,00	@ 1	%
1	1480.0	101.0	35.62	17.56	17.56	55.8
2	1480.0	90.2	43.65	17.24	17.24	62.2
3	1480.0	80.2	50.54	16.66	16.66	66.3
4	1480.0	70.6	56.71	15.89	15.89	68.6
5	1480.0	59.7	61.99	14.84	14.84	68.0
6	1480.0	50.1	66.02	13.75	13.75	65.6
7	1480.0	39.9	68.40	12.42	12.42	59.9
8	1480.0	30.2	71.16	11.03	11.03	53.1
9	1480.0	20.3	72.67	9.57	9.57	42.1
10	1480.0	9.9	74.03	8.18	8.18	24.5
11	1480.0	0.0	75.22	7.08	7.08	0.0
12						
13						
14						
15						

### Malzemeler / Materials

Gövde / Casing :  
Difüzör / Diffuser :  
Çark / Impeller :  
Mil / Shaft :

### Açıklamalar / Comments





# Appendix **C**

## **HSE Risk Assessments**

The risk assessments for the LDV system and the test rig are displayed here.

# Risk Assessment Report

## Centrifugal Pump Rig

<b>Prosjektnavn</b>	LDA measurements in a Centrifugal Pump
<b>Apparatur</b>	Laser modell 177-GO232, serienr T10502
<b>Enhet</b>	EPT
<b>Apparaturansvarlig</b>	Bård Brandåstrø
<b>Prosjektleder</b>	Torbjørn K. Nielsen
<b>HMS-koordinator</b>	Morten Grønli
<b>HMS-ansvarlig (linjeleder)</b>	Olav Bolland
<b>Plassering</b>	Waterpower Laboratory
<b>Romnummer</b>	11
<b>Risikovurdering utført av</b>	Karl Oskar Pires Bjørgen and Alessandro Nocente, with help from Halvor Haukvik

### *Approval:*

<b>Apparatur kort (UNIT CARD) valid for:</b>	
<b>Forsøk pågår kort (EXPERIMENT IN PROGRESS) valid for:</b>	

Rolle	Navn	Dato	Signatur
<b>Prosjektleder</b>	Torbjørn K. Nielsen		
<b>HMS koordinator</b>	Morten Grønli		
<b>HMS ansvarlig (linjeleder)</b>	Olav Bolland		



## TABLE OF CONTENTS

1	INTRODUCTION	1
2	CONCLUSION	1
3	ORGANISATION	1
4	RISK MANAGEMENT IN THE PROJECT	1
5	DESCRIPTIONS OF EXPERIMENTAL SETUP	2
6	EVACUATION FROM THE EXPERIMENTAL AREA	2
7	WARNING	2
7.1	Before experiments.....	2
7.2	Non-conformance.....	2
8	ASSESSMENT OF TECHNICAL SAFETY	3
8.1	HAZOP.....	3
8.2	Flammable, reactive and pressurized substances and gas.....	3
8.3	Pressurized equipment.....	4
8.4	Effects on the environment (emissions, noise, temperature, vibration, smell).....	4
8.5	Radiation.....	4
8.6	Chemicals.....	4
8.7	Electricity safety (deviations from the norms/standards).....	4
9	ASSESSMENT OF OPERATIONAL SAFETY	5
9.1	Procedure HAZOP.....	5
9.2	Operation and emergency shutdown procedure.....	5
9.3	Training of operators.....	5
9.4	Technical modifications.....	5
9.5	Personal protective equipment.....	5
9.5.1	General Safety.....	5
9.6	Safety equipment.....	6
9.7	Special predations.....	6
10	QUANTIFYING OF RISK - RISK MATRIX	6
11	REGULATIONS AND GUIDELINES	7
12	DOCUMENTATION	8
13	GUIDANCE TO RISK ASSESSMENT TEMPLATE	8

## 1 INTRODUCTION

LDA measurements will be conducted operation of the centrifugal pump in the Waterpower Laboratory. The measurements will take place in October and November of 2014.

## 2 ORGANISATION

Rolle	
Prosjektleder	Torbjørn K. Nielsen
Apparaturansvarlig	Bård Brandåstrø
Romansvarlig	Bård Brandåstrø
HMS koordinator	Morten Grønli
HMS ansvarlig (linjeleder):	Olav Bolland

## 3 RISK MANAGEMENT IN THE PROJECT

Hovedaktiviteter risikostyring	Nødvendige tiltak, dokumentasjon	DATE
Prosjekt initiering	Prosjekt initiering mal	
Veiledningsmøte Guidance Meeting	Skjema for Veiledningsmøte med pre-risikovurdering	
Innledende risikovurdering Initial Assessment	Fareidentifikasjon – HAZID Skjema grovanalyse	
Vurdering av teknisk sikkerhet Evaluation of technical security	Prosess-HAZOP Tekniske dokumentasjoner	
Vurdering av operasjonell sikkerhet Evaluation of operational safety	Prosedyre-HAZOP Opplæringsplan for operatører	
Sluttvurdering, kvalitetssikring Final assessment, quality assurance	Uavhengig kontroll Utstedelse av apparaturkort Utstedelse av forsøk pågå kort	

## 4 DESCRIPTIONS OF EXPERIMENTAL SETUP

- Drawings and photos describing the setup.
- Process and Instrumentation Diagram (PID) with list of components
- Location of the operator, gas bottles, shutdown valves for water / air.

## 5 EVACUATION FROM THE EXPERIMENTAL AREA

Evacuate at signal from the alarm system or local gas alarms with its own local alert with sound and light outside the room in question, see 6.2

Evacuation from the rigging area takes place through the marked emergency exits to the assembly point, (corner of Old Chemistry Kjelhuset or parking 1a-b.)

### Action on rig before evacuation:

*Describe in which condition the rig should be left in case of evacuation (emergency shutdown procedure, water, gas, electric supply, etc.)*

## 6 WARNING

### 6.1 Before experiments

Send an e-mail with information about the planned experiment to:

[iept-experiments@ivt.ntnu.no](mailto:iept-experiments@ivt.ntnu.no)

### The e-mail must include the following information:

- Name of responsible person:
- Experimental setup/rig:
- Start Experiments: (date and time)
- Stop Experiments: (date and time)

You must get the approval back from the laboratory management before start up. All running experiments are notified in the activity calendar for the lab to be sure they are coordinated with other activity.

### 6.2 Non-conformance

#### FIRE

If you are NOT able to extinguish the fire, activate the nearest fire alarm and evacuate area. Be then available for fire brigade and building caretaker to detect fire place.

If possible, notify:

NTNU	SINTEF
Morten Grønli, Mob: 918 97 515	Harald Mæhlum, Mob: 930 14 986
Olav Bolland: Mob: 918 97 209	Anne Karin T. Hemmingsen Mob: 930 19 669

NTNU – SINTEF Beredskapstelefon	800 80 388
---------------------------------	------------

### **GAS ALARM**

If a gas alarm occurs, close gas bottles immediately and ventilate the area. If the level of the gas concentration does not decrease within a reasonable time, activate the fire alarm and evacuate the lab. Designated personnel or fire department checks the leak to determine whether it is possible to seal the leak and ventilate the area in a responsible manner.

### **PERSONAL INJURY**

- First aid kit in the fire / first aid stations
- Shout for help
- Start life-saving first aid
- **CALL 113** if there is any doubt whether there is a serious injury

### **OTHER NON-CONFORMANCE (AVVIK)**

#### **NTNU:**

You will find the reporting form for non-conformance on:

<https://innsida.ntnu.no/wiki/-/wiki/Norsk/Melde+avvik>

#### **SINTEF:**

Synergi

## **7 ASSESSMENT OF TECHNICAL SAFETY**

### **7.1 HAZOP**

*See Chapter 13 "Guide to the report template".*

The experiment set up is divided into the following nodes:

Node 1	Traverse table
Node 2	Laser class IV

**Attachments, Form: Hazop\_mal**

**Conclusion:**

#### **Node 1:**

- Pinch points clearly marked

#### **Node 2:**

- Radiation area shielded

**Appropriate signalling and lights in place, light active during operation**

### **7.2 Flammable, reactive and pressurized substances and gas**

Are any flammable, reactive and pressurized substances and gases in use?

NO	
----	--

### **7.3 Pressurized equipment**

Is any pressurized equipment in use?

NO	
----	--

#### 7.4 Effects on the environment (emissions, noise, temperature, vibration, smell)

NO	
----	--

#### 7.5 Radiation

*See Chapter 13 "Guide to the report template".*

YES	Radiation Sources need to have an own risk assessment
-----	-------------------------------------------------------

**Attachments: Radiation risk assessment**

**Conclusion:**

#### 7.6 Chemicals

NO	
----	--

#### 7.7 Electricity safety (deviations from the norms/standards)

NO	
----	--

## 8 ASSESSMENT OF OPERATIONAL SAFETY

Ensure that the procedures cover all identified risk factors that must be taken care of. Ensure that the operators and technical performance have sufficient expertise.

### 8.1 Procedure HAZOP

*See Chapter 13 "Guide to the report template".*

The method is a procedure to identify causes and sources of danger to operational problems.

**Attachments:** HAZOP\_MAL\_Proseedyre

### 8.2 Operation procedure and emergency shutdown procedure

*See Chapter 13 "Guide to the report template".*

The operating procedure is a checklist that must be filled out for each experiment.

Emergency procedure should attempt to set the experiment set up in a harmless state by unforeseen events.

**Attachments:** Procedure for running experiments

**Emergency shutdown procedure:**

### 8.3 Training of operators

### 8.4 Technical modifications

### 8.5 Personal protective equipment

- *It is mandatory use of eye protection in the rig zone*

### 8.6 General Safety

- *The area around the staging attempts shielded.*
- *Operator has to be present during experiments.*

### 8.7 Safety equipment

- *Warning signs, see the Regulations on Safety signs and signalling in the workplace*

### 8.8 Special predations

## 9 QUANTIFYING OF RISK - RISK MATRIX

*See Chapter 13 "Guide to the report template".*

The risk matrix will provide visualization and an overview of activity risks so that management and users get the most complete picture of risk factors.

IDnr	Aktivitet-hendelse	Frekv-Sans	Kons	RV
1	<i>Unintentional rarefaction/reflection of laser beam</i>	1	A	1A
2	<i>People without protective goggles entering radiation area</i>	1	C	1C
3	<i>Traverse table damaging lab equipment</i>	2	B	2B

**Conclusion:** There is little remaining risk. The most prominent risk is that people unintentionally wander into the radiation area without protective goggles, but proper signalling and blocking should prevent this. The risk is therefore acceptable.

## 10 REGULATIONS AND GUIDELINES

Se <http://www.arbeidstilsynet.no/regelverk/index.html>

- Lov om tilsyn med elektriske anlegg og elektrisk utstyr (1929)
- Arbeidsmiljøloven
- Forskrift om systematisk helse-, miljø- og sikkerhetsarbeid (HMS Internkontrollforskrift)
- Forskrift om sikkerhet ved arbeid og drift av elektriske anlegg (FSE 2006)
- Forskrift om elektriske forsyningsanlegg (FEF 2006)
- Forskrift om utstyr og sikkerhetssystem til bruk i eksplosjonsfarlig område NEK 420
- Forskrift om håndtering av brannfarlig, reaksjonsfarlig og trykksatt stoff samt utstyr og anlegg som benyttes ved håndteringen
- Forskrift om Håndtering av eksplosjonsfarlig stoff
- Forskrift om bruk av arbeidsutstyr.
- Forskrift om Arbeidsplasser og arbeidslokaler
- Forskrift om Bruk av personlig verneutstyr på arbeidsplassen
- Forskrift om Helse og sikkerhet i eksplosjonsfarlige atmosfærer
- Forskrift om Høytrykkspyling
- Forskrift om Maskiner
- Forskrift om Sikkerhetsskilting og signalgivning på arbeidsplassen
- Forskrift om Stillaser, stiger og arbeid på tak m.m.
- Forskrift om Sveising, termisk skjæring, termisk sprøyting, kullbuemeisling, lodding og sliping (varmt arbeid)
- Forskrift om Tekniske innretninger
- Forskrift om Tungt og ensformig arbeid
- Forskrift om Vern mot eksponering for kjemikalier på arbeidsplassen (Kjemikalieforskriften)
- Forskrift om Vern mot kunstig optisk stråling på arbeidsplassen
- Forskrift om Vern mot mekaniske vibrasjoner
- Forskrift om Vern mot støy på arbeidsplassen

Veiledninger fra arbeidstilsynet

se: <http://www.arbeidstilsynet.no/regelverk/veiledninger.html>

## 11 DOCUMENTATION

- Tegninger, foto, beskrivelser av forsøksoppsetningen
- Hazop\_mal
- Sertifikat for trykkpåkjent utstyr
- Håndtering avfall i NTNU
- Sikker bruk av LASERE, retningslinje
- HAZOP\_MAL\_Prosegyre
- Forsøksprosedyre
- Opplæringsplan for operatører
- Skjema for sikker jobb analyse, (SJA)
- Apparatorkortet
- Forsøk pågår kort

## 12 GUIDANCE TO RISK ASSESSMENT TEMPLATE

### **Chapter 7 Assessment of technical safety.**

Ensure that the design of the experiment set up is optimized in terms of technical safety.

Identifying risk factors related to the selected design, and possibly to initiate re-design to ensure that risk is eliminated as much as possible through technical security.

This should describe what the experimental setup actually are able to manage and acceptance for emission.

#### **7.1 HAZOP**

The experimental set up is divided into nodes (eg motor unit, pump unit, cooling unit.). By using guidewords to identify causes, consequences and safeguards, recommendations and conclusions are made according to if necessary safety is obtained. When actions are performed the HAZOP is completed.

(e.g. "No flow", cause: the pipe is deformed, consequence: pump runs hot, precaution: measurement of flow with a link to the emergency or if the consequence is not critical used manual monitoring and are written into the operational procedure.)

#### **7.2 Flammable, reactive and pressurized substances and gas.**

*According to the Regulations for handling of flammable, reactive and pressurized substances and equipment and facilities used for this:*

**Flammable material:** Solid, liquid or gaseous substance, preparation, and substance with occurrence or combination of these conditions, by its flash point, contact with other substances, pressure, temperature or other chemical properties represent a danger of fire.

**Reactive substances:** Solid, liquid, or gaseous substances, preparations and substances that occur in combinations of these conditions, which on contact with water, by its pressure, temperature or chemical conditions, represents a potentially dangerous reaction, explosion or release of hazardous gas, steam, dust or fog.

**Pressurized :** Other solid, liquid or gaseous substance or mixes having fire or hazardous material response, when under pressure, and thus may represent a risk of uncontrolled emissions

Further criteria for the classification of flammable, reactive and pressurized substances are set out in Annex 1 of the Guide to the Regulations "Flammable, reactive and pressurized substances"

<http://www.dsb.no/Global/Publikasjoner/2009/Veiledning/Generell%20veiledning.pdf>

[http://www.dsb.no/Global/Publikasjoner/2010/Tema/Temaveiledning\\_bruk\\_av\\_farlig\\_stoff\\_Del\\_1.pdf](http://www.dsb.no/Global/Publikasjoner/2010/Tema/Temaveiledning_bruk_av_farlig_stoff_Del_1.pdf)

Experiment setup area should be reviewed with respect to the assessment of Ex zone

- Zone 0: Always explosive atmosphere, such as inside the tank with gas, flammable liquid.
- Zone 1: Primary zone, sometimes explosive atmosphere such as a complete drain point
- Zone 2: secondary discharge could cause an explosive atmosphere by accident, such as flanges, valves and connection points



## 7.4 Effects on the environment

With pollution means: bringing solids, liquid or gas to air, water or ground, noise and vibrations, influence of temperature that may cause damage or inconvenience effect to the environment.

Regulations: <http://www.lovddata.no/all/hi-19810313-006.html#6>

NTNU guidance to handling of waste: <http://www.ntnu.no/hms/retningslinjer/HMSR18B.pdf>

## 7.5 Radiation

Definition of radiation

<b>Ionizing radiation:</b> Electromagnetic radiation (in radiation issues with wavelength <100 nm) or rapid atomic particles (e.g. alpha and beta particles) with the ability to stream ionized atoms or molecules.
<b>Non ionizing radiation:</b> Electromagnetic radiation (wavelength >100 nm), og ultrasound <sub>1</sub> with small or no capability to ionize.
<b>Radiation sources:</b> All ionizing and powerful non-ionizing radiation sources.
<b>Ionizing radiation sources:</b> Sources giving ionizing radiation e.g. all types of radiation sources, x-ray, and electron microscopes.
<b>Powerful non ionizing radiation sources:</b> Sources giving powerful non ionizing radiation which can harm health and/or environment, e.g. class 3B and 4. MR <sub>2</sub> systems, UVC <sub>3</sub> sources, powerful IR sources <sub>4</sub> .
<sub>1</sub> Ultrasound is an acoustic radiation ("sound") over the audible frequency range (> 20 kHz). In radiation protection regulations are referred to ultrasound with electromagnetic non-ionizing radiation.
<sub>2</sub> MR (e.g. NMR) - nuclear magnetic resonance method that is used to "depict" inner structures of different materials.
<sub>3</sub> UVC is electromagnetic radiation in the wavelength range 100-280 nm.
<sub>4</sub> IR is electromagnetic radiation in the wavelength range 700 nm - 1 mm.

For each laser there should be an information binder (HMSRV3404B) which shall include:

- General information
- Name of the instrument manager, deputy, and local radiation protection coordinator
- Key data on the apparatus
- Instrument-specific documentation
- References to (or copies of) data sheets, radiation protection regulations, etc.
- Assessments of risk factors
- Instructions for users
- Instructions for practical use, startup, operation, shutdown, safety precautions, logging, locking, or use of radiation sensor, etc.
- Emergency procedures
- See NTNU for laser: <http://www.ntnu.no/hms/retningslinjer/HMSR34B.pdf>

## 7.6 The use and handling of chemicals.

In the meaning chemicals, a element that can pose a danger to employee safety and health

See: <http://www.lovddata.no/cgi-wift/ldles?doc=/sf/sf/sf-20010430-0443.html>

Safety datasheet is to be kept in the HSE binder for the experiment set up and registered in the database for chemicals.

## **Chapter 8 Assessment of operational procedures.**

Ensures that established procedures meet all identified risk factors that must be taken care of through operational barriers and that the operators and technical performance have sufficient expertise.

### **8.1 Procedure Hazop**

Procedural HAZOP is a systematic review of the current procedure, using the fixed HAZOP methodology and defined guidewords. The procedure is broken into individual operations (nodes) and analyzed using guidewords to identify possible nonconformity, confusion or sources of inadequate performance and failure.

### **8.2 Procedure for running experiments and emergency shutdown.**

Have to be prepared for all experiment setups.

*The operating procedure has to describe stepwise preparation, startup, during and ending conditions of an experiment. The procedure should describe the assumptions and conditions for starting, operating parameters with the deviation allowed before aborting the experiment and the condition of the rig to be abandoned.*

*Emergency procedure describes how an emergency shutdown have to be done, (conducted by the uninitiated),*

*what happens when emergency shutdown, is activated. (electricity / gas supply) and which events will activate the emergency shutdown (fire, leakage).*

## **Chapter 9 Quantifying of RISK**

Quantifying of the residue hazards, Risk matrix

To illustrate the overall risk, compared to the risk assessment, each activity is plotted with values for the probability and consequence into the matrix. Use task IDnr.

Example: If activity IDnr. 1 has been given a probability 3 and D for consequence the risk value become D3, red. This is done for all activities giving them risk values.

In the matrix are different degrees of risk highlighted in red, yellow or green. When an activity ends up on a red risk (= unacceptable risk), risk reducing action has to be taken

<b>CONSEQUENCES</b>	Catastrophic	<b>E1</b>	<b>E2</b>	<b>E3</b>	<b>E4</b>	<b>E5</b>
	Major	<b>D1</b>	<b>D2</b>	<b>D3</b>	<b>D4</b>	<b>D5</b>
	Moderate	<b>C1</b>	<b>C2</b>	<b>C3</b>	<b>C4</b>	<b>C5</b>
	Minor	<b>B1</b>	<b>B2</b>	<b>B3</b>	<b>B4</b>	<b>B5</b>
	Insignificant	<b>A1</b>	<b>A2</b>	<b>A3</b>	<b>A4</b>	<b>A5</b>
		Rare	Unlikely	Possible	Likely	Almost
		<b>PROBABILITY</b>				

Table 8. Risk's Matrix

Table 9. The principle of the acceptance criterion. Explanation of the colors used in the matrix

COLOUR	DESCRIPTION
Red	Unacceptable risk Action has to be taken to reduce risk
Yellow	Assessment area. Actions has to be considered
Green	Acceptable risk. Action can be taken based on other criteria

# Attachment to Risk Assessment report

## Centrifugal Pump Rig

<b>Prosjektnavn</b>	LDA measurements in a Centrifugal Pump
<b>Apparatur</b>	Laser modell 177-GO232, serienr T10502
<b>Enhet</b>	EPT
<b>Apparaturansvarlig</b>	Bård Brandåstrø
<b>Prosjektleder</b>	Torbjørn K. Nielsen
<b>HMS-koordinator</b>	Morten Grønli
<b>HMS-ansvarlig (linjeleder)</b>	Olav Bolland
<b>Plassering</b>	Waterpower Laboratory
<b>Romnummer</b>	11
<b>Risikovurdering utført av</b>	Karl Oskar Pires Bjørgen and Alessandro Nocente, with help from Halvor Haukvik

### TABLE OF CONTENTS

ATTACHMENT A: PROCESS AND INSTRUMENTATION DIAGRAM	1
ATTACHMENT B: HAZOP TEMPLATE	2
ATTACHMENT C: TEST CERTIFICATE FOR LOCAL PRESSURE TESTING	4
ATTACHMENT D: HAZOP PROCEDURE (TEMPLATE)	5
ATTACHMENT E: PROCEDURE FOR RUNNING EXPERIMENTS	6
ATTACHMENT F: TRAINING OF OPERATORS	8
ATTACHMENT G: FORM FOR SAFE JOB ANALYSIS	9
APPARATURKORT / UNITCARD	11
FORSØK PÅGÅR / EXPERIMENT IN PROGRESS	12

**ATTACHMENT A: PROCESS AND INSTRUMENTATION DIAGRAM**

**ATTACHMENT B: HAZOP TEMPLATE**

Project: Node: Laser							Page
Ref	Guideword	Causes	Consequences	Safeguards	Recommendations	Action	Date/Sign
	Unintentional rarefaction of beam	Poor alignment of laser beam, unintentional beam obstruction	Damage to personnel, damage to equipment	Laser emitter latched in place, radiation area enclosed	Careful instrument handling		
	Laser generation unit temperature rise	Cooling fan failure	Equipment will overheat and break	-	Be aware of equipment condition		
	Unprotected personnel entering radiation area	Insufficient signalling, radiation area too accessible	Possibility of severe damage to personnel	Signalling and warning light in place, radiation area enclosed with physical obstruction	Always run experiments with warning light on		
	Electrical failures in apparatuses	Wear, poor construction	Equipment failure				
	Fire hazard	Laser beam hitting flammable material	Fire	Enclosing fabric approved for shielding laser experiments.	Make sure a fire extinguisher is easily available		
	Beam interception by operator	Careless equipment handling, obstructed work area	Damage to personnel, severe if lacking protective gear	Goggles approved for laser in use worn by operator	Careful instrument handling		

**ATTACHMENT C: TEST CERTIFICATE FOR LOCAL PRESSURE TESTING**

Trykkpåkjent utstyr:	
Benyttes i rigg:	
Design trykk for utstyr (bara):	
Maksimum tillatt trykk (bara): (i.e. burst pressure om kjent)	
Maksimum driftstrykk i denne rigg:	

**Prøvetrykket skal fastlegges i følge standarden og med hensyn til maksimum tillatt trykk.**

Prøvetrykk (bara):	
X maksimum driftstrykk: I følge standard	
Test medium:	
Temperatur (°C)	
Start tid:	Trykk (bara):
Slutt tid:	Trykk (bara):
Maksimum driftstrykk i denne rigg:	

Eventuelle repetisjoner fra atm. trykk til maksimum prøvetrykk:.....

Test trykket, dato for testing og maksimum tillatt driftstrykk skal markers på (skilt eller innslått)

\_\_\_\_\_  
Sted og dato

\_\_\_\_\_  
Signatur

**ATTACHMENT D: HAZOP PROCEDURE (TEMPLATE)**

Project: Node: 1							Page
Ref#	Guideword	Causes	Consequences	Safeguards	Recommendations	Action	Date/Sign
	Not clear procedure	Procedure is too ambitious, or confusingly					
	Step in the wrong place	The procedure can lead to actions done in the wrong pattern or sequence					
	Wrong actions	Procedure improperly specified					
	Incorrect information	Information provided in advance of the specified action is wrong					
	Step missing	Missing step, or step requires too much of operator					
	Step unsuccessful	Step has a high probability of failure					
	Influence and effects from other	Procedure's performance can be affected by other sources					



## ATTACHMENT E: PROCEDURE FOR RUNNING EXPERIMENTS

<b>Prosjekt</b> LDV measurements in the centrifugal pump	<b>Dato</b>	<b>Signatur</b>
<b>Apparatur</b> Laser modell 177-GO232, serienr T10502		
<b>Prosjektleder</b> Torbjørn K. Nielsen		

	<b>Conditions for the experiment:</b>	<b>Completed</b>
	Experiments should be run in normal working hours, 08:00-16:00 during winter time and 08.00-15.00 during summer time. Experiments outside normal working hours shall be approved.	
	One person must always be present while running experiments, and should be approved as an experimental leader.	
	An early warning is given according to the lab rules, and accepted by authorized personnel.	
	Be sure that everyone taking part of the experiment is wearing the necessary protecting equipment and is aware of the shut down procedure and escape routes.	
	<b>Preparations</b>	<b>Carried out</b>
	Post the "Experiment in progress" sign.	
	<i>Start computer with red cable inserted</i>	
	<i>Set Local Area IP to 10.x.x.x (10.10.100.25) and subnet mask to 255.0.0.0</i>	
	<i>Turn on power supply (huge box)</i>	
	<i>Start BSA software when the "Ready" lamp is lit, and start/open a project</i>	
	<i>When connected, the "On-line" lamp should be lit. If problems connecting, make sure that the IP of the processor is set to 10.10.100.100</i>	
	<i>Prepare experiment</i>	
	<i>Double check that the area is properly shielded and signalled</i>	
	<i>Turn on laser – Mode switch:Power</i>	
	<i>Mode switch: Run</i>	
	<i>Power knob: Minimum</i>	
	<i>Discharge: On</i>	
	<i>Power switch: On</i>	
	<i>Turn key on (display goes to ~40 after 35 seconds)</i>	
	<b>During the experiment</b>	
	<i>Keep unauthorized personnel out of radiation area</i>	
	<i>Avoid wearing jewellery and/or shiny objects</i>	
	<b>End of experiment</b>	
	<i>Turn off power supply (huge box)</i>	
	<i>Power knob: minimum</i>	
	<i>Mode switch: Standby</i>	
	<i>Turn key to off position</i>	
	<i>Discharge: Off</i>	

	<i>Wait until the cooling fans have stopped</i>	
	<i>Power switch: Off</i>	
	<i>Remove all obstructions/barriers/signs around the experiment.</i>	
	<i>Tidy up and return all tools and equipment.</i>	
	<i>Tidy and cleanup work areas.</i>	
	Return equipment and systems back to their normal operation settings <i>(fire alarm)</i>	
	<b>To reflect on before the next experiment and experience useful for others</b>	
	Was the experiment completed as planned and on scheduled in professional terms?	
	Was the competence which was needed for security and completion of the experiment available to you?	
	Do you have any information/ knowledge from the experiment that you should document and share with fellow colleagues?	

**Operator(s):**

Navn	Dato	Signatur

## ATTACHMENT F: TRAINING OF OPERATORS

Prosjekt	Dato	Signatur
LDV measurements on the centrifugal rig		
<b>Apparatur</b> Laser modell 177-GO232, serienr T10502		
<b>Prosjektleder</b> Torbjørn K. Nielsen		

	<b>Knowledge about EPT LAB in general</b>	
	Lab <ul style="list-style-type: none"> <li>• Access</li> <li>• routines and rules</li> <li>• working hour</li> </ul>	
	Knowledge about the evacuation procedures.	
	Activity calendar for the Lab	
	Early warning, <a href="mailto:iept-experiments@ivt.ntnu.no">iept-experiments@ivt.ntnu.no</a>	
	<b>Knowledge about the experiments</b>	
	Procedures for the experiments	
	Emergency shutdown.	
	Nearest fire and first aid station.	

I hereby declare that I have read and understood the regulatory requirements has received appropriate training to run this experiment and are aware of my personal responsibility by working in EPT laboratories.

### Operator(s):

Navn	Dato	Signatur
Alessandro Nocente		
Karl Oskar Pires Bjørgen		

## ATTACHMENT G: FORM FOR SAFE JOB ANALYSIS

<b>SJA name:</b>	
Date:	Location:
Mark for completed checklist:	

<b>Participators:</b>		
SJA-responsible:		

Specification of work (What and how?):
Risks associated with the work:
Safeguards: (plan for actions, see next page):
Conclusions/comments:

Recommended/approved	Date/Signature:	Recommended/approved	Date/Signature:
SJA-responsible:		HSE responsible:	
Responsible for work:		Other, (position):	

HSE aspect	Yes	No	NA	Comments / actions	Resp.
<b>Documentation, experience, qualifications</b>					
Known operation or work?	X				
Knowledge of experiences / incidents from similar operations?		X			
Necessary personnel?	X				
<b>Communication and coordinating</b>					
Potential conflicts with other operations?		X			
Handling of an eventually incident (alarm, evacuation)?		X			
Need for extra assistance / watch?		X			
<b>Working area</b>					
Unusual working position		X			
Work in tanks, manhole?		X			
Work in ditch, shaft or pit?		X			
Clean and tidy?	X				
Protective equipment beyond the personal?		X			
Weather, wind, visibility, lighting, ventilation?	X				
Usage of scaffolding/lifts/belts/ straps, anti-falling device?		X			
Work at heights?		X			
Ionizing radiation?		X			
Influence of escape routes?		X			
<b>Chemical hazards</b>					
Usage of hazardous/toxic/corrosive chemicals?		X			
Usage of flammable or explosive chemicals?		X			
Risk assessment of usage?	X				
Biological materials/substances?		X			
Dust/asbestos/dust from insulation?		X			
<b>Mechanical hazards</b>					
Stability/strength/tension?		X			
Crush/clamp/cut/hit?		X			
Dust/pressure/temperature?		X			
Handling of waste disposal?		X			
Need of special tools?		X			
<b>Electrical hazards</b>					
Current/Voltage/over 1000V?		X			
Current surge, short circuit?		X			
Loss of current supply?		X			
<b>Area</b>					
Need for inspection?	X				
Marking/system of signs/rope off?	X				
Environmental consequences?		X			
<b>Key physical security systems</b>					
Work on or demounting of safety systems?		X			
<b>Other</b>					

## APPARATURKORT / UNITCARD

**Dette kortet SKAL henges godt synlig på apparaturen!**  
***This card MUST be posted on a visible place on the unit!***

<b>Apparatur (Unit)</b> LDV measurements in centrifugal rig	
<b>Prosjektleder (Project Leader)</b> Torbjørn K. Nielsen	<b>Telefon mobil/privat (Phone no. mobile/private)</b>
<b>Apparaturansvarlig (Unit Responsible)</b> Bård Brandåstrø	<b>Telefon mobil/privat (Phone no. mobile/private)</b>
<b>Sikkerhetsrisikoer (Safety hazards)</b> Laser light	
<b>Sikkerhetsregler (Safety rules)</b> -Wear appropriate safety goggles for laser wavelength -no shiny objects (eg. Jewellery) worn	
<b>Nødstop prosedyre (Emergency shutdown)</b> Turn off or unplug the laser from the power supply	

**Her finner du (Here you will find):**

<b>Prosedyrer (Procedures)</b>	Apparaturperm ved laser
<b>Bruksanvisning (Users manual)</b>	Apparaturperm ved laser

**Nærmeste (Nearest)**

<b>Brannslukningsapparat (fire extinguisher)</b>	Vestveggen i Lab
<b>Førstehjelpsskap (first aid cabinet)</b>	Vestveggen i Lab

**NTNU**  
**Institutt for energi og prosessteknikk**

**SINTEF Energi**  
**Avdeling energiprosesser**

**Dato**

**Dato**

**Signert**

**Signert**

## FORSØK PÅGÅR / EXPERIMENT IN PROGRESS

**Dette kortet SKAL henges opp før forsøk kan starte!**  
***This card MUST be posted on the unit before the experiment startup!***

<b>Apparatur (Unit)</b> LDV measurements in centrifugal pump	
<b>Prosjektleder (Project Leader)</b> Torbjørn K. Nielsen	<b>Telefon mobil/privat (Phone no. mobile/private)</b>
<b>Apparaturansvarlig (Unit Responsible)</b> Bård Brandåstrø	<b>Telefon mobil/privat (Phone no. mobile/private)</b>
<b>Godkjente operatører (Approved Operators)</b> Alessandro Nocente Karl Oskar Pires Bjørgen	<b>Telefon mobil/privat (Phone no. mobile/private)</b>
<b>Prosjekt (Project)</b> LDV measurements in centrifugal pump	
<b>Forsøksstid / Experimental time (start - stop)</b> 01.10.2014 – 31.11.2014	
<b>Kort beskrivelse av forsøket og relaterte farer (Short description of the experiment and related hazards)</b> Laser measurements with class IV laser on the centrifugal pump rig, danger of eye injury and skin injury. Radiation area clearly marked.	

**NTNU**  
**Institutt for energi og prosesseteknikk**

**SINTEF Energi**  
**Avdeling energiprosesser**

**Dato**

---

**Dato**

---

**Signert**

---

**Signert**

---

# Risk Assessment Report

## Centrifugal Pump Rig

<b>Prosjektnavn</b>	LDA measurements in a Centrifugal Pump
<b>Apparatur</b>	Singlestage Centrifugal Pump
<b>Enhet</b>	EPT
<b>Apparaturansvarlig</b>	Bård Brandåstrø
<b>Prosjektleder</b>	Torbjørn K. Nielsen
<b>HMS-koordinator</b>	Morten Grønli
<b>HMS-ansvarlig (linjeleder)</b>	Olav Bolland
<b>Plassering</b>	Waterpower Laboratory
<b>Romnummer</b>	11
<b>Risikovurdering utført av</b>	Karl Oskar Pires Bjørgen and Alessandro Nocente, with help from Halvor Haukvik

### *Approval:*

<b>Apparatur kort (UNIT CARD) valid for:</b>	
<b>Forsøk pågår kort (EXPERIMENT IN PROGRESS) valid for:</b>	

Rolle	Navn	Dato	Signatur
<b>Prosjektleder</b>	Torbjørn K. Nielsen		
<b>HMS koordinator</b>	Morten Grønli		
<b>HMS ansvarlig (linjeleder)</b>	Olav Bolland		



## TABLE OF CONTENTS

1	INTRODUCTION	1
2	CONCLUSION	1
3	ORGANISATION	1
4	RISK MANAGEMENT IN THE PROJECT	1
5	DESCRIPTIONS OF EXPERIMENTAL SETUP	2
6	EVACUATION FROM THE EXPERIMENTAL AREA	2
7	WARNING	2
7.1	Before experiments.....	2
7.2	Non-conformance.....	2
8	ASSESSMENT OF TECHNICAL SAFETY	3
8.1	HAZOP.....	3
8.2	Flammable, reactive and pressurized substances and gas.....	3
8.3	Pressurized equipment.....	4
8.4	Effects on the environment (emissions, noise, temperature, vibration, smell).....	4
8.5	Radiation.....	4
8.6	Chemicals.....	4
8.7	Electricity safety (deviations from the norms/standards).....	4
9	ASSESSMENT OF OPERATIONAL SAFETY	5
9.1	Procedure HAZOP.....	5
9.2	Operation and emergency shutdown procedure.....	5
9.3	Training of operators.....	5
9.4	Technical modifications.....	5
9.5	Personal protective equipment.....	5
9.5.1	General Safety.....	5
9.6	Safety equipment.....	6
9.7	Special predations.....	6
10	QUANTIFYING OF RISK - RISK MATRIX	6
11	REGULATIONS AND GUIDELINES	7
12	DOCUMENTATION	8
13	GUIDANCE TO RISK ASSESSMENT TEMPLATE	8

## 1 INTRODUCTION

LDA measurements will be conducted. Operation of the centrifugal pump will take place in the Waterpower Laboratory at NTNU. The measurements will take place in October and November of 2014.

## 2 ORGANISATION

Rolle	
Prosjektleder	Torbjørn K. Nielsen
Apparaturansvarlig	Bård Brandåstrø
Romansvarlig	Bård Brandåstrø
HMS koordinator	Morten Grønli
HMS ansvarlig (linjeleder):	Olav Bolland

## 3 RISK MANAGEMENT IN THE PROJECT

Hovedaktiviteter risikostyring	Nødvendige tiltak, dokumentasjon	DATE
Prosjekt initiering	Prosjekt initiering mal	
Veiledningsmøte Guidance Meeting	Skjema for Veiledningsmøte med pre-risikovurdering	
Innledende risikovurdering Initial Assessment	Fareidentifikasjon – HAZID Skjema grovanalyse	
Vurdering av teknisk sikkerhet Evaluation of technical security	Prosess-HAZOP Tekniske dokumentasjoner	
Vurdering av operasjonell sikkerhet Evaluation of operational safety	Prosedyre-HAZOP Opplæringsplan for operatører	
Sluttvurdering, kvalitetssikring Final assessment, quality assurance	Uavhengig kontroll Utstedelse av apparaturkort Utstedelse av forsøk pågår kort	

## 4 DESCRIPTIONS OF EXPERIMENTAL SETUP

- Drawings and photos describing the setup.
- Process and Instrumentation Diagram (PID) with list of components
- Location of the operator, gas bottles, shutdown valves for water / air.

## 5 EVACUATION FROM THE EXPERIMENTAL AREA

Evacuate at signal from the alarm system or local gas alarms with its own local alert with sound and light outside the room in question, see 6.2

Evacuation from the rigging area takes place through the marked emergency exits to the assembly point, (corner of Old Chemistry Kjelhuset or parking 1a-b.)

### Action on rig before evacuation:

*Describe in which condition the rig should be left in case of evacuation (emergency shutdown procedure, water, gas, electric supply, etc.)*

## 6 WARNING

### 6.1 Before experiments

Send an e-mail with information about the planned experiment to:

[iept-experiments@ivt.ntnu.no](mailto:iept-experiments@ivt.ntnu.no)

### The e-mail must include the following information:

- Name of responsible person:
- Experimental setup/rig:
- Start Experiments: (date and time)
- Stop Experiments: (date and time)

You must get the approval back from the laboratory management before start up. All running experiments are notified in the activity calendar for the lab to be sure they are coordinated with other activity.

### 6.2 Non-conformance

#### FIRE

If you are NOT able to extinguish the fire, activate the nearest fire alarm and evacuate area. Be then available for fire brigade and building caretaker to detect fire place.

If possible, notify:

NTNU	SINTEF
Morten Grønli, Mob: 918 97 515	Harald Mæhlum, Mob: 930 14 986
Olav Bolland: Mob: 918 97 209	Anne Karin T. Hemmingsen Mob: 930 19 669

NTNU – SINTEF Beredskapstelefon	800 80 388
---------------------------------	------------

### **GAS ALARM**

If a gas alarm occurs, close gas bottles immediately and ventilate the area. If the level of the gas concentration does not decrease within a reasonable time, activate the fire alarm and evacuate the lab. Designated personnel or fire department checks the leak to determine whether it is possible to seal the leak and ventilate the area in a responsible manner.

### **PERSONAL INJURY**

- First aid kit in the fire / first aid stations
- Shout for help
- Start life-saving first aid
- **CALL 113** if there is any doubt whether there is a serious injury

### **OTHER NON-CONFORMANCE (AVVIK)**

#### **NTNU:**

You will find the reporting form for non-conformance on:

<https://innsida.ntnu.no/wiki/-/wiki/Norsk/Melde+avvik>

#### **SINTEF:**

Synergi

## **7 ASSESSMENT OF TECHNICAL SAFETY**

### **7.1 HAZOP**

*See Chapter 13 "Guide to the report template".*

The experiment set up is divided into the following nodes:

Node 1	Electrical motor
Node 2	Test rig
Node 3	Tank

**Attachments, Form: Hazop\_mal**

**Conclusion:**

#### **Node 1:**

- **Shutdown button is clearly marked.**

### **7.2 Flammable, reactive and pressurized substances and gas**

Are any flammable, reactive and pressurized substances and gases in use?

NO	
----	--

### **7.3 Pressurized equipment**

Is any pressurized equipment in use?

NO	
----	--

#### 7.4 Effects on the environment (emissions, noise, temperature, vibration, smell)

NO	
----	--

#### 7.5 Radiation

*See Chapter 13 "Guide to the report template".*

NO	
----	--

**Attachments:**

**Conclusion:**

#### 7.6 Chemicals

NO	
----	--

#### 7.7 Electricity safety (deviations from the norms/standards)

YES	Electrical danger from the motor
-----	----------------------------------

## 8 ASSESSMENT OF OPERATIONAL SAFETY

Ensure that the procedures cover all identified risk factors that must be taken care of. Ensure that the operators and technical performance have sufficient expertise.

### 8.1 Procedure HAZOP

*See Chapter 13 "Guide to the report template".*

The method is a procedure to identify causes and sources of danger to operational problems.

**Attachments:** HAZOP\_MAL\_Proseedyre

### 8.2 Operation procedure and emergency shutdown procedure

*See Chapter 13 "Guide to the report template".*

The operating procedure is a checklist that must be filled out for each experiment.

Emergency procedure should attempt to set the experiment set up in a harmless state by unforeseen events.

**Attachments:** Procedure for running experiments

**Emergency shutdown procedure:**

### 8.3 Training of operators

### 8.4 Technical modifications

### 8.5 Personal protective equipment

- *It is mandatory use of eye protection in the rig zone*

### 8.6 General Safety

- *The area around the staging attempts shielded.*
- *Operator has to be present during experiments.*

### 8.7 Safety equipment

- *Warning signs, see the Regulations on Safety signs and signalling in the workplace*

### 8.8 Special predations

## 9 QUANTIFYING OF RISK - RISK MATRIX

*See Chapter 13 "Guide to the report template".*

The risk matrix will provide visualization and an overview of activity risks so that management and users get the most complete picture of risk factors.

IDnr	Aktivitet-hendelse	Frekv-Sans	Kons	RV
1	<i>Rotating machinery could break and possibly damage people or equipment nearby</i>	1	D	D1
2	<i>Noise</i>	2	B	B2
3	<i>Contact with the rotating machinery</i>	1	C	B1
4	<i>Debris from the rotating machinery</i>	1	B	B1

**Conclusion:** There is little risk involved in using the test rig. However by coming in contact with the rotating machinery, or operating it without knowing the risks and how to operate it, significant damage could occur. Noise is also a hazard, ear protection should be used.

## 10 REGULATIONS AND GUIDELINES

Se <http://www.arbeidstilsynet.no/regelverk/index.html>

- Lov om tilsyn med elektriske anlegg og elektrisk utstyr (1929)
- Arbeidsmiljøloven
- Forskrift om systematisk helse-, miljø- og sikkerhetsarbeid (HMS Internkontrollforskrift)
- Forskrift om sikkerhet ved arbeid og drift av elektriske anlegg (FSE 2006)
- Forskrift om elektriske forsyningsanlegg (FEF 2006)
- Forskrift om utstyr og sikkerhetssystem til bruk i eksplosjonsfarlig område NEK 420
- Forskrift om håndtering av brannfarlig, reaksjonsfarlig og trykksatt stoff samt utstyr og anlegg som benyttes ved håndteringen
- Forskrift om Håndtering av eksplosjonsfarlig stoff
- Forskrift om bruk av arbeidsutstyr.
- Forskrift om Arbeidsplasser og arbeidslokaler
- Forskrift om Bruk av personlig verneutstyr på arbeidsplassen
- Forskrift om Helse og sikkerhet i eksplosjonsfarlige atmosfærer
- Forskrift om Høytrykkspyling
- Forskrift om Maskiner
- Forskrift om Sikkerhetsskilting og signalgivning på arbeidsplassen
- Forskrift om Stillaser, stiger og arbeid på tak m.m.
- Forskrift om Sveising, termisk skjæring, termisk sprøyting, kullbuemeisling, lodding og sliping (varmt arbeid)
- Forskrift om Tekniske innretninger
- Forskrift om Tungt og ensformig arbeid
- Forskrift om Vern mot eksponering for kjemikalier på arbeidsplassen (Kjemikalieforskriften)
- Forskrift om Vern mot kunstig optisk stråling på arbeidsplassen
- Forskrift om Vern mot mekaniske vibrasjoner
- Forskrift om Vern mot støy på arbeidsplassen

Veiledninger fra arbeidstilsynet

se: <http://www.arbeidstilsynet.no/regelverk/veiledninger.html>

## 11 DOCUMENTATION

- Tegninger, foto, beskrivelser av forsøksoppsetningen
- Hazop\_mal
- Sertifikat for trykkpåkjent utstyr
- Håndtering avfall i NTNU
- Sikker bruk av LASERE, retningslinje
- HAZOP\_MAL\_Prosekyre
- Forsøksprosedyre
- Opplæringsplan for operatører
- Skjema for sikker jobb analyse, (SJA)
- Apparatkortet
- Forsøk pågår kort

## 12 GUIDANCE TO RISK ASSESSMENT TEMPLATE

### **Chapter 7 Assessment of technical safety.**

Ensure that the design of the experiment set up is optimized in terms of technical safety.

Identifying risk factors related to the selected design, and possibly to initiate re-design to ensure that risk is eliminated as much as possible through technical security.

This should describe what the experimental setup actually are able to manage and acceptance for emission.

#### **7.1 HAZOP**

The experimental set up is divided into nodes (eg motor unit, pump unit, cooling unit.). By using guidewords to identify causes, consequences and safeguards, recommendations and conclusions are made according to if necessary safety is obtained. When actions are performed the HAZOP is completed.

(e.g. "No flow", cause: the pipe is deformed, consequence: pump runs hot, precaution: measurement of flow with a link to the emergency or if the consequence is not critical used manual monitoring and are written into the operational procedure.)

#### **7.2 Flammable, reactive and pressurized substances and gas.**

*According to the Regulations for handling of flammable, reactive and pressurized substances and equipment and facilities used for this:*

**Flammable material:** Solid, liquid or gaseous substance, preparation, and substance with occurrence or combination of these conditions, by its flash point, contact with other substances, pressure, temperature or other chemical properties represent a danger of fire.

**Reactive substances:** Solid, liquid, or gaseous substances, preparations and substances that occur in combinations of these conditions, which on contact with water, by its pressure, temperature or chemical conditions, represents a potentially dangerous reaction, explosion or release of hazardous gas, steam, dust or fog.

**Pressurized :** Other solid, liquid or gaseous substance or mixes having fire or hazardous material response, when under pressure, and thus may represent a risk of uncontrolled emissions

Further criteria for the classification of flammable, reactive and pressurized substances are set out in Annex 1 of the Guide to the Regulations "Flammable, reactive and pressurized substances"

<http://www.dsb.no/Global/Publikasjoner/2009/Veiledning/Generell%20veiledning.pdf>

[http://www.dsb.no/Global/Publikasjoner/2010/Tema/Temaveiledning\\_bruk\\_av\\_farlig\\_stoff\\_Del\\_1.pdf](http://www.dsb.no/Global/Publikasjoner/2010/Tema/Temaveiledning_bruk_av_farlig_stoff_Del_1.pdf)

Experiment setup area should be reviewed with respect to the assessment of Ex zone

- Zone 0: Always explosive atmosphere, such as inside the tank with gas, flammable liquid.
- Zone 1: Primary zone, sometimes explosive atmosphere such as a complete drain point
- Zone 2: secondary discharge could cause an explosive atmosphere by accident, such as flanges, valves and connection points



## 7.4 Effects on the environment

With pollution means: bringing solids, liquid or gas to air, water or ground, noise and vibrations, influence of temperature that may cause damage or inconvenience effect to the environment.

Regulations: <http://www.lovddata.no/all/hi-19810313-006.html#6>

NTNU guidance to handling of waste: <http://www.ntnu.no/hms/retningslinjer/HMSR18B.pdf>

## 7.5 Radiation

Definition of radiation

<b>Ionizing radiation:</b> Electromagnetic radiation (in radiation issues with wavelength <100 nm) or rapid atomic particles (e.g. alpha and beta particles) with the ability to stream ionized atoms or molecules.
<b>Non ionizing radiation:</b> Electromagnetic radiation (wavelength >100 nm), og ultrasound <sub>1</sub> with small or no capability to ionize.
<b>Radiation sources:</b> All ionizing and powerful non-ionizing radiation sources.
<b>Ionizing radiation sources:</b> Sources giving ionizing radiation e.g. all types of radiation sources, x-ray, and electron microscopes.
<b>Powerful non ionizing radiation sources:</b> Sources giving powerful non ionizing radiation which can harm health and/or environment, e.g. class 3B and 4. MR <sub>2</sub> systems, UVC <sub>3</sub> sources, powerful IR sources <sub>4</sub> .
<sub>1</sub> Ultrasound is an acoustic radiation ("sound") over the audible frequency range (> 20 kHz). In radiation protection regulations are referred to ultrasound with electromagnetic non-ionizing radiation.
<sub>2</sub> MR (e.g. NMR) - nuclear magnetic resonance method that is used to "depict" inner structures of different materials.
<sub>3</sub> UVC is electromagnetic radiation in the wavelength range 100-280 nm.
<sub>4</sub> IR is electromagnetic radiation in the wavelength range 700 nm - 1 mm.

For each laser there should be an information binder (HMSRV3404B) which shall include:

- General information
- Name of the instrument manager, deputy, and local radiation protection coordinator
- Key data on the apparatus
- Instrument-specific documentation
- References to (or copies of) data sheets, radiation protection regulations, etc.
- Assessments of risk factors
- Instructions for users
- Instructions for practical use, startup, operation, shutdown, safety precautions, logging, locking, or use of radiation sensor, etc.
- Emergency procedures
- See NTNU for laser: <http://www.ntnu.no/hms/retningslinjer/HMSR34B.pdf>

## 7.6 The use and handling of chemicals.

In the meaning chemicals, a element that can pose a danger to employee safety and health

See: <http://www.lovddata.no/cgi-wift/ldles?doc=/sf/sf/sf-20010430-0443.html>

Safety datasheet is to be kept in the HSE binder for the experiment set up and registered in the database for chemicals.

## **Chapter 8 Assessment of operational procedures.**

Ensures that established procedures meet all identified risk factors that must be taken care of through operational barriers and that the operators and technical performance have sufficient expertise.

### **8.1 Procedure Hazop**

Procedural HAZOP is a systematic review of the current procedure, using the fixed HAZOP methodology and defined guidewords. The procedure is broken into individual operations (nodes) and analyzed using guidewords to identify possible nonconformity, confusion or sources of inadequate performance and failure.

### **8.2 Procedure for running experiments and emergency shutdown.**

Have to be prepared for all experiment setups.

*The operating procedure has to describe stepwise preparation, startup, during and ending conditions of an experiment. The procedure should describe the assumptions and conditions for starting, operating parameters with the deviation allowed before aborting the experiment and the condition of the rig to be abandoned.*

*Emergency procedure describes how an emergency shutdown have to be done, (conducted by the uninitiated),*

*what happens when emergency shutdown, is activated. (electricity / gas supply) and which events will activate the emergency shutdown (fire, leakage).*

## **Chapter 9 Quantifying of RISK**

Quantifying of the residue hazards, Risk matrix

To illustrate the overall risk, compared to the risk assessment, each activity is plotted with values for the probability and consequence into the matrix. Use task IDnr.

Example: If activity IDnr. 1 has been given a probability 3 and D for consequence the risk value become D3, red. This is done for all activities giving them risk values.

In the matrix are different degrees of risk highlighted in red, yellow or green. When an activity ends up on a red risk (= unacceptable risk), risk reducing action has to be taken

<b>CONSEQUENCES</b>	Catastrophic	<b>E1</b>	<b>E2</b>	<b>E3</b>	<b>E4</b>	<b>E5</b>
	Major	<b>D1</b>	<b>D2</b>	<b>D3</b>	<b>D4</b>	<b>D5</b>
	Moderate	<b>C1</b>	<b>C2</b>	<b>C3</b>	<b>C4</b>	<b>C5</b>
	Minor	<b>B1</b>	<b>B2</b>	<b>B3</b>	<b>B4</b>	<b>B5</b>
	Insignificant	<b>A1</b>	<b>A2</b>	<b>A3</b>	<b>A4</b>	<b>A5</b>
		Rare	Unlikely	Possible	Likely	Almost
		<b>PROBABILITY</b>				

Table 8. Risk's Matrix

Table 9. The principle of the acceptance criterion. Explanation of the colors used in the matrix

COLOUR	DESCRIPTION
Red	Unacceptable risk Action has to be taken to reduce risk
Yellow	Assessment area. Actions has to be considered
Green	Acceptable risk. Action can be taken based on other criteria

# Attachment to Risk Assessment report

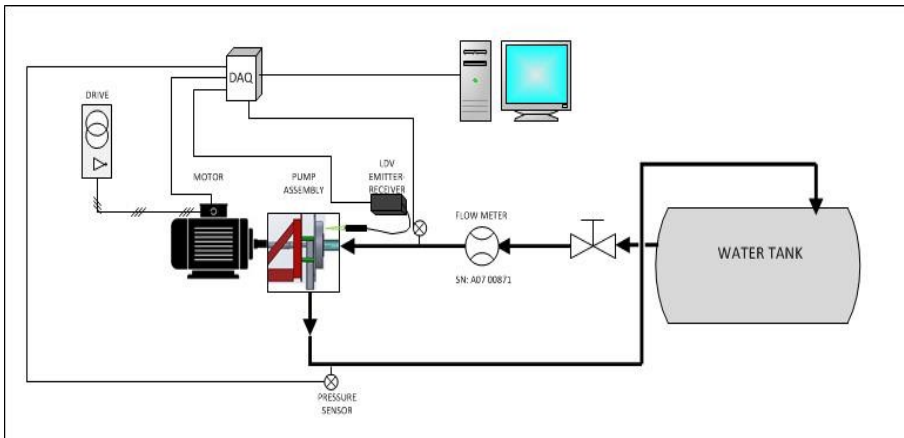
## Centrifugal Pump Rig

<b>Prosjektnavn</b>	LDA measurements in a Centrifugal Pump
<b>Apparatur</b>	Singlestage Centrifugal Pump
<b>Enhet</b>	EPT
<b>Apparaturansvarlig</b>	Bård Brandåstrø
<b>Prosjektleder</b>	Torbjørn K. Nielsen
<b>HMS-koordinator</b>	Morten Grønli
<b>HMS-ansvarlig (linjeleder)</b>	Olav Bolland
<b>Plassering</b>	Waterpower Laboratory
<b>Romnummer</b>	11
<b>Risikovurdering utført av</b>	Karl Oskar Pires Bjørgen and Alessandro Nocente, with help from Halvor Haukvik

### TABLE OF CONTENTS

ATTACHMENT A: PROCESS AND INSTRUMENTATION DIAGRAM	1
ATTACHMENT B: HAZOP TEMPLATE	2
ATTACHMENT C: TEST CERTIFICATE FOR LOCAL PRESSURE TESTING	4
ATTACHMENT D: HAZOP PROCEDURE (TEMPLATE)	5
ATTACHMENT E: PROCEDURE FOR RUNNING EXPERIMENTS	6
ATTACHMENT F: TRAINING OF OPERATORS	8
ATTACHMENT G: FORM FOR SAFE JOB ANALYSIS	9
APPARATURKORT / UNITCARD	11
FORSØK PÅGÅR / EXPERIMENT IN PROGRESS	12

ATTACHMENT A: PROCESS AND INSTRUMENTATION DIAGRAM



**ATTACHMENT B: HAZOP TEMPLATE**

Project: Node: Electrical engine							Page
Ref	Guideword	Causes	Consequences	Safeguards	Recommendations	Action	Date/Sign
	Damage on rotating parts	Vital parts of the rig is poorly covered	Damage to personnel, damage to equipment	Vital parts of the rig is well covered	Make sure that the rotating parts of the rig is covered so that nothing can damage the rig or get damaged.		
	Noise from the rig	Rotating machinery	Damage to personnels hearing	Personnel operating the rig and personnel in the vicinity should wear ear protection	Personnel working in the vicinity should be warned before the rig is running.		
	Debris from the rotating machinery		Damage to personnels eyes	Personnel operating the rig and personnel in the vicinity should wear ear protection	Personnel working in the vicinity should be warned before the rig is running.		
	Getting objects (hair) into the rotating shaft	Rotating shaft is poorly covered or personnel is unaware of the danger	Damage to personnel	The rotating parts should be properly covered.	Personnel should not keep their long hair loose. Other objects that can get into the rotating shaft should not be kept close to the shaft when the rig is running.		

**ATTACHMENT C: TEST CERTIFICATE FOR LOCAL PRESSURE TESTING**

Trykkpåkjent utstyr:	
Benyttes i rigg:	
Design trykk for utstyr (bara):	
Maksimum tillatt trykk (bara): (i.e. burst pressure om kjent)	
Maksimum driftstrykk i denne rigg:	

**Prøvetrykket skal fastlegges i følge standarden og med hensyn til maksimum tillatt trykk.**

Prøvetrykk (bara):	
X maksimum driftstrykk: I følge standard	
Test medium:	
Temperatur (°C)	
Start tid:	Trykk (bara):
Slutt tid:	Trykk (bara):
Maksimum driftstrykk i denne rigg:	

Eventuelle repetisjoner fra atm. trykk til maksimum prøvetrykk:.....

Test trykket, dato for testing og maksimum tillatt driftstrykk skal markers på (skilt eller innslått)

\_\_\_\_\_  
Sted og dato

\_\_\_\_\_  
Signatur

**ATTACHMENT D: HAZOP PROCEDURE (TEMPLATE)**

Project: Node: 1							Page
Ref#	Guideword	Causes	Consequences	Safeguards	Recommendations	Action	Date/Sign
	Not clear procedure	Procedure is too ambitious, or confusingly					
	Step in the wrong place	The procedure can lead to actions done in the wrong pattern or sequence					
	Wrong actions	Procedure improperly specified					
	Incorrect information	Information provided in advance of the specified action is wrong					
	Step missing	Missing step, or step requires too much of operator					
	Step unsuccessful	Step has a high probability of failure					
	Influence and effects from other	Procedure's performance can be affected by other sources					



## ATTACHMENT E: PROCEDURE FOR RUNNING EXPERIMENTS

<b>Prosjekt</b> LDV measurements in the centrifugal pump	<b>Dato</b>	<b>Signatur</b>
<b>Apparatur</b> Singlestage Centrifugal Pump		
<b>Prosjektleder</b> Torbjørn K. Nielsen		

	<b>Conditions for the experiment:</b>	<b>Completed</b>
	Experiments should be run in normal working hours, 08:00-16:00 during winter time and 08.00-15.00 during summer time. Experiments outside normal working hours shall be approved.	
	One person must always be present while running experiments, and should be approved as an experimental leader.	
	An early warning is given according to the lab rules, and accepted by authorized personnel.	
	Be sure that everyone taking part of the experiment is wearing the necessary protecting equipment and is aware of the shut down procedure and escape routes.	
	<b>Preparations</b>	<b>Carried out</b>
	Post the "Experiment in progress" sign.	
	Check that nothing is in contact with the pump shaft	
	Check the water level in the water tank	
	Open the valve between the pump and the water tank	
	Wait until the water level has been stabilized and check that there is enough water.	
	Make sure the switch on the pump control panel is switched to "PUMPE DRIFT".	
	Make sure the knob is turned to the minimum by turning it counter-clockwise	
	Turn the key so that the light labelled "DRIFTSKLAR" is glowing	
	Start the pump by pressing the green button.	
	<b>During the experiment</b>	
	Increase the rotational speed of the pump to between 1000-2000 rpm by carefully turning the knob in the clockwise direction.	
	<b>End of experiment</b>	
	Turn the pump off by pressing the red button on the pump control panel.	
	Turn the knob down to the minimum.	
	Turn the key and remove it, put it on top of the control panel.	
	Close the valve between the water tank and the pump.	

	<b>To reflect on before the next experiment and experience useful for others</b>	
	Was the experiment completed as planned and on scheduled in professional terms?	
	Was the competence which was needed for security and completion of the experiment available to you?	
	Do you have any information/ knowledge from the experiment that you should document and share with fellow colleagues?	

**Operator(s):**

Navn	Dato	Signatur
Alessandro Nocente		
Karl Oskar Pires Bjørgen		

## ATTACHMENT F: TRAINING OF OPERATORS

Prosjekt	Dato	Signatur
LDV measurements on the centrifugal rig		
<b>Apparatur</b> Singlestage Centrifugal Pump		
<b>Prosjektleder</b> Torbjørn K. Nielsen		

Knowledge about EPT LAB in general		
Lab		
<ul style="list-style-type: none"> <li>• Access</li> <li>• routines and rules</li> <li>• working hour</li> </ul>		
Knowledge about the evacuation procedures.		
Activity calendar for the Lab		
Early warning, <a href="mailto:iept-experiments@ivt.ntnu.no">iept-experiments@ivt.ntnu.no</a>		
Knowledge about the experiments		
Procedures for the experiments		
Emergency shutdown.		
Nearest fire and first aid station.		

I hereby declare that I have read and understood the regulatory requirements has received appropriate training to run this experiment and are aware of my personal responsibility by working in EPT laboratories.

### Operator(s):

Navn	Dato	Signatur
Alessandro Nocente		
Karl Oskar Pires Bjørgen		

### ATTACHMENT G: FORM FOR SAFE JOB ANALYSIS

<b>SJA name:</b>	
Date:	Location:
Mark for completed checklist:	

<b>Participators:</b>		
<b>SJA-responsible:</b>		

Specification of work (What and how?):
Risks associated with the work:
Safeguards: (plan for actions, see next page):
Conclusions/comments:

Recommended/approved	Date/Signature:	Recommended/approved	Date/Signature:
SJA-responsible:		HSE responsible:	
Responsible for work:		Other, (position):	

HSE aspect	Yes	No	NA	Comments / actions	Resp.
<b>Documentation, experience, qualifications</b>					
Known operation or work?	X				
Knowledge of experiences / incidents from similar operations?		X			
Necessary personnel?	X				
<b>Communication and coordinating</b>					
Potential conflicts with other operations?		X			
Handling of an eventually incident (alarm, evacuation)?		X			
Need for extra assistance / watch?		X			
<b>Working area</b>					
Unusual working position		X			
Work in tanks, manhole?		X			
Work in ditch, shaft or pit?		X			
Clean and tidy?	X				
Protective equipment beyond the personal?		X			
Weather, wind, visibility, lighting, ventilation?	X				
Usage of scaffolding/lifts/belts/ straps, anti-falling device?		X			
Work at heights?		X			
Ionizing radiation?		X			
Influence of escape routes?		X			
<b>Chemical hazards</b>					
Usage of hazardous/toxic/corrosive chemicals?		X			
Usage of flammable or explosive chemicals?		X			
Risk assessment of usage?	X				
Biological materials/substances?		X			
Dust/asbestos/dust from insulation?		X			
<b>Mechanical hazards</b>					
Stability/strength/tension?		X			
Crush/clamp/cut/hit?		X			
Dust/pressure/temperature?		X			
Handling of waste disposal?		X			
Need of special tools?		X			
<b>Electrical hazards</b>					
Current/Voltage/over 1000V?		X			
Current surge, short circuit?		X			
Loss of current supply?		X			
<b>Area</b>					
Need for inspection?	X				
Marking/system of signs/rope off?	X				
Environmental consequences?		X			
<b>Key physical security systems</b>					
Work on or demounting of safety systems?		X			
<b>Other</b>					

## APPARATURKORT / UNITCARD

**Dette kortet SKAL henges godt synlig på apparaturen!**  
***This card MUST be posted on a visible place on the unit!***

<b>Apparatur (Unit)</b> LDV measurements in centrifugal rig	
<b>Prosjektleder (Project Leader)</b> Torbjørn K. Nielsen	<b>Telefon mobil/privat (Phone no. mobile/private)</b> 91897572
<b>Apparaturansvarlig (Unit Responsible)</b> Bård Brandåstrø	<b>Telefon mobil/privat (Phone no. mobile/private)</b> 91897257
<b>Sikkerhetsrisikoer (Safety hazards)</b> Rotating parts	
<b>Sikkerhetsregler (Safety rules)</b> -Wear appropriate safety goggles	
<b>Nødstop prosedyre (Emergency shutdown)</b> Hit the marked emergency shutdown button	

**Her finner du (Here you will find):**

<b>Prosedyrer (Procedures)</b>	Apparaturperm
<b>Bruksanvisning (Users manual)</b>	Apparaturperm

**Nærmeste (Nearest)**

<b>Brannslukningsapparat (fire extinguisher)</b>	Vestveggen i Lab
<b>Førstehjelpsskap (first aid cabinet)</b>	Vestveggen i Lab

**NTNU**  
**Institutt for energi og prosessteknikk**

**SINTEF Energi**  
**Avdeling energiprosesser**

**Dato**

**Dato**

**Signert**

**Signert**

## FORSØK PÅGÅR / EXPERIMENT IN PROGRESS

**Dette kortet SKAL henges opp før forsøk kan starte!**  
***This card MUST be posted on the unit before the experiment startup!***

<b>Apparatur (Unit)</b> LDV measurements in centrifugal pump	
<b>Prosjektleder (Project Leader)</b> Torbjørn K. Nielsen	<b>Telefon mobil/privat (Phone no. mobile/private)</b> 91897572
<b>Apparaturansvarlig (Unit Responsible)</b> Bård Brandåstrø	<b>Telefon mobil/privat (Phone no. mobile/private)</b> 91897257
<b>Godkjente operatører (Approved Operators)</b> Alessandro Nocente Karl Oskar Pires Bjørgen	<b>Telefon mobil/privat (Phone no. mobile/private)</b> 90861780 (Karl Oskar)
<b>Prosjekt (Project)</b> LDV measurements in centrifugal pump	
<b>Forsøkestid / Experimental time (start - stop)</b> 01.10.2014 – 15.12.2014	
<b>Kort beskrivelse av forsøket og relaterte farer (Short description of the experiment and related hazards)</b> Centrifugal pump test rig. Rotating parts and noise are possible dangers while the experiment is running.	

**NTNU**  
**Institutt for energi og prosesseteknikk**

**SINTEF Energi**  
**Avdeling energiprosesser**

**Dato**

---

**Dato**

---

**Signert**

---

**Signert**

---